Deformation Transitions and their Effects on the Long-term Performance of Polyethylene and its Pressure Pipe

by

Na Tan

A thesis submitted in partial fulfillment of the requirements for the degree of

Doctor of Philosophy

Department of Mechanical Engineering

University of Alberta

Abstract

Ductile-to-brittle (DB) transition is of tremendous importance for lifetime prediction of polyethylene (PE). Majority of current methods for determining critical stress for the DB transition of PE products use notched coupon specimens in order to shorten the test timeframe. However, those work are mainly for characterization of the crack resistance performance, not for determining critical stress level for the DB transition. Therefore, the ultimate goal of this research is to develop a new short-term test, based on notch-free specimens, to predict critical stress for the DB transition of PE for load-carrying applications. The key assumption for the approach used in the research is that below a critical stress level, brittle failure occurs as a result of the limited extent of deformation due to the constraint of deformation in the amorphous phase; above this critical stress level, ductile failure dominates the failure mode due to the activation of collective crystallographic slips which accommodate large plastic strain. Thus, it is expected that critical stress for the DB transition should not exceed the stress level for the onset of global yielding in the crystalline phase. Also, the critical stress contains two components, one is the time-dependent viscous stress and the other the time-independent quasi-static stress. In view that the quasi-static stress should dominate the long-term load-carrying performance of PE, the viscous stress should be excluded from the critical stress that is considered for the long-term applications.

Based on the above assumption, uniaxial creep tests are firstly conducted on three PE plaques differing mainly in mass density, and master time-to-failure curves are constructed through the use of a stress-time-temperature (StT) parametric method. PE with the highest density shows the well-known DB transition; PE with the medium density shows a different transition which was detected through the change in the dependence of failure time on the applied stress, but the failure

mode remained ductile. Therefore, this transition is named ductile-ductile (DD) transition. To investigate the correlation between creep deformation and activation energy at the secondary creep stage, Norton Power Law (NPL) and Eyring's Law are used to analyze the results. The analysis suggests a strong correlation between the DB transition and activation energy at the secondary creep stage, and that the Monkman-Grant relationship is applicable to ductile failure, even with the DD transition. Therefore, rather than the use of creep tests with failure time up to 13 months, short-term creep tests have been investigated, and found to have the potential for predicting the critical stress for the DB transition.

The study also included development of a new short-term test, named multi-relaxation (MR) test which is proven to be capable of detecting two critical quasi-static stresses for change of mechanisms involved in deformation. Six PE plaques with different mass densities were studied and the results show that the 1st critical stroke has very similar values among six PEs of different mass densities. More interestingly, ratio of the quasi-static stress at the 1st critical stroke to the yield stress from the standard tensile test shows little dependence on PE density. Therefore, it is possible to use the popular short-term tensile test to characterize the critical quasi-static component of the applied stress to initiate plastic deformation in the crystalline phase, which is expected to play a significant role on the long-term, load-carrying applications of PE.

Finally, the study has correlated the critical quasi-static stresses from the MR test with the critical stress for the DB transition from the creep test. The results on compression-molded PE plaque show that the critical quasi-static stress for the onset of global yielding in the crystalline phase correlates well with the critical stress for the DB transition. Therefore, such a concept is also transferred to PE pipe. The results suggest that critical quasi-static stress for the onset of plastic deformation in the crystalline phase is close to the hydrostatic design basis (HDB) value based on

the long-term hydrostatic strength (LTHS) determined from hydrostatic pressure tests, but the MR test takes less than two weeks to complete, while the LTHS requires more than 1 year to measure. Therefore, the MR test can be used as an alternative method to characterize PE pipe performance, especially for preliminary screening or in-service monitoring of PE pipe performance.

Preface

The thesis is an original work by Na Tan under the supervision of Dr. P.-Y. Ben Jar. The main body of this thesis is composed of three published/submitted journal papers and two conference papers.

Chapter 2 is based on one published journal paper: N. Tan and P.Y. Ben Jar, 2020. Deformation transitions of ethylene-hexene copolymers under creep loading. *Polymer*, 208, pp.122905. I was responsible for the data collection and analysis as well as the manuscript composition. Dr. Jar assisted with the data collection and contributed to manuscript edits. Dr. Jar was the supervisory author and was involved with concept formation and manuscript composition.

Chapter 3 is based on one submitted journal paper: N. Tan and P.Y. Ben Jar, 2021. Creep deformation and failure behaviour of polyethylene and its copolymers. Submitted to *Polymer*. I was responsible for the data collection and analysis as well as the manuscript composition. Dr. Jar assisted with the data collection and contributed to manuscript edits. Dr. Jar was the supervisory author and was involved with concept formation and manuscript composition.

Chapter 4 is based on one published journal paper: N. Tan and P.Y. Ben Jar, 2019. Determining deformation transition in polyethylene under tensile loading. *Polymers*, 11, pp.1415. I was responsible for the data collection and analysis as well as the manuscript composition. Dr. Jar assisted with the data collection and contributed to manuscript edits. Dr. Jar was the supervisory author and was involved with concept formation and manuscript composition.

The work presented in Chapter 5 is based on two published conference papers: N. Tan and P.Y. Ben Jar, 2020. Establishing ductile-to-brittle transition of unimodal high density polyethylene under creep test. In *SPE ANTEC 2020: Annual Technical Conference for Plastic Professionals*; N.

Tan and P.Y. Ben Jar, 2019. Multi-relaxation test to characterize PE pipe performance. *Plastics Engineering*, 75, pp.40-45. I was responsible for the data collection and analysis as well as the manuscript composition. Dr. Jar assisted with the data collection and contributed to manuscript edits. Dr. Jar was the supervisory author and was involved with concept formation and manuscript composition.

Acknowledgements

First of all, I wish to express my sincere gratitude to my supervisor Dr. P.-Y. Ben Jar without whom it would not be possible to complete the work on time. I am fully indebted to Dr. Jar for his wisdom, patience and invaluable guidance and for pushing me further than I thought I could go. His rigorous attitude toward research always reminds me to be a more humble and decent person. It is a great honor to conduct research under his supervision.

To my committee, Dr. Cagri Ayranci and Dr. Xiaodong Wang, I am extremely grateful for your assistance and suggestions throughout my project.

Sincere appreciation goes to Ron Cooke in Imperial Oil, Ernest Lever in Gas Technology Institute and Wajdy Ateerah in Polytubes for the supply of PEs used in the project, and machine shop staff in the Department of Mechanical Engineering for preparation of specimens used for the testing and especially Bernie Faulkner for the fabrication of extensometers used for the testing.

I would like to acknowledge the financial support from China Scholarship Council (CSC) and Natural Sciences and Engineering Research Council of Canada (NSERC).

I would like especially to thank my husband Yuanyuan Pu for his unconditional love, support and for always encouraging me and having more faith than I had in myself. It was an amazing experience to live and study with you in Edmonton. I do treasure all the ups and downs we went through together and these unforgettable moments had turned me into a more optimistic person. Finally, I would like to thank our parents, Dingying Liu, Haoming Tan, Qiulan Shu and Jianyou Pu for being the source of energy and inspiration.

Table of Contents

Abstract ..... **ii**

Preface ..... **v**

Acknowledgements ..... **vii**

Table of Contents ..... **viii**

List of Tables ..... **xii**

List of Figures ..... **xiii**

List of Symbols and Abbreviations ..... **xix**

Chapter 1 Introduction **1**

1.1 Background and motivation 2

1.2 Literature review 5

1.2.1 Characterization of the DB transition using notched-coupon specimens 5

1.2.2 Characterization of the DB transition using notch-free specimens and its comparison with that using notched-coupon specimens 7

1.3 Research objectives and methodology 9

1.4 Thesis organization 11

References 13

Chapter 2 Deformation transitions of ethylene-hexene copolymers under creep Loading . 22

2.1 Introduction 23

2.2 Experiments 26

2.2.1 Materials and specimens 26

2.2.2 Creep test 28

2.2.3 Scanning electron microscopy (SEM) 29

2.3 Results 29

2.3.1 Creep test 29

2.3.2 Fractographic analysis 38

2.4 Discussions 39

2.4.1 Deformation transition under creep loading 39

2.4.2 Relationship between stroke rate and failure time under creep loading 46

2.5 Conclusions 48

References 49

Chapter 3 Creep deformation and failure behaviour of polyethylene and its copolymers.. 56

3.1 Introduction 57

3.2 Experiments 59

3.2.1 Materials and specimens 59

3.2.2 Mechanical testing 60

3.2.3 Scanning electron microscopy (SEM) 60

3.3 Results 61

3.3.1 Creep test 61

3.3.2 Fractographic analysis 76

3.4 Discussion 77

3.4.1 Applicability of the Monkman-Grant relationship 77

3.4.2 Mechanisms and comparison of Eyring's parameters for the four PEs 79

3.5 Conclusions 82

References 83

Chapter 4 Determining deformation transition in polyethylene under tensile loading 89

4.1 Introduction 90

4.2 Multi-relaxation (MR) test 92

4.3 Experimental details 97

4.3.1 Materials and specimen dimensions 97

4.3.2 Multi-relaxation (MR) test 99

4.3.3 Wide-angle X-ray scattering (WAXS) 99

4.4 Results and discussion 101

4.4.1 MR test 101

4.4.2 WAXS 104

4.4.3 Discussion 109

4.5 Conclusions 112

References 113

Chapter 5 Multi-relaxation test to characterize the long-term performance of PE and its pressure pipe 119

5.1 Introduction 120

5.2 Experiments 121

5.2.1 Materials and sample preparation 121

5.2.2 Multi-relaxation (MR) test 123

5.3 Idea of using MR test to predict critical stress for the DB transition 125

5.4 Results and discussions 128

5.5 Conclusions 135

References 135

Chapter 6 Conclusions and future work 139

6.1 Main conclusions 140

6.2 Future work 143

References 146

Bibliography 148

List of Tables

Tab. 2.1 Material characteristics of PEs used in the study. 27

Tab. 2.2 Values for parameters *A*, *B*, *C* and *D* in Eq. (2.1)..... 36

Tab. 3.1 Summary of characteristics for PEs used in this study. 59

Tab. 3.2 Fitting parameters of the Eyring's Law for the four PEs..... 72

Tab. 3.3 Activation energy (in kJ/mol) in literature for deformation of PE using two Eyring's processes. 82

Tab. 4.1 Material characteristics of PEs used in the study. 98

Tab. 5.1 Material characteristics for pipes used in the study. 122

Tab. 5.2 Summary of results from the multi-relaxation tests and those from standard test methods (HDB and LTHS). 134

List of Figures

Fig. 1.1 Schematic plot of the typical hoop stress versus failure time for PE pipes. 3

Fig. 2.1 Schematic plot of applied hoop stress versus failure time for PE pipes. 24

Fig. 2.2 Geometry and dimensions of the modified dog-bone specimens. 27

Fig. 2.3 Sample specimens in ductile failure. 30

Fig. 2.4 Sample of specimens for #3 HDPE that fractured in a brittle manner (left and centre) and in a mix of brittle initiation and ductile stretch (right)..... 31

Fig. 2.5 Typical creep curves at different applied stresses and temperatures (selected from #3 HDPE). 33

Fig. 2.6 Plots of applied stress versus time for ductile or brittle failures at different temperatures: (a) #1 LLDPE-ductile, (b) #2 HDPE-ductile, (c) #3 HDPE-ductile and (d) #3 HDPE-brittle. 34

Fig. 2.7 Summary of intercepts (a) and slopes (b) used for the fitting functions in Fig. 2.6, plotted as a function of $1/T$ ('D' and 'B' in the legends indicate ductile and brittle failures, respectively). 35

Fig. 2.8 Sample master curves generated based on Eq. (2.1): (a) #1 LLDPE, (b) #2 HDPE and (c) #3 HDPE. 37

Fig. 2.9 SEM micrographs of selected brittle failure surfaces for #3 HDPE: (a) 353 K and (b) 358 K..... 39

Fig. 2.10 Data from the second batch of creep tests on #3 HDPE (squares), with the line plots identical to those shown in Fig. 2.8(c). 40

Fig. 2.11 Creep test results for #2 HDPE at 323 K. 42

Fig. 2.12 Summary of slope and intercept values for #2 HDPE, including those presented in Figs. 2.6(b) and 2.11. The trend lines are based on the same expressions as those for #2 HDPE in Fig. 2.7. 44

Fig. 2.13 Double logarithmic plot of failure time versus stroke rate for ductile and brittle failures for all specimens used in the study, that is, #1 LLDPE (□), #2 HDPE (△ and ▲), and #3 HDPE (○ and ●). Open and solid symbols represent before and after DD and DB transitions, respectively (DD transition for #2 HDPE and DB transition for #3 HDPE). Different colours for #3 HDPE in the electronic version represent results from different temperatures. 48

Fig. 3.1 Typical creep curves for four PEs used in the study, with temperatures indicated by the numbers next to each curve, followed by DF (ductile failure), LTBF (low-temperature brittle failure) and HTBF (high-temperature brittle failure). 63

Fig. 3.2 Typical strain-time curves to demonstrate the determination of the critical failure point and the corresponding secondary creep strain rate. 64

Fig. 3.3 Summary of strains to failure as a function of the applied stress for the four PEs. #1 LLDPE (□), #2 HDPE (△), #3 HDPE (○ and ●), and #4 HDPE (◇ and ◆), in which unfilled and filled symbols represent ductile and brittle failures, respectively. 64

Fig. 3.4 Natural logarithmic plots of strain rate in the secondary creep stage versus the applied stress. 67

Fig. 3.5 Summary of the NPL-based analysis: (a) slopes (n) of the expressions in Fig. 3.4 versus T, and (b) intercepts of expressions in Fig. 3.4 versus $1/T$. Unfilled symbols are for ductile failure and filled symbols for brittle failure. 67

Fig. 3.6 Plots of σ/T versus ln ($\dot{\varepsilon}_s$) for the four PEs used in the study. 70

Fig. 3.7 Plots of σ/T versus ln ($\dot{\varepsilon}_s$) at two highest temperatures used in the experimental testing, for determining the V_1 values. 71

Fig. 3.8 Summary of analysis for process 1 based on the Eyring's model: (a) The intercept values for the solid trend lines in Fig. 3.7, and (b) values for $\frac{\dot{\varepsilon}_s}{\dot{\varepsilon}_{01}} \exp\left(\frac{E_1}{RT}\right)$ versus T. 72

Fig. 3.9 (a) The left-hand side (LHS) of Eq. (3.8) generated using the temporary V_2 values, and (b) plots of $\frac{\dot{\varepsilon}_s}{\dot{\varepsilon}_{02}} \exp\left(\frac{E_2}{RT}\right)$ versus T, using temporary E_2 and $\dot{\varepsilon}_{02}$ values based on the temporary V_2 values. 75

Fig. 3.10 Summary of results for determining V_2, E_2 and $\dot{\varepsilon}_{02}$: (a) creep data at room temperature to determine V_2 based on Eq. (3.5b), and (b) plot of values from the LHS of Eq. (3.8) generated using the true V_2 values, as a function of $1/T$. 75

Fig. 3.11 SEM micrographs of surfaces generated by brittle failure of #4 HDPE: (a) LTBF at 296 K, (b) HTBF at 333 K and (c) HTBF at 353 K. 77

Fig. 3.12 The Monkman-Grant (MG) plot for all data reported here: #1 LLDPE (□), #2 HDPE (△), #3 HDPE (○ and ●) and #4 HDPE (◇ and ◆) in which unfilled symbols represent ductile failure and filled symbols brittle failure..... 78

Fig. 3.13 Comparison of experimental measurements (unfilled and filled symbols of large size in black) with predictions based on the Eyring's Law using parameters listed in Tab. 3.2 (unfilled symbols of small size in red). 80

Fig. 4.1 Schematic diagram of the standard, visco-elastic model used in this work. 93

Fig. 4.2 Examples of stress drop obtained from the MR tests (open circles) and generated based on Eq. (4.8) (solid lines) for all stress relaxation stages: (a) with time in the linear scale, and (b) with time in the logarithmic scale. 97

Fig. 4.3 Geometry and dimensions of the modified dog-bone specimens. 98

Fig. 4.4 Schematic description of the set-up for the WAXS experiment. 100

Fig. 4.5 Typical curves from the MR test, of total stress versus stroke with the total stress measured at the beginning of each stress relaxation stage, in which peak points are highlighted using open blue boxes. 102

Fig. 4.6 Summary of MR test results: (a) sample curves showing the approach used to determine the stroke for the 1st critical point, (b) typical variation of σ_0 with stroke, (c) typical variation of σ_{st} with stroke (highlighted open red circles and open blue boxes indicate the 1st critical point and the yield point, respectively)..... 104

Fig. 4.7 Typical WAXS spectra with different strokes (from #2 HDPE) (Peak intensity for (110) decreases with increase of stroke applied to specimens). 105

Fig. 4.8 Absolute intensity of peak (110) from the orthorhombic structure of PE, as a function of stroke used to stretch the specimens. 107

Fig. 4.9 Comparison of critical strokes in Fig. 4.8 and those for the 1st critical point from the MR test. 109

Fig. 4.10 Summary of σ_{st} and σ_t values at the 1st critical point and yield point from the MR tests (σ_{st}-1st, σ_{st}-yield, σ_t-1st, and σ_t-yield), and yield strength listed in Tab. 4.1 (σ_{yld}-mono), plotted as functions of PE density. 110

Fig. 4.11 Ratio of σ_{st} at the 1st critical point from the MR test (σ_{st}-1st) to yield stress from the standard tensile test (σ_{yld}-mono) listed in Tab. 4.1, plotted as a function of PE density. 112

Fig. 5.1 Schematic description of specimen preparation. 123

Fig. 5.2 Set-up of the D-split tensile test. 125

Fig. 5.3 Master curves of engineering stress versus time, including the DB transition and creep test results. 126

Fig. 5.4 Critical stresses for the DB transition (■) from creep tests, first critical quasi-static stresses (●) and critical quasi-static stress for global yielding (○) from short-term MR tests at different temperatures. 127

Fig. 5.5 A typical engineering stress-stroke curve (from #5 u-MDPE). 128

Fig. 5.6 Curves of applied engineering stress versus stroke for the six PE pipes. 129

Fig. 5.7 Curves of applied true stress versus area strain for the six PE pipes. 129

Fig. 5.8 Curve fitting of experimental data according to the Eyring's Law. 131

Fig. 5.9 Plot of reference stress (σ_0) as a function of stroke for a NPR specimen, and depiction of the process to determine the first critical point for deformation transition. 132

Fig. 5.10 Reference stress (σ_0) as a function of (a) stroke, and (b) area strain. 132

Fig. 5. 11 Two stress components determined from the multi-relaxation tests as a function of stroke for the six PE pipes: (a) $\sigma_r(0)$ and (b) σ_{st}. 133

Fig. 6.1 Typical WAXS spectra (from #1 LLDPE with stroke of 5 mm) and the individual contribution of each peak from the deconvolution procedure. 145

List of Symbols and Abbreviations

A, B, C, D	Fitting parameters in a parametric method
A_1	Material constant
ASTM	American Society for Testing and Materials
BD	Brittle-ductile
CDNT	Circumferentially deep notched tensile
CRB	Cracked round bar
DB	Ductile-brittle
DD	Ductile-ductile
DF	Ductile failure
e	Shape parameter of Pearson VII function
E	Activation energy
E_1, E_2	Activation energy in process 1 and 2
E_N	Activation energy in Norton Power Law
E_r	Modulus for the spring in the viscous branch in the standard visco-elastic model
ESCR	Environmental stress cracking resistance
$f(2\theta)$	Peak profile
F	Load
F_a	Peak area of crystalline peak
F_c	Peak area of amorphous halo

FNCT	Full-notch creep test
G	Peak height
HDB	Hydrostatic design basis
HDPE	High-density polyethylene
HTBF	High-temperature brittle failure
ISO	International Organization for Standardization
LLDPE	Linear low-density polyethylene
LTBF	Low-temperature brittle failure
LTHS	Long-term hydrostatic strength
m, C_{MG}	Constants for Monkman-Grant relationship
MDPE	Medium-density polyethylene
MG	Monkman-Grant
MR	Multi-relaxation
MWD	Molecular weight distribution
n	Power law exponent
NPL	Norton Power Law
NPR	Notched-pipe-ring
NPT	Notched pipe test
PE	Polyethylene
PENT	Pennsylvania edge-notch tensile test
R	The Boltzmann constant
SCG	Slow crack growth

SEM	Scanning electron microscopy
SEN	Single-edge notched
StT	Stress-time-temperature
t	Failure time
T	Temperature
T_0	Initial thickness
V	Activation volume
V_1, V_2	Activation volume in process 1 and 2
w, w_0	Initial and deformed width
WAXS	Wide-angle X-ray scattering
X_c	Crystallinity
σ	Stress
σ_0	Reference stress
σ_1, σ_2	Stress in process 1 and 2
σ_A	Applied stress in the standard visco-elastic model
σ_{eng}	Engineering tress
$\sigma_r(t)$	Time-dependent viscous stress
σ_{st}	Quasi-static stress
σ_{st}-1st	First critical quasi-static stress
σ_{st}-yield	Critical quasi-static stress for global yielding
σ_t-1st	First critical total stress from MR test
σ_t-yield	Total stress for global yielding from MR test

σ_{yld}-mono	Yield stress from monotonic tensile test
$\Delta\sigma_t$, $\Delta\sigma_r$	Decay of total stress, change of viscous stress
ε_{area}	Area strain
$\dot{\varepsilon}_0$	Reference strain rate
$\dot{\varepsilon}_{01}$, $\dot{\varepsilon}_{02}$	Reference strain rate in process 1 and 2
$\dot{\varepsilon}_D$	Strain rate of the damper in the standard visco-elastic model
$\dot{\varepsilon}_s$	Strain rate at the secondary creep stage
$\dot{\delta}$	Stroke rate at the secondary creep stage
τ_r	Relaxation time
θ_{hkl}	Bragg angle
2θ	Diffraction angle
$\Delta(2\theta_{hkl})$	Full width at half maximum

Chapter 1 Introduction

Chapter 1 is an overview at this thesis, which provides the research background, motivations, literature review, objectives and methodologies. The thesis organization is also outlined at the end of this chapter.

1.1 Background and motivation

Polyethylene (PE) has long been an attractive option for load-carrying applications, ranging from plastic pipes for water and gas transportation to containers and film for material packaging, because of its light weight, corrosion resistance and excellent ductility [1-4]. In addition, easy installation and low maintenance costs make PE pipe the most popular candidate for the newly installed low-pressure gas pipeline systems [5-7]. Therefore, there is considerable interest to address the mechanical behaviors of PE pipe for load carrying applications.

For the use of PE in such applications, a ductile-to-brittle (DB) transition of failure mode is a major concern [8-9], since PE can fracture in either a ductile or a brittle manner, depending on the loading conditions [10-15]. Using hydrostatic pressure test on full-sized PE pipes, as suggested in ASTM D2837 [16], the LTHS (long-term hydrostatic strength) of PE pipe is typically obtained through standard extrapolation methods. However, the standard test requires a long duration (some more than 14 months) to complete in order to cover the service life of 50 years. And this standard test is yet to be able to determine time and stress level for the DB transition. Better understanding of the DB transition will help in predicting the failure mode and lifetime of PE. Hence, it is of great importance to develop an accurate and time-efficient test to predict critical stress for the DB transition.

Typically, failure mechanisms of PE under creep loading can be divided into three characteristic regions, depending on the applied stress level, schematically shown in Fig. 1.1 [17]. At a relatively high stress level, corresponding to region I in the figure, PE fails in a ductile manner as a large scale of plastic deformation occurs before fracture. At a lower stress level, region II, the

failure mode changes to brittle, as little indication of plastic deformation occurs, which is also known as slow crack growth (SCG) [18]. The DB transition is where the inflection point is between regions I and II. Region III is nearly stress independent, where failure occurs via chemical aging or polymer degradation, usually after a very long period [19].

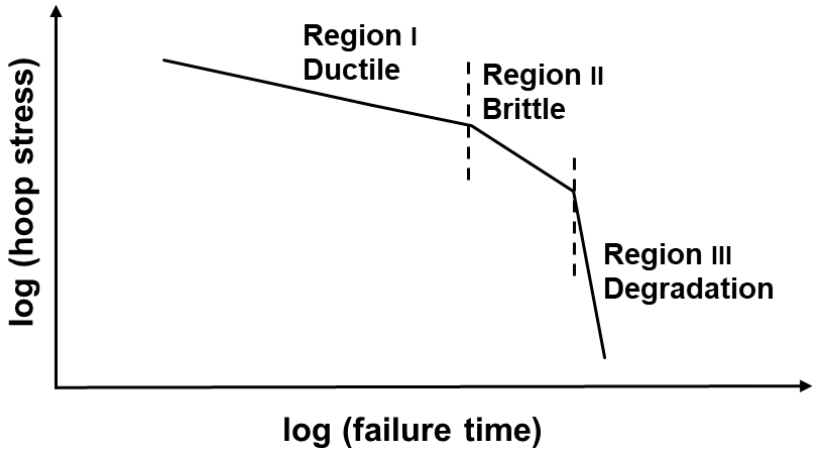

Fig. 1.1 Schematic plot of the typical hoop stress versus failure time for PE pipes.

As brittle failure is mainly characterized by SCG, some standard test methods, such as notched pipe test (NPT) [20], full-notch creep test (FNCT) [21] and Pennsylvania edge-notch tensile test (PENT) [22] and cracked round bar (CRB) test [23] have been developed to promote SCG at the notch tip. Notched specimens are effective in reducing test time for detecting the DB transition. However, use of the notches prevents the test results from predicting critical stress and time for the DB transition in PE products that do not contain any notch [24]. In addition to the use of sharp notches to promote SCG, environmental stress cracking agents such as Igepal are also used to facilitate the formation of crazes and reduce time for initiation of crack growth [25-26]. For semi-crystalline polymers such as PE, the crystalline lamellae are packed together by the tie

molecules in the amorphous phase, which play a decisive role in the load transmission in the deformation process [27-29]. The pull-out and disentanglement of tie molecules from the crystalline lamellae can initiate crack, which are favored by the use of stress cracking agents. However, the above test is mainly for characterization of the environmental stress cracking resistance (ESCR) performance, not for determining the critical stress level for the DB transition. Therefore, in this study, without the use of environmental stress cracking agents, notch-free specimens are used to characterize critical stress for the DB transition.

As a semicrystalline polymer, PE's deformation involves both crystalline and amorphous phases. Although both phases are involved from the beginning of the deformation process, their role of involvement varies with the applied stress level [30]. A widely accepted concept is that deformation of PE is initially dominated by the amorphous phase, due to its relatively low resistance to deformation [31]. The crystalline phase is involved at this stage through inter-lamellar shear, inter-lamellar separation, and lamellar stack rotation [31-34], of which the contribution depends on the loading mode and the stress level. Majority of the recoverable deformation can be attributed to the reversible inter-lamellar shear due to the rubber-like behaviour of the amorphous phase [35]. In an engineering stress-strain curve from tensile loading, PE is known to yield at the peak point, at which the lamellar structure starts to disintegrate. However, Strobl and co-workers [36-38] reported that local plastic strain started to occur before the global yielding, and transition from amorphous-phase-dominant deformation to that involving plastic deformation in the crystalline phase is detectable. Based on this concept, we believe that the brittle-like failure behavior in PE at a low stress level is caused by the limited extent of deformation due to the constraint in the inter-lamellar, amorphous phase.

Following the work described above, this study proposed a new short-term test method to detect critical stresses for deformation transitions. On the other hand, creep tests were also conducted to predict critical stress and time for the DB transition, based on a stress-time-temperature (StT) parametric method that is similar to the method introduced in ISO 9080 [39] and ASTM D2837 [16]. Results from short-term and creep tests were correlated to demonstrate the feasibility of using a short-term test to characterize DB transition of PE.

1.2 Literature review

1.2.1 Characterization of the DB transition using notched-coupon specimens

Over the last few decades, many researchers have shown considerable interests in predicting the DB transition and long-term performance of PE using short-term laboratory tests [19, 40-43]. To my knowledge, majority of these studies introduce artificial notches to specimens to use high stress concentration at the notch tip to encourage SCG development. Such coupon specimens are chosen to be able to characterize the DB transition in a very short period.

Brown and his co-workers have studied extensively the DB transition and long-term performance of PE and its copolymer [11, 14, 25, 44-45]. In Ref. [44], they conducted creep tests on linear PE at 30 °C to generate ductile failure. In order to generate brittle failure, they used single-edge notched (SEN) specimens to initiate the fracture process and then to measure crack growth speed. The notch opening under different loading conditions was obtained from scanning electron microscopy (SEM), which was used to determine crack growth speed for brittle failure. By expressing time for the ductile failure as a power law function of applied stress, the location of the DB transition is in qualitative agreement with results from hydrostatic pressure tests (notch-free) [46]. However, the quantitative comparison is not given.

Brown and his co-workers also investigated the effect of the side chains of PE molecules on the occurrence of the DB transition [14]. The SCG behaviours of a high-density homopolymer and an ethylene-hexene copolymer were studied using SEN specimens. The results suggest that the major effect of the side chains is to decrease the rate of disentanglement which governs the process of SCG. In other words, the homopolymer has a lower resistance to SCG. Later, they studied the effects of crack tip blunting [11], environmental stress cracking agent [25] and thermal history [45] on the long-term performance of PE. Following the aforementioned work, Brown and his co-workers developed an accelerated test to evaluate SCG resistance and DB transition of polymer pipe [47]. The test later became an international standard, and is known as PENT test [22]. However, many researchers [17, 48] have shown concerns in quantitative evaluation of the DB transition of PE grades using the PENT test.

Other accelerated tests using coupon specimens have also been developed by many investigators. Frank and Pinter [40] conducted cyclic fatigue test to predict the failure time and DB transition of PE using cracked round bar (CRB) specimens. Based on linear elastic fracture mechanics, stress intensity factor was used to characterize the crack growth kinetics. The fatigue crack growth (FCG) curves were generated by plotting the crack growth rate against R-ratio (ratio of minimum to maximum loads). These curves were then extrapolated to static loading conditions (i.e., R-ratio = 1). Without considering the crack initiation time, the DB transition determined was compared to results from hydrostatic pressure tests (notch-free), to show a good agreement with an initial crack size of 0.4 mm. However, the strong dependency of the DB transition on initial crack size remains a concern for its universal applicability.

Schilling et al. [49] used FNCT test to characterize the DB transition of HDPE. Location of the DB transition was investigated and compared when performing FNCT test among different

media, i.e. water, air and 4-nonylphenyl-polyethylene glycol. It was found that location of the DB transition was strongly dependent on the surfactant used in the study. Time for the DB transition was significantly shortened and the corresponding stress lowered in 4-nonylphenyl-polyethylene glycol. Although such an accelerated test is effective in ranking different PEs, it is ineffective for lifetime prediction under the in-service loading conditions.

Adib et al. [50] studied the influence of specimen geometry on the SCG testing of HDPE pipes. They suggested that different specimen geometries adopted by PENT test and circumferentially deep notched tensile (CDNT) test can lead to different ranking for the PE pipes. Such phenomena leave uncertainties in quantitatively evaluating the DB transition of PE pipes in service.

In addition, coupon specimens were also widely adopted in Refs. [12, 15, 51-56], to shorten the timeframe for characterizing the DB transition. However, results from these studies cannot be used to determine the DB transition of PE pipes in service because of the use of artificial notches [24]. Moreover, those work are mainly for characterization of the crack resistance performance, not for determining critical stress level for the DB transition.

1.2.2 Characterization of the DB transition using notch-free specimens and its comparison with that using notched-coupon specimens

On the other hand, to my knowledge, only a few groups have tried to use notch-free specimens to predict the DB transition, and to apply the test results to prediction of service life of PE under the in-service loading conditions. The DB transition is known to cause brittle failure at a low stress level, occurring often after a long incubation period [10, 14]. Hence, one problem for

the use of notch-free specimens is that the DB transition may not be detected for a long period, even at elevated temperatures.

Using dumbbell specimens, Crissman [57] investigated the long-term creep and lifetime behavior of linear low density PE (LLDPE) under different loading conditions. The concept of time-temperature superposition was applied to construct a master curve to predict long-term creep response for LLDPE. For all tested specimens, none of them showed brittle failure. In other words, the DB transition cannot be detected by this type of creep test within a year. This was not surprising, as LLDPE contained a large amount of amorphous structure, making it relatively ductile.

Crissman and Zapas [58] conducted creep test on HDPE with mass density of 0.970 g/cm^3. They have shown that brittle failure of their HDPE occurs after 10 days under a low stress level at ambient temperature. For HDPE, the mass density is around 0.94 to 0.97 g/cm^3 [59]. Therefore, the high mass density PE used in their work reaches the upper density limit and is prone to brittle failure because of the high degree of crystallinity [60]. For this type of PE, creep test can be performed within a very short timeframe to measure the DB transition.

Lang et al. [15] also studied the failure behavior of HDPE pipes under constant internal pressure and characterized the DB transition at several temperatures using an extrapolation method in ISO 9080. A transition from ductile failure to brittle or quasi-brittle failure is clearly visible at elevated temperatures. Although no brittle failure was detected at room temperature within the test, the extrapolation method in ISO 9080 was capable of predicting the location of DB transition at room temperature. However, the test is quite time-consuming (more than three months) even with the acceleration factor of temperature. Krishnaswamy [61] also investigated the creep rupture behavior of PE pressure pipes with mass density of 0.952 g/cm^3 at room temperature and 80 °C.

Only ductile failure was evident for all tested conditions at room temperature. Although the DB transition was observed at 80 °C, the long time required for gathering rupture data is more than a year. It is therefore expected to be very time-consuming to characterize the DB transition of HDPE of different mass density.

Due to the improved crack resistance of newly installed PE pipe, only a few works addressed the comparison of the DB transition in notched and notch-free specimens. Krishnaswamy [17] compared the DB transition for two different HDPEs using PENT test and hydrostatic pressure test (notch-free). In the PENT test, the applied stress was increased to 3.8 MPa to accelerate the fracture process. For both HDPE pipes, the DB transition was detected from the two tests. However, contradictory results were obtained.

Nezbedová et al. [48] compared PENT test result with hydrostatic stress pressure tests. They suggested that PENT test may underestimate the SCG rate and thus overestimate lifetime. Considering that PENT test is carried out at elevated temperatures, the obtained failure time does not allow us to estimate the absolute lifetime of PE in the ambient temperature that is common in service.

1.3 Research objectives and methodology

The overall objective of this research project is to develop a short-term test, using notch-free specimens, to detect critical points for deformation transitions of PE and predict critical stress for the DB transition. In this research project, six compression-molded PE plaques with different mass densities, all from ExxonMobil Chemical provided by Imperial Oil, are selected as sample materials. Due to PE's popularity in pipeline industry, another six commercial PE pressure pipes, provided by Gas Technology Institute and Polytubes, are also studied. However, the main focus

of this research is on PE plaques, as the residual stress within PE pipes may have unknown effects on the characterization of the DB transition. Nevertheless, feasibility of transferring the concept used for PE plaques to PE pipes was examined.

Here are the specific objectives for the study:

(1) To establish master time-to-failure curves for creep test results using a stress-time-temperature (StT) parametric method.

(2) To quantify the occurrence of DB transition and to identify deformation mechanisms in notch-free specimens.

(3) To develop a new short-term test to detect the critical points for transitions of deformation mechanisms.

(4) To correlate the short-term test results with creep stress for DB transition.

To achieve the above objectives, the following tasks have been completed:

(1) Creep tests are conducted to collect test data for three ethylene-hexene copolymers, with different failure modes observed. Collecting enough creep data for each failure mode, a StT parametric method, similar to that described in ISO 9080, can be adopted to construct master time-to-failure curves. Master time-to-failure curve for ductile failure should be obtained by pure ductile failure data. Similarly, master time-to-failure curve for brittle failure is generated using pure brittle failure data. The intersection of two master curves is the location where DB transition is expected. The master time-to-failure curves were constructed for the three PE plaques.

(2) In order to investigate the deformation mechanisms for different failure modes, Eyring's Law and Norton Power Law are used to analyze deformation behaviour at the secondary creep stage. With the analyses, activation energy at the secondary creep stage is correlated with

the transition of failure modes. The analysis was based on creep test results from four PE plaques, three being ethylene-hexene copolymers and one homopolymer.

(3) A new short-term test method is developed to detect critical stress for deformation transitions, based on the concept that the stress relaxation behavior can characterize the material state of PE during the tensile deformation. Wide-angle X-ray Scattering (WAXS) is also performed to provide supporting evidence for the short-term test results. The critical stresses for deformation transitions are characterized for both six PE plaques and six PE pipes.

(4) To investigate the possibility of using the new short-term test to characterize DB transition of PE plaque, the critical stresses detected from the short-term test are evaluated with stresses for the DB transition. For PE pipes, the critical stresses are compared with their hydrostatic design basis (HDB) values which were provided by suppliers.

1.4 Thesis organization

The thesis provides a detailed description of the proposed short-term test and deformation transitions under creep test, and demonstrates the correlation between short-term test results with creep test results. The remainder of this thesis is composed of five chapters as follows:

In Chapter 2, creep tests were performed on three ethylene-hexene copolymers to obtain master time-to-failure curves with the help of a StT parametric method. Two deformation transitions, i.e., ductile-ductile (DD) transition and ductile-brittle (DB) transition, are detected through the change in the dependence of failure time on the applied stress. The critical stress for the DB transition is obtained and verified by addition creep test data. This chapter also examines applicability of the Monkman-Grant relationship for PEs that involve DD or DB transition.

Chapter 3 presents a study on the analyses of creep deformation and its correlation with activation energy at the secondary creep stage for three ethylene-hexene copolymers and one homopolymer. Different from the three copolymers, the homopolymer exhibits a third failure behaviour, referred to as low-temperature brittle failure (LTBF). The Norton Power Law (NPL) and the Eyring's Law are used to analyze the creep deformation at the secondary creep stage. The analysis suggests a strong correlation between DB transition and activation energy at the secondary creep stage. The results also suggest that Monkman-Grant relationship is applicable to both ductile and LTBF failures.

Chapter 4 proposes a new short-term multi-relaxation (MR) test to characterize the critical points for deformation transitions based on the concept that stress relaxation behavior can be used to reflect the material state of PE under tension. The first critical point is for the onset of plastic deformation in the crystalline phase and the second critical point for global yielding in the crystalline phase. WAXS is also performed to examine the change of the crystalline phase in PE during deformation. The corresponding quasi-static stresses at two critical points are obtained, which are expected to play a significant role on the long-term, load-carrying applications of PE. Materials used in Chapter 4 are six PE plaques, including four ethylene-hexene copolymers, one ethylene-butene copolymer and one homopolymer.

Chapter 5 provides a quantitative comparison of short-term MR test results and long-term performance for both PE plaques and PE pipes. For PE plaques, critical stress for the DB transition correlates well with the second critical quasi-static stress. For PE pipes, the HDB value which is a material property determined using the LTHS according to ASTM D2837, is found to be close to the first critical quasi-static stress. The good correlations shade a light on the possibility of using short-term MR test to predict the long-term behaviour of PE in load-carrying applications.

Chapter 6 summarizes the main contributions of this work and provides recommendation for the future work.

References

[1] A. Peacock, Handbook of polyethylene: structures, properties, and applications, CRC press, New York, 2000. doi:10.1201/9781482295467.

[2] D. Li, H. Garmestani, S.R. Kalidindi, R. Alamo, Crystallographic texture evolution in high-density polyethylene during uniaxial tension, Polymer (Guildf). 42 (2001) 4903–4913. doi:10.1016/S0032-3861(00)00829-6.

[3] Y. Zhang, P.Y. Ben Jar, Phenomenological modelling of tensile fracture in PE pipe by considering damage evolution, Mater. Des. 77 (2015) 72–82. doi:10.1016/j.matdes.2015.04.011.

[4] Z. Qi, N. Hu, G. Li, D. Zeng, X. Su, Constitutive modeling for the elastic-viscoplastic behavior of high density polyethylene under cyclic loading, Int. J. Plast. 113 (2019) 125–144. doi:10.1016/j.ijplas.2018.09.010.

[5] K.Q. Nguyen, C. Mwiseneza, K. Mohamed, P. Cousin, M. Robert, B. Benmokrane, Long-term testing methods for HDPE pipe-advantages and disadvantages: a review, Eng. Fract. Mech. 246 (2021) 107629. doi:10.1016/j.engfracmech.2021.107629.

[6] N. Kiass, R. Khelif, L. Boulanouar, K. Chaoui, Experimental approach to mechanical property variability through a high-density polyethylene gas pipe wall, J. Appl. Polym. Sci. 97 (2005) 272–281. doi:10.1002/app.21713.

[7] J. Fawaz, S. Deveci, V. Mittal, Molecular and morphological studies to understand slow crack growth (SCG) of polyethylene, Colloid Polym. Sci. 294 (2016) 1269–1280. doi:10.1007/s00396-016-3888-5.

[8] P.Y. Ben Jar, Determining critical stress for ductile-brittle transition of polyethylene pipe under creep loading, Annu. Tech. Conf.-ANTEC, Conf. Proc. 2018-May (2018).

[9] A. Lustiger, R.D. Corneliussen, The role of crazes in the crack growth of polyethylene, J. Mater. Sci. 22 (1987) 2470–2476. doi:10.1007/BF01082132.

[10] P.A. O'Connell, R.A. Duckett, I.M. Ward, Brittle-ductile transitions in polyethylene, Polym. Eng. Sci. 42 (2002) 1493–1508. doi:10.1002/pen.11046.

[11] X. Lu, N. Brown, The transition from ductile to slow crack growth failure in a copolymer of polyethylene, J. Mater. Sci. 25 (1990) 411–416. doi:10.1007/BF00714048.

[12] H.B.H. Hamouda, M. Simoes-betbeder, F. Grillon, P. Blouet, N. Billon, R. Piques, Creep damage mechanisms in polyethylene gas pipes, Polymer (Guildf). 42 (2001) 5425–5437. doi:10.1016/S0032-3861(00)00490-0.

[13] G.C. Derringer, A model for service life of polyethylene pipe exhibiting ductile–brittle transition in failure mode, J. Appl. Polym. Sci. 37 (1989) 215–224. doi:10.1002/app.1989.070370116.

[14] X. Lu, X. Wang, N. Brown, Slow fracture in a homopolymer and copolymer of polyethylene, J. Mater. Sci. 23 (1988) 643–648. doi:10.1007/BF01174699.

[15] R.W. Lang, A. Stern, G. Doerner, Applicability and limitations of current lifetime prediction

models for thermoplastics pipes under internal pressure, Angew. Makromol. Chemie. 247 (1997) 131–145. doi:10.1002/apmc.1997.052470109.

[16] ASTM D2837-13, Standard test method for obtaining hydrostatic design basis for thermoplastic pipe materials or pressure design basis for thermoplastic pipe products, ASTM Int. (2013). doi:10.1520/D2837-13.cable.

[17] R.K. Krishnaswamy, Analysis of ductile and brittle failures from creep rupture testing of high-density polyethylene (HDPE) pipes, Polymer (Guildf). 46 (2005) 11664–11672. doi:10.1016/j.polymer.2005.09.084.

[18] J. Poduška, P. Hutař, J. Kučera, A. Frank, J. Sadílek, G. Pinter, L. Náhlík, Residual stress in polyethylene pipes, Polym. Test. 54 (2016) 288–295. doi:10.1016/j.polymertesting.2016.07.017.

[19] A. Frank, G. Pinter, R.W. Lang, Prediction of the remaining lifetime of polyethylene pipes after up to 30 years in use, Polym. Test. 28 (2009) 737–745. doi:10.1016/j.polymertesting.2009.06.004.

[20] ISO 13479, Polyolefin pipes for the conveyance of fluids-Determination of resistance to crack propagation-Test method for slow crack growth on notched pipes (notch test), Int. Organ. Stand. (2009).

[21] ISO 16770, Plastics-Determination of the environmental stress cracking (ESC) of polyethylene-Full-notch creep test (FNCT), Int. Organ. Stand. (2004).

[22] ISO 16421, Notch tensile test to measure the resistance to slow crack growth of

polyethylene materials for pipe and fitting products (PENT), Int. Organ. Stand. (2015).

[23] G. Pinter, M. Haager, W. Balika, R.W. Lang, Cyclic crack growth tests with CRB specimens for the evaluation of the long-term performance of PE pipe grades, Polym. Test. 26 (2007) 180–188. doi:10.1016/j.polymertesting.2006.09.010.

[24] P. Y. Ben Jar, Transition of neck appearance in polyethylene and effect of the associated strain rate on the damage generation, Polym. Eng. Sci. 54 (2014) 1871–1878. doi:10.1002/pen.23735.

[25] A.L. Ward, X. Lu, Y. Huang, N. Brown, The mechanism of slow crack growth in polyethylene by an environmental stress cracking agent, Polymer (Guildf). 32 (1991) 2172–2178. doi:10.1016/0032-3861(91)90043-I.

[26] J. Cazenave, R. Seguela, B. Sixou, Y. Germain, Short-term mechanical and structural approaches for the evaluation of polyethylene stress crack resistance, Polymer (Guildf). 47 (2006) 3904–3914. doi:10.1016/j.polymer.2006.03.094.

[27] A. Lustiger, R.D. Corneliusen, The effect of an environmental stress cracking agent on interlamellar links in polyethylene, J. Polym. Sci. Part B Polym. Phys. 24 (1986) 1625–1629. doi:10.1002/polb.1986.090240719.

[28] Y. Chen, X. Nie, S. Zhou, H. Zou, M. Liang, P. Liu, Investigations of environmental stress cracking resistance of HDPE/UHMWPE and LDPE/UHMWPE blends, J. Polym. Res. 20 (2013) 1-7. doi:10.1007/s10965-013-0141-5.

[29] J.M. Lagarón, G. Capaccio, L.J. Rose, K.J. Bert, Craze morphology and molecular

orientation in the slow crack growth failure of polyethylene, J. Appl. Polym. Sci. 77 (2000) 283–296. doi:10.1002/(SICI)1097-4628(20000711)77:2<283::AID-APP5>3.0.CO;2-0.

[30] R. Hiss, S. Hobeika, C. Lynn, G. Strobl, Network stretching, slip processes, and fragmentation of crystallites during uniaxial drawing of polyethylene and related copolymers. A comparative study, Macromolecules. 32 (1999) 4390–4403. doi:10.1021/ma981776b.

[31] L. Farge, J. Boisse, J. Dillet, S. André, P.A. Albouy, F. Meneau, Wide-angle X-ray scattering study of the lamellar/fibrillar transition for a semi-crystalline polymer deformed in tension in relation with the evolution of volume strain, J. Polym. Sci. Part B Polym. Phys. 53 (2015) 1470–1480. doi:10.1002/polb.23790.

[32] M.F. Butler, A.M. Donald, W. Bras, G.R. Mant, G.E. Derbyshire, A.J. Ryan, A real-time simultaneous small- and wide-angle X-ray scattering study of in-situ deformation of isotropic polyethylene, Macromolecules. 28 (1995) 6383–6393. doi:10.1021/ma00123a001.

[33] R. Hiss, S. Hobeika, C. Lynn, G. Strobl, General scheme derived from video-controlled stretching tests and WAXS for describing tensile deformations of polyethylenes, J. Macromol. Sci. Part B. 38 (1999) 37–41. doi:10.1080/00222349908248143.

[34] D.J. Louse, R.J. Gaylord, The amorphous contribution to the modulus of a semi-crystalline polymer, Polym. Eng. Sci. 18 (1978) 512–517. doi:10.1002/pen.760180614.

[35] Z. Bartczak, A. Galeski, Plasticity of semicrystalline polymers, Macromol. Symp. 294 (2010) 67–90. doi:10.1002/masy.201050807.

[36] Q. Fu, Y. Men, G. Strobl, Understanding of the tensile deformation in HDPE/LDPE blends based on their crystal structure and phase morphology, Polymer (Guildf). 44 (2003) 1927–1933. doi:10.1016/S0032-3861(02)00940-0.

[37] K. Hong, A. Rastogi, G. Strobl, A model treating tensile deformation of semicrystalline polymers: quasi-static stress-strain relationship and viscous stress determined for a sample of polyethylene, Macromolecules. 37 (2004) 10165–10173. doi:10.1021/ma049174h.

[38] Y. Men, G. Strobl, Critical strains in poly(ε-caprolactone) and blends with poly(vinyl methyl ether) and poly(styrene-co-acrylonitrile), Macromolecules. 36 (2003) 1889–1898. doi:10.1021/ma025955b.

[39] ISO 9080, Plastics piping and ducting systems—Determination of the long-term hydrostatic strength of thermoplastics materials in pipe form by extrapolation, Int. Organ. Stand. (2012). doi:10.31030/1908468.

[40] A. Frank, G. Pinter, Lifetime prediction of polyethylene pipes based on an accelerated extrapolation concept for creep crack growth with fatigue tests on cracked round bar specimens, in: Antec, Chicago, 2009: pp. 2169–2174. doi:10.13140/RG.2.1.3718.1845.

[41] P. Hutař, M. Ševčík, L. Náhlík, G. Pinter, A. Frank, I. Mitev, A numerical methodology for lifetime estimation of HDPE pressure pipes, Eng. Fract. Mech. 78 (2011) 3049–3058. doi:10.1016/j.engfracmech.2011.09.001.

[42] C. Tischler, T.R. Kratochvilla, H. Muschik, H. Dragaun, Notched ring test for measuring slow cracking resistance in plastics pipes and fittings, Macromol. Symp. 296 (2010) 626–631. doi:10.1002/masy.201051082.

[43] E. Nezbedová, G. Pinter, A. Frank, P. Hutař, J. Poduška, J. Hodan, Accelerated tests for lifetime prediction of PE-HD pipe grades, Macromol. Symp. 373 (2017) 1–8. doi:10.1002/masy.201600096.

[44] N. Brown, J. Donofrio, X. Lu, The transition between ductile and slow-crack-growth failure in polyethylene, Polymer (Guildf). 28 (1987) 1326–1330. doi:10.1016/0032-3861(87)90446-0.

[45] X. Lu, N. Brown, Effect of thermal history on the initiation of slow crack growth in linear polyethylene, Polymer (Guildf). 28 (1987) 1505–1511. doi:10.1016/0032-3861(87)90350-8.

[46] J.L. Cooney, Effect of morphology on biaxial stress rupture of polyethylene, J. Appl. Polym. Sci. 8 (1964) 1889–1901. doi:10.1002/app.1964.070080435.

[47] X. Lu, N. Brown, A test for slow crack growth failure in polyethylene under a constant load, Polym. Test. 11 (1992) 309–319. doi:10.1016/0142-9418(92)90025-7.

[48] E. Nezbedová, P. Hutař, M. Zouhar, Z. Knésl, J. Sadílek, L. Náhlík, The applicability of the Pennsylvania Notch Test for a new generation of PE pipe grades, Polym. Test. 32 (2013) 106–114. doi:10.1016/j.polymertesting.2012.09.009.

[49] M. Schilling, U. Niebergall, M. Böhning, Full notch creep test (FNCT) of PE-HD–Characterization and differentiation of brittle and ductile fracture behavior during environmental stress cracking (ESC), Polym. Test. 64 (2017) 156–166. doi:10.1016/j.polymertesting.2017.09.043.

[50] A. Adib, C. Domínguez, R.A. García, M.A. Garrido, J. Rodríguez, Influence of specimen geometry on the slow crack growth testing of HDPE for pipe applications, Polym. Test. 48 (2015) 104–110. doi:10.1016/j.polymertesting.2015.09.012.

[51] S.H. Beech, E.Q. Clutton, Interpretation of results of full notch creep test and comparison with notched pipe test, Plast. Rubber Compos. 34 (2005) 294–300. doi:10.1179/174328905X59791.

[52] A. Frank, W. Freimann, G. Pinter, R.W. Lang, A fracture mechanics concept for the accelerated characterization of creep crack growth in PE-HD pipe grades, Eng. Fract. Mech. 76 (2009) 2780–2787. doi:10.1016/j.engfracmech.2009.06.009.

[53] S. Choi, S. Pyo, Y.S. Suh, Y. Seo, Development of notched ring test for measuring slow cracking resistance in plastics pipes and fittings, Plast. Rubber Compos. 36 (2007) 219–225. doi:10.1179/174328907x191314.

[54] Y. Zhao, B.H. Choi, A. Chudnovsky, Characterization of the fatigue crack behavior of pipe grade polyethylene using circular notched specimens, Int. J. Fatigue. 51 (2013) 26–35. doi:10.1016/j.ijfatigue.2013.01.016.

[55] G. Pinter, M. Haager, W. Balika, R.W. Lang, Fatigue crack growth in PE-HD pipe grades, Plast. Rubber Compos. 34 (2005) 25–33. doi:10.1179/174328905X29758.

[56] E. Nezbedová, A. Zahradnickova, Z. Salajka, Brittle failure versus structure of HDPE pipe resins, J. Macromol. Sci. Part B. 40 (2001) 507–515. doi:10.1081/MB-100106173.

[57] J.M. Crissman, On the long time creep and lifetime behavior in uniaxial extension of a linear

low density polyethylene, Polym. Eng. Sci. 31 (1991) 541–547. doi:10.1002/pen.760310802.

[58] J.M. Crissman, L.J. Zapas, Creep failure and fracture of polyethylene in uniaxial extension, Polym. Eng. Sci. 19 (1979) 99–103. doi:10.1002/pen.760190208.

[59] H.F. Enderle, Encyclopedia of materials, Science and Technology, Amsterdam, the Netherlands: Elsevier (2001).

[60] R.H. Carey, Creep and stress-rupture behavior of polyethylene resins, Ind. Eng. Chem. 50 (2005) 1045–1048. doi:10.1021/ie50583a040.

[61] R.K. Krishnaswamy, Influence of wall thickness on the creep rupture performance of polyethylene pipe, Polym. Eng. Sci. 47 (2007) 516–521. doi:10.1002/pen.20729.

Chapter 2 Deformation transitions of ethylene-hexene copolymers under creep Loading

In this chapter, creep tests were conducted in the temperature range from 296 to 358 K, on three commercial ethylene-hexene copolymers (PE) with mass density of 0.938, 0.941 and 0.952 g/cc. PE with the highest density shows the well-known ductile-brittle (DB) transition in the relationship between applied stress and failure time, and PE with the medium density a different transition which was detected through the change in the dependence of failure time on the applied stress, but the failure mode remained ductile. Therefore, this transition is named ductile-ductile (DD). The work shows feasibility of establishing creep master curves to include the two transitions, and discusses exclusiveness between DD and DB transitions so that detection of the DD transition can be used to determine the likelihood of the DB transition to occur in the long-term service. The work also examines applicability of the Monkman-Grant relationship to PEs that involve DD or DB transition.

2.1 Introduction

Polyethylene (PE) has long been an attractive material candidate for load-carrying applications because of its light weight, strong corrosion resistance and excellent ductility[1-3]. Such advantages, however, have been hampered by the possibility of a ductile-brittle (DB) transition that is known to cause a sharp decrease of the material performance. Because of the impact of DB transition on PE's long-term performance, standard short-term tests for some applications have required the consideration of DB transition to determine the maximum service life. For plastic gas pipe, for example, the standard test needs more than 13 months to complete [4] in order to cover the service life of 50 years, but this standard test is yet to be able to determine time and stress level for the DB transition. As a result, great efforts have been made by various groups to develop short-term tests that can be completed in a period much shorter than 13 months, and provide accurate measurement on time and stress level for the DB transition [5-8].

Many test methods proposed to detect the DB transition in PE are based on the creep loading [9]. As illustrated in Fig. 2.1 which is commonly used to describe creep failure in PE pipe, failure in region I is for creep failure under a relatively high stress level. Failure in this region is ductile, due to extensive plastic deformation before the final fracture. By decreasing the stress below a critical level, failure occurs in region II, also known as slow crack growth (SCG) [10], which is to generate brittle failure from a single crack with little plastic deformation at the macroscopic scale. Intersection between two lines in Fig. 2.1 which represent regions I and II, respectively, is the critical point for the DB transition, also known as the "knee" point in the plastic pipe industry. Further decrease of the stress level from region II is to enter region III which is also for brittle failure, but with a large scale of multiple cracks. Failure in region III is often caused by

chemical aging or polymer degradation, and time for its failure is nearly independent of the applied stress level [11].

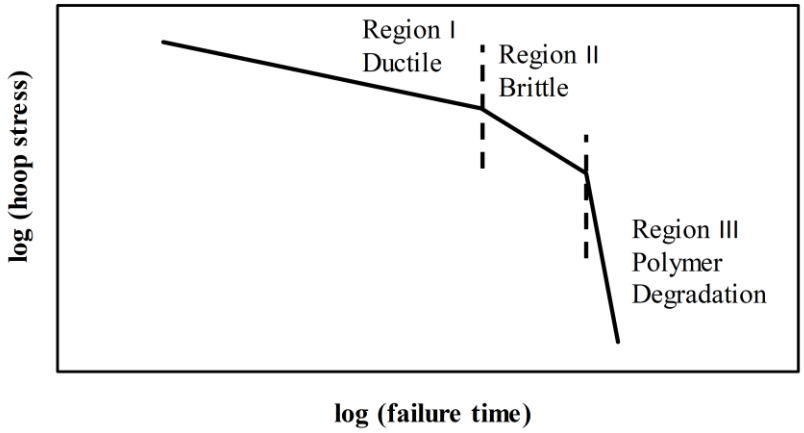

Fig. 2.1 Schematic plot of applied hoop stress versus failure time for PE pipes.

Majority of short-term coupon tests developed to predict long-term performance of PE use specimens with pre-notches in order to encourage SCG development from the notch tip [12-15]. Results from such tests can detect the DB transition using a relatively short test period. But due to crack growth from a sharp notch, the results cannot quantify the critical stress level for the DB transition or time for its occurrence in the load-carrying applications.

Among studies for developing coupon tests to characterize the long-term performance of PE, extensive works were carried out by Brown and his co-workers. Work in Ref. [16] shows that ductile failure can be easily generated in all types of coupon specimens of PE under creep loading at 30°C, but brittle failure at the same temperature requires the use of notched specimens with specific dimensions. The study also used notch opening displacement to determine crack growth speed for brittle failure. By expressing time for the ductile failure as a power law function of

applied stress, Brown and his co-workers showed that critical condition for the DB transition has a qualitative agreement with results from the hydrostatic pressure tests on notch-free pipe sections. They used notched-coupon specimens to investigate the effects of molecular side chains [17], crack tip blunting [18], environmental stress cracking agent [19] and thermal history [20] on the long-term performance of PE. The results provided a database for the development of an accelerating test method, known as Pennsylvania Edge-Notched Tensile (PENT) test [21], to evaluate SCG resistance of PE pipes. The PENT test is now an international standard for characterizing SCG resistance of PE pipes and their resins [22], though some researchers [9, 23-24] are still concerned about validity of the PENT test for quantitative evaluation of SCG resistance of the pipe grade PE.

Other research groups have proposed other than creep loading to characterize DB transition of PE. For example, Frank and Pinter [25] used cyclic fatigue test and simulation tools on cracked round bar (CRB) specimens to predict failure time and DB transition of PE. The CRB test is based on linear elastic fracture mechanics, using stress intensity factor to characterize the crack growth kinetics. However, main concerns are that conditions used to generate the DB transition in this type of tests show a strong dependence on the initial notch size, and that the use of a notch has limited the test to measurement of crack growth time, not crack initiation time.

Other tests proposed based on the similar approach are also to provide a qualitative comparison among PEs for their long-term performance [26-29]. None of them could quantify the critical condition for the DB transition. Furthermore, studies have indicated that results from the notched specimens can be inconsistent with results from notch-free specimens. For example, Krishnaswamy [9] compared results from PENT test for two HDPEs with results from the hydrostatic pressure test on their pipe sections. The comparison indicated that resistance to SCG

failure from the two types of tests are contradictory to each other. In another study, Adib et al. [30] showed that PENT test and circumferentially deep notched tensile (CDNT) test can lead to different ranking among PE pipes of the same group. Such inconsistency provides uncertainties on the validity of these test methods, which need to be resolved before these tests could be considered for characterizing the long-term performance of PE products.

In view of the above shortcomings for the use of notched specimens, we decide to use notch-free specimens for the study. Work presented here is about results collected from creep tests at room and elevated temperatures, and analyzed based on a stress-time-temperature (StT) parametric method that is similar to the method introduced in ISO 9080 [4]. The StT method is to construct master curves of creep stress versus time-to-failure in order to explore the possibility of detecting the DB transition. The work also reports another failure transition that does not cause any change in the ductile failure behaviour, and examines the use of the Monkman-Grant relationship to predict the creep failure time when the two failure transitions are involved.

2.2 Experiments

2.2.1 Materials and specimens

Plaques of three commercial ethylene-hexene copolymers were used in this study, all from ExxonMobil Chemical provided by Imperial Oil. Commercial names of the PEs and their basic properties are given in Tab. 2.1. For convenience, the three PEs are referred to as #1 LLDPE, #2 HDPE and #3 HDPE, respectively. Rectangular PE plaques with nominal thickness of 3 mm and dimensions of 17.5 × 17.5 cm^2 were compression-molded according to the conditions specified in ASTM D4703 [31]. A pre-determined quantity of polymer beads was placed into a metal “picture frame” mold, heated to 177 ºC in a platen press, and subjected to 10 MPa for 10 minutes before

being cooled down at a rate of 15 ºC/min. All plaques of 3 PEs were prepared using the same process. Specimens of a modified dog-bone geometry, as shown in Fig. 2.2, were prepared from PE plaques using a milling machine with a single point cutter which has been sharpened and used only for cutting polyethylene specimens. No evidence for melting or any other kind of machining damage could be found for specimen surfaces using this milling process.

Tab. 2.1 Material characteristics of PEs used in the study.

Material	Commercial name	Density (g/cc)	Yield strength (MPa)	Crystallinity (%)	Melt index (g/10 min) at 190 ºC/2.16 Kg	Peak melting temperature (ºC)
#1 LLDPE	LL 8460.29	0.938	17	63	3.3	126
#2 HDPE	HD 8660.29	0.941	19	64	2.0	129
#3 HDPE	HD 6706.17	0.952	26	71	6.7	132

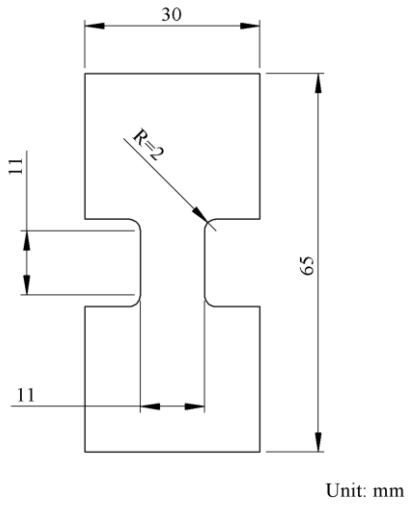

Fig. 2.2 Geometry and dimensions of the modified dog-bone specimens.

2.2.2 Creep test

Creep tests were conducted using a universal test machine (Qualitest Quasar 100), with a personal computer to control the test program and data acquisition. The two ends of each specimen were clamped in home-made fixtures. Each specimen was centered with respect to the fixtures and aligned to the loading direction. Also, the clamping edge is at a distance of 11 mm from the end of the gauge section, to avoid stress concentration in the gauge section, introduced by the teeth along the clamping edges. Load was applied to the specimen within 30 seconds. In view that total number of creep tests could be large, levels of the applied stress were chosen to ensure that each test could be completed within 10 days, but results for failure time less than 4 hours were discarded as the time was deemed to be too short to be considered as creep. In this study, stroke was used to quantify the deformation under the creep loading. For specimens failing in a ductile manner, 20 mm was selected to be the maximum stroke before the test was terminated, so that the deformation could be well into the tertiary creep stage. This allows proper determination of the creep failure time under ductile deformation, as to be shown in Section 2.3.1.

Two batches of creep tests were conducted in this study. The first batch is to establish the database for constructing master curves for creep deformation, which includes results obtained at temperatures of 296, 315, 333, 353 and 358 K. The second batch is to verify the trend lines generated from the first batch and includes results obtained at temperatures of 343, 353 and 358 K for ductile and brittle failures of #3 HDPE and 323 K for transition of ductile failure in #2 HDPE. Total number of specimens used in this study was 20 for #1 LLDPE, 23 for #2 HDPE, and 32 for #3 HDPE. Note that temperatures reported here are based on the readout from a thermocouple that was placed close to the specimen gauge section, with the variation of ±1 K. For creep tests at

elevated temperatures, the specimens were subjected to a preheating period of 2 hours at zero load, to ensure that the specimens had reached the thermal equilibrium state before the load was applied.

2.2.3 Scanning electron microscopy (SEM)

Surfaces generated from brittle failure were examined using a Zeiss Sigma field emission scanning electron microscope (SEM), focusing on the surface topography at the crack initiation sites. The specimens were not coated with any conductive layer. Rather, the SEM chamber was back-filled with nitrogen gas to minimize the surface charging, and a backscattering detector was used to collect the signals.

2.3 Results

2.3.1 Creep test

Fig. 2.3 presents typical post-test specimens with ductile failure. All ductile failures involve extensive plastic deformation and necking. The figure indicates that necks in #1 LLDPE and #2 HDPE are slightly more translucent than that in #3 HDPE. Variation in the neck translucency was also reported by Pae and Bhateja [32] and Jar [33], and is believed to be caused by the difference of cavity content generated in the neck-forming process.

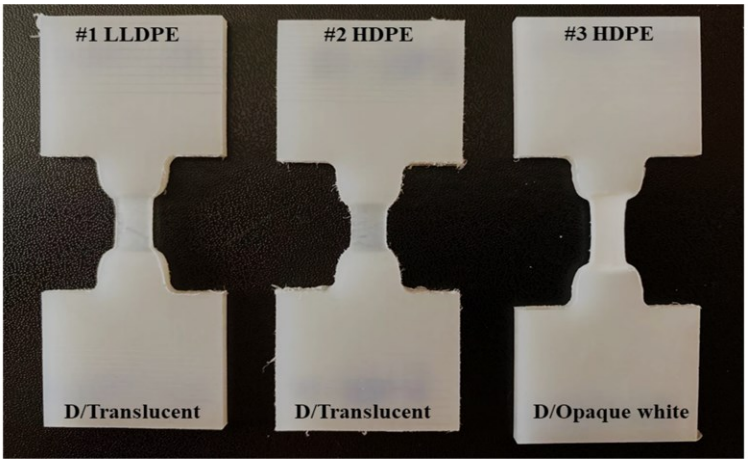

Fig. 2.3 Sample specimens in ductile failure.

As shown in Fig. 2.4, all brittle failures were observed from #3 HDPE which were generated by testing at or above 333 K. Most of the brittle failures were initiated in regions close to one end of the gauge section, as shown by the very left specimen in Fig. 2.4. Fracture at such a location was possibly caused by stress concentration in that region, due to change of the specimen width. Two of #3 HDPE specimens had brittle failure initiated away from the end of the gauge section, as depicted by the middle specimen in Fig. 2.4. Failure time for these two specimens turned out to be much shorter than the trend line generated by the other specimens tested at the same temperature. Therefore, fracture initiated away from the end of the gauge section is possibly due to the presence of defects in the gauge section, and the results were then excluded from the analysis. The specimen on the right of Fig. 2.4 shows a combination of brittle failure initiation from both sides of the gauge width and ductile stretch of the remaining ligament. This type of failure behaviour occurred only in two #3 HDPE specimens tested at 333 K.

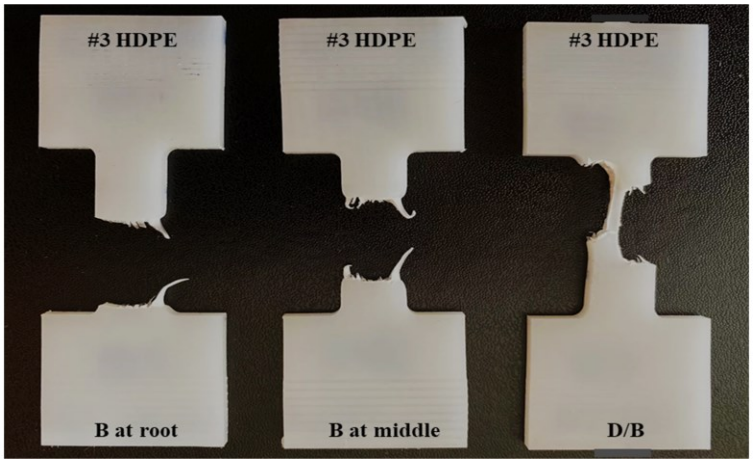

Fig. 2.4 Sample of specimens for #3 HDPE that fractured in a brittle manner (left and centre) and in a mix of brittle initiation and ductile stretch (right).

Fig. 2.5 summarizes typical curve profiles generated from the creep tests. The curves in Fig. 2.5 were selected from #3 HDPE as this is the only PE that showed both ductile failure and brittle failure, but its curve profiles for ductile failure also represent the curve profiles for the other two PEs used in the study. Each of these curves in Fig. 2.5 contains three characteristic creep stages, i.e., the primary stage that corresponds to a rapid stroke increase, but at a decreasing rate, the secondary stage that shows virtually a constant stroke rate, and the tertiary stage at which the stroke increment accelerates till the end of the test. All curves in (a) and (b) of Fig. 2.5 and the left four curves in (c) are typical for ductile failure, and all curves in (d) and (e) for brittle failure. The right two curves in (c), marked "mixed behaviour," are from specimens with a mixed mode of brittle initiation and ductile stretch, as depicted by the specimen on the right of Fig. 2.4 which as mentioned earlier, occurred only in #3 HDPE. Since the mixed behaviour is an indication that the testing condition was close to the DB transition, results from these two specimens were put in the data set for the validation of the master curves, not for the construction of the master curves.

Number next to each curve in Fig. 2.5 denotes the applied stress used for the testing. Point for ductile failure or brittle failure is defined by the intersection of two trend lines, one for the secondary creep stage and the other for the tertiary creep stage, as demonstrated by one curve in Fig. 2.5(a) and one in 2.5(e), for ductile and brittle failures, respectively. Fig. 2.5 suggests that regardless of ductile or brittle failures, all curves have similar profiles. The main difference is that the curves for ductile failure have a relatively smooth transition from the secondary to the tertiary creep stages, and those for brittle failure have a relatively sharp transition. Note that time for the ductile failure is essentially the time for the onset of necking [34].

Fig. 2.6 presents double logarithmic plots of applied stress versus time for ductile failure (open symbol) and brittle failure (solid symbol) from the first batch of creep tests. As shown in the figure, the data can be fitted quite well by linear regression, with the correlation coefficient greater than 0.95. However, in contrast to that reported by Lu and Brown [8], the fitting lines in Fig. 2.6 are not always parallel to each other. Rather, the lines become increasingly flat with the increase of the test temperature.

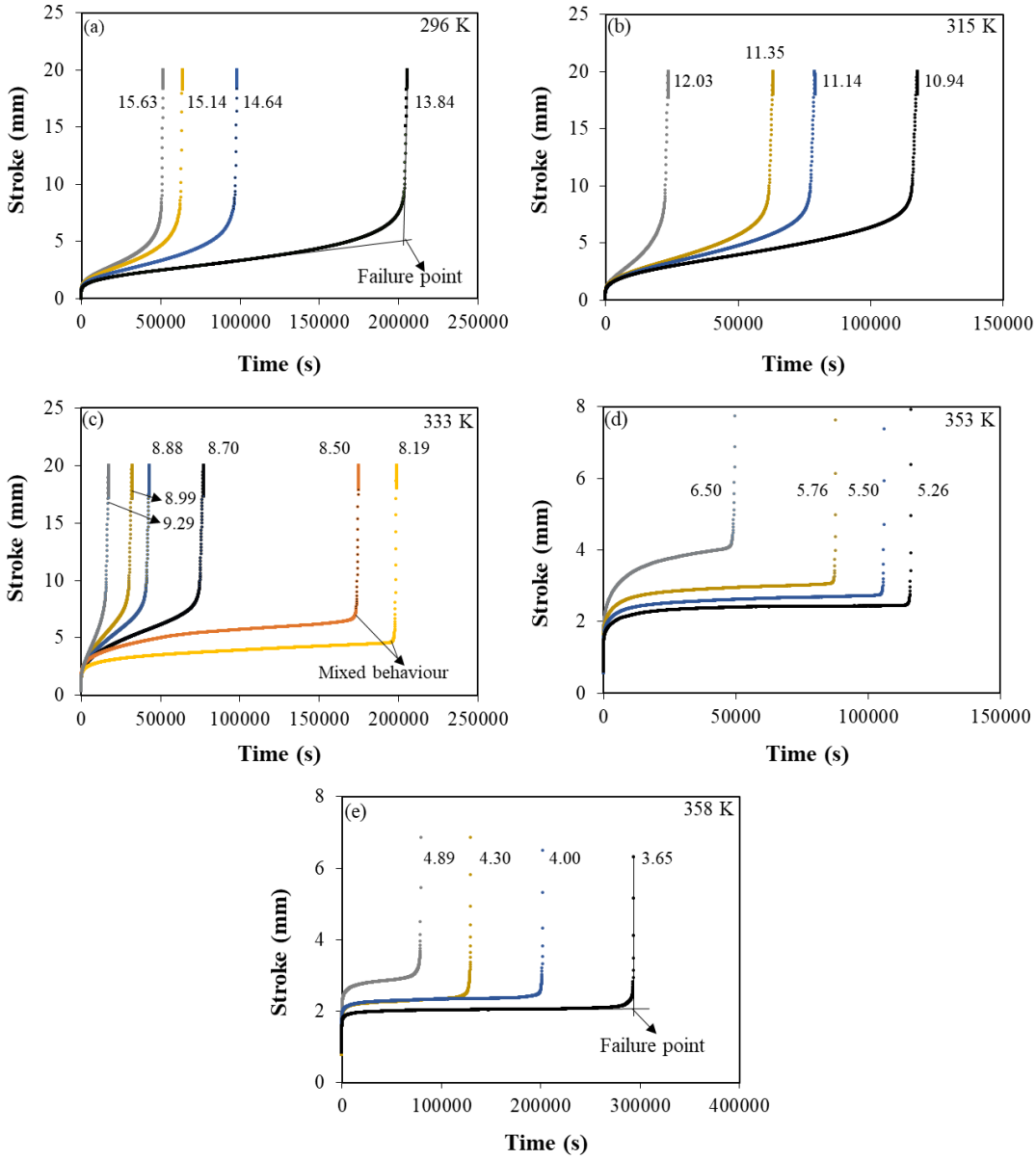

Fig. 2.5 Typical creep curves at different applied stresses and temperatures (selected from #3 HDPE).

The StT parametric method with four fitting parameters (A, B, C and D), as expressed in Eq. (2.1) below, is used to correlate the applied stress (σ), time for ductile or brittle failures (t) and temperature (T) for the creep tests. As mentioned earlier, Eq. (2.1) is similar to that given in ISO 9080 [4], except that in ISO 9080, log t is expressed in terms of a function of log σ and $1/T$.

$$\log(\sigma) = \left[A + \frac{B}{T}\right] + \left[C + \frac{D}{T}\right]\log(t) \tag{2.1}$$

Values for A, B, C and D in Eq. (2.1) were determined by plotting intercept and slope values for the fitting lines in Fig. 2.6 as functions of $1/T$, as shown in Fig. 2.7 in which the trend lines for the intercept values, Fig. 2.7(a), are used to determine A and B, and the trend lines for the slope values, Fig. 2.7(b), to determine C and D. For clarity, these A, B, C and D values are summarized in Tab. 2.2.

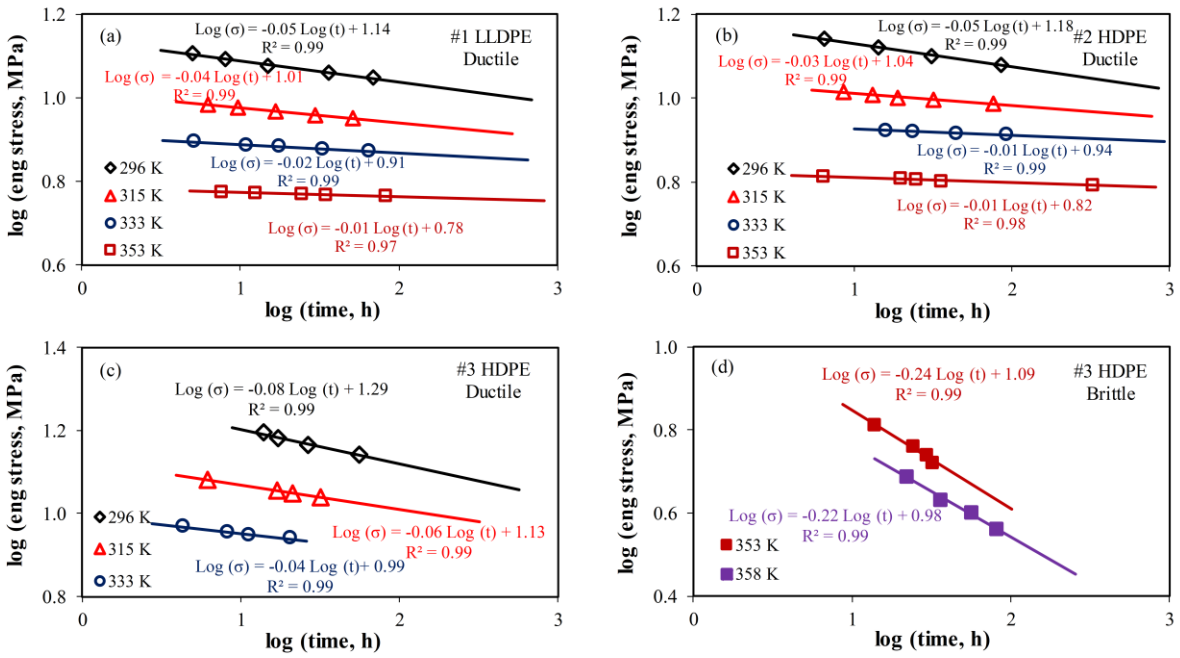

Fig. 2.6 Plots of applied stress versus time for ductile or brittle failures at different temperatures: (a) #1 LLDPE-ductile, (b) #2 HDPE-ductile, (c) #3 HDPE-ductile and (d) #3 HDPE-brittle.

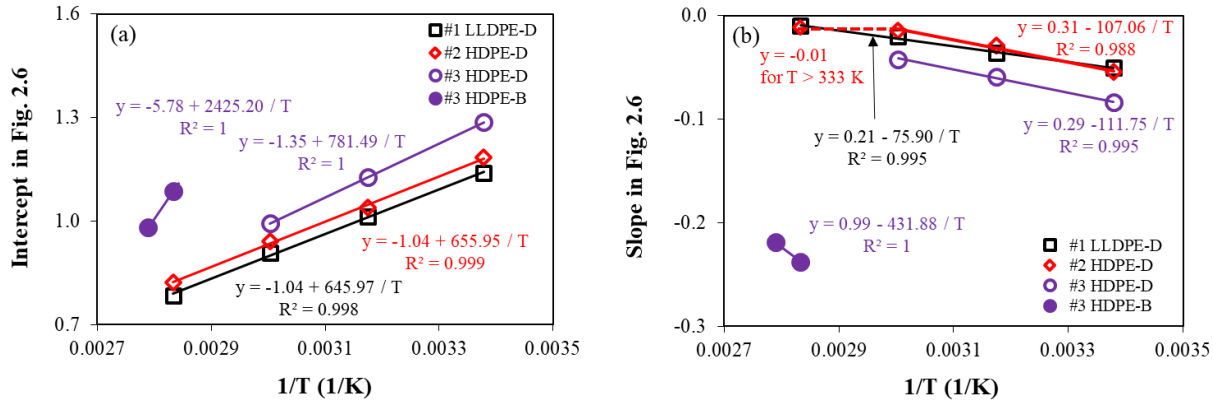

Fig. 2.7 Summary of intercepts (a) and slopes (b) used for the fitting functions in Fig. 2.6, plotted as a function of $1/T$ ('D' and 'B' in the legends indicate ductile and brittle failures, respectively).

Note that each of the two figures in Fig. 2.7 contains two trend lines for #3 HDPE, one for temperatures up to 333 K and the other from 353 to 358 K. The corresponding sets of A, B, C and D values in Tab. 2.2 are referred to as 'Ductile' and 'Brittle', respectively. For #2 HDPE, there is only one trend line in Fig. 2.7(a), but two in Fig. 2.7(b). One of the trend lines in Fig. 2.7(b) (in solid line) is for temperatures up to 333 K, and the other (in dashed line) from 333 to 353 K. Since all failures for #2 HDPE are ductile, the corresponding two sets of A, B, C and D values in Tab. 2.2 are referred to as 'Ductile-Low temp' and 'Ductile-High temp', respectively. Also, since the change of the trend lines for the slope of #2 HDPE does not affect the creep failure behaviour, the change is referred to as a ductile-ductile (DD) transition. For #1 LLDPE, neither slope nor intercept in the temperature range showed any change in the trend lines, and thus only one set of values are listed in Tab. 2.2.

Tab. 2.2 Values for parameters *A*, *B*, *C* and *D* in Eq. (2.1).

Material	A	B	C	D
#1 LLDPE-Ductile	-1.04	645.97	0.21	-75.90
#2 HDPE-Ductile-Low temp	-1.04	655.95	0.31	-107.06
#2 HDPE-Ductile-High temp	-1.04	655.95	-0.01	0
#3 HDPE-Ductile	-1.35	781.49	0.29	-111.75
#3 HDPE-Brittle	-5.78	2425.20	0.99	-431.88

Based on values listed in Tab. 2.2, master curves for creep deformation could be constructed using Eq. (2.1), which for #3 HDPE should include both ductile and brittle failures, but for #1 LLDPE and #2 HDPE only ductile failure as these two PEs did not show any brittle failure in the experimental testing. Fig. 2.8 presents the master curves at temperatures used for the testing, with symbols in the figure representing values determined experimentally which are identical to those presented in Fig. 2.6. Note that since these master curves do not consider the possibility of aging or environmental degradation during the long-term loading, their use for the performance evaluation is limited to the conditions that do not involve any aging- or degradation-related change in the mechanical properties [7]. Furthermore, since slope values for #2 HDPE at 333 and 353 K are very close to each other, as shown in Fig. 2.7(b), the corresponding master curves in Fig. 2.8(b) at these temperatures differ mainly by a vertical shift that is equivalent to the difference of the intercept values between these two temperatures. Also, because the DD transition was detected only through the trend line change of slope versus temperature, as shown in Fig. 2.7(b), none of the master curves for #2 HDPE show any change in the trend line to indicate the

DD transition at that temperature. This issue will later be discussed with additional test data, to depict the effect of DD transition on the creep test results at a given temperature.

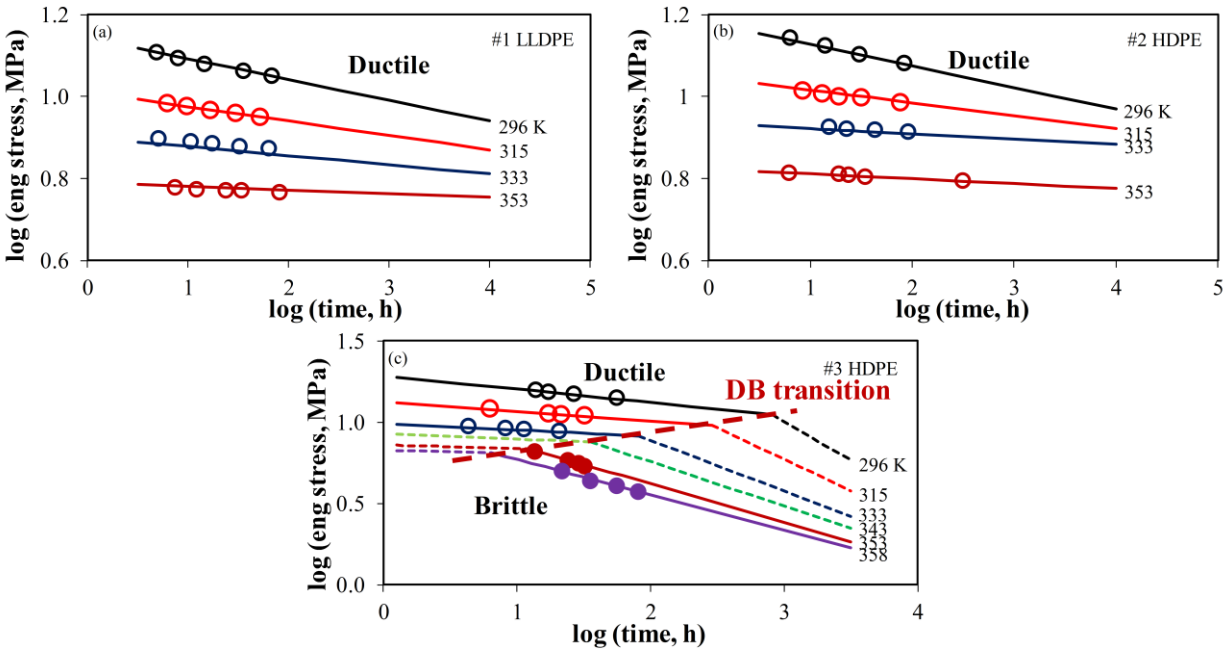

Fig. 2.8 Sample master curves generated based on Eq. (2.1): (a) #1 LLDPE, (b) #2 HDPE and (c) #3 HDPE.

For #3 HDPE, trend lines for ductile and brittle failures at each temperature, as shown in Fig. 2.8(c), can be generated using the corresponding sets of A, B, C, and D values listed in Tab. 2.2, based on the form of Eq. (2.1). Fig. 2.8(c) presents the two sets of trend lines for #3 HDPE at each temperature used for the testing, and the corresponding intersection points are connected using a dashed line which is marked as 'DB transition' in the figure. Note that each master curve in Fig. 2.8(c) consists of one solid line and one dashed line. The solid line contains symbols that represent the experimental measurements, but the dashed line does not. In addition, Fig. 2.8(c) includes a master curve at 343 K which does not contain any experimental measurement. This curve is included in the figure because based on Eq. (2.1), DB transition at this temperature should

occur in a test period between 10 and 100 hours which is suitable for the experimental testing, and thus the data can be collected to verify the validity of the predicted master curve. As mentioned in Section 2.2.2, this part of experiment has been included in the second batch of creep tests. The results will be presented in Section 2.4.1.

2.3.2 Fractographic analysis

Fig. 2.9 presents typical SEM micrographs for #3 HDPE, on the initiation site of the brittle failure surface. All micrographs are from specimens that fractured close to the end of the gauge section. The micrographs on the right-hand side in Fig. 2.9 are the enlarged views of the boxed regions on the left. These micrographs suggest that fracture was initiated from the surface along the thickness of the cross section. The enlarged views also suggest that in spite of little plastic deformation from the naked eyes, micro-scaled plastic deformation still exists on the fracture initiation site. This is consistent with that reported previously using notched specimens of pipe grade PE under fatigue loading [24], and no differences can be identified among surfaces formed in #3 HDPE specimens by the brittle failure.

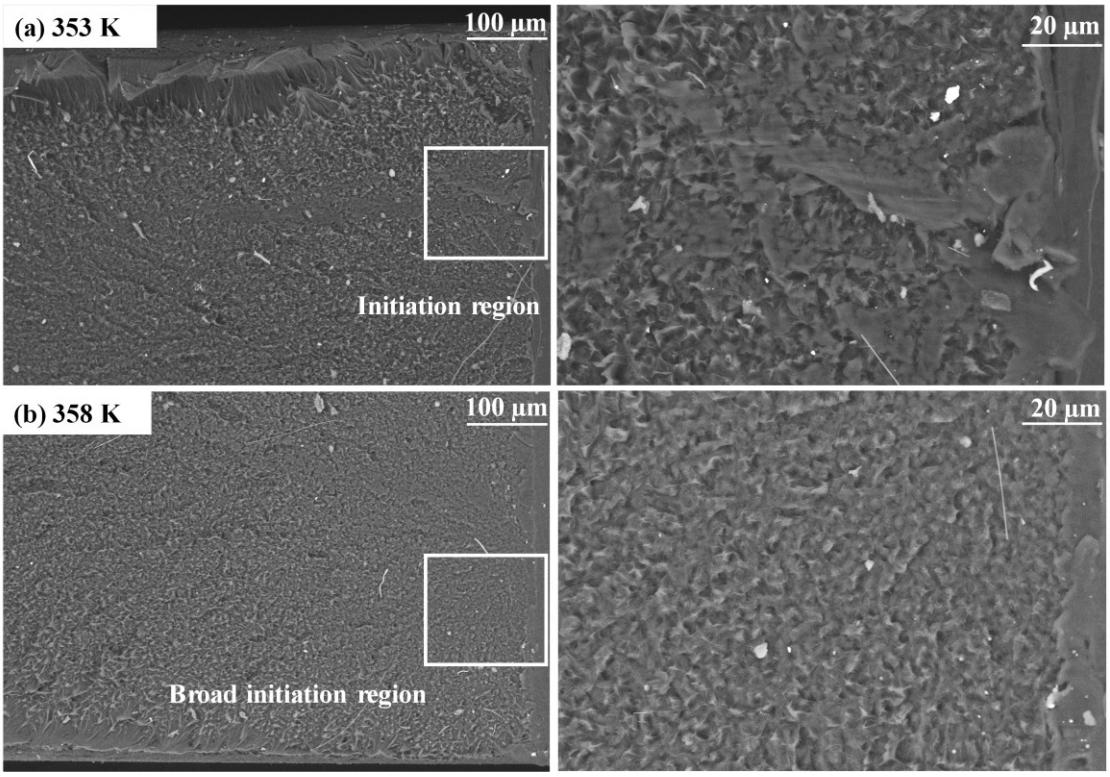

Fig. 2.9 SEM micrographs of selected brittle failure surfaces for #3 HDPE: (a) 353 K and (b) 358 K.

2.4 Discussions

2.4.1 Deformation transition under creep loading

Two types of deformation transitions, DB and DD, have been detected from the study. The DB transition was detected in #3 HDPE through the increase of test temperatures. However, none of the master curves in Fig. 2.8(c), established using Eq. (2.1), contains experimental data for both ductile and brittle failures. Therefore, a second batch of creep tests were conducted on #3 HDPE so that some of the master curves have experimental data for both ductile and brittle failures.

Results from these additional creep tests at 343, 353 and 358 K are summarized in Fig. 2.10 using square symbols, solid for brittle failure and open for ductile failure. The trend lines in Fig. 2.10 are identical to those shown in Fig. 2.8(c), i.e., solid lines containing experimental data from the first batch of creep tests and dashed lines not. In addition to the experimental data from the second batch of creep tests, Fig. 2.10 includes two data points at 333 K that are from the first batch of creep tests, for specimens showing a mixed mode of brittle initiation and ductile stretch, as depicted by the right specimen in Fig. 2.4. Overall, Fig. 2.10 indicates clearly that the experimental data show a fairly good agreement with the trend lines generated from Eq. (2.1), and thus support the validity of using the StT parametric method to construct a master curve that includes both ductile and brittle failures under the creep loading.

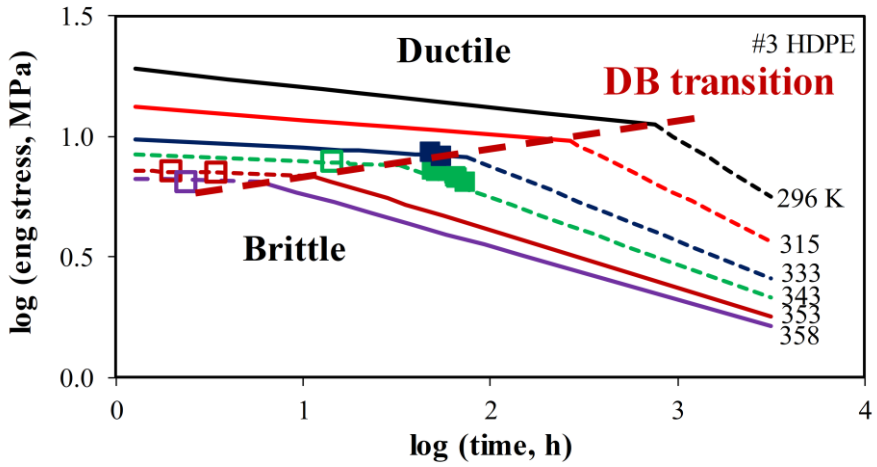

Fig. 2.10 Data from the second batch of creep tests on #3 HDPE (squares), with the line plots identical to those shown in Fig. 2.8(c).

Fig. 2.10 also suggests that critical stress for the DB transition decreases significantly with the increase of test temperature, from 11.1 MPa at 296 K to 6.5 MPa at 358 K. The critical time

for the DB transition also decreases with the increase of test temperature, from about 800 hours at 296 K to about 6 hours at 358 K.

Although the DB transition has been well recognized for PE under creep loading, the DD transition is not. In this study, the DD transition is detected from the change of the trend line for #2 HDPE, as indicated in Fig. 2.7(b). Occurrence of the DD transition has avoided the slope value to become positive. Otherwise, a positive slope would represent an impossible scenario where an increase of the applied stress level increases the creep failure time.

A linear relationship between $1/T$ and slope for the trend line in the double logarithmic plot of applied stress versus failure time was also observed from the long-term hydrostatic strength (LTHS) test of PE pipe [35, 36]. However, most of the studies on PE pipe were to detect the DB transition at an elevated temperature. Little attention was paid to the possibility of the trend line change for the slope which is shown for #2 HDPE in Fig. 2.7(b). As a result, presence of the DD transition in PE pipe was not recognized in the past.

Although a clear change is shown for #2 HDPE in Fig. 2.7(b) for the trend line of the slope with $1/T$, the corresponding trend line for the intercept values in Fig. 2.7(a) does not seem to show any change. This results in two sets of C and D values in Eq. (2.1) for one set of A and B values, as listed in Tab. 2.2. The corresponding master curve of applied stress versus failure time at a given temperature, in a double logarithmic plot, is then represented by two straight lines that are discontinuous at the point for the DD transition. This issue was clarified by conducting additional creep tests on #2 HDPE, as part of the tests in the second batch of creep tests, to establish a double logarithmic plot of applied stress versus failure time at a given temperature, which includes the DD transition.

Temperature chosen for the additional creep tests is 323 K which is about halfway between 315 and 333 K used in the first batch of creep tests, as slope at 315 K is smaller than -0.01 (i.e., before the DD transition) and slope at 333 K equal to -0.01 (after the DD transition). Results from these additional creep tests are presented in Fig. 2.11 in which two trend lines can be identified and intercept of the two trend lines, marked as "DD transition," happened to be one of the data points. Note that two trend lines in Fig. 2.11 were generated through connecting two points at the high applied stresses and two points at low applied stresses. As shown in Fig. 2.11, slopes for the two trend lines agree well with the prediction based on the plot for #2 HDPE in Fig. 2.7(b).

Fig. 2.11 also suggests that occurrence of DD transition causes an upward swing of the data points with the increase of the failure time, while the DB transition, as shown in Fig. 2.9, the downward swing of the data points. Therefore, occurrence of the DD transition increases the sensitivity of failure time to the change of the applied stress, while the DB transition decreases the sensitivity.

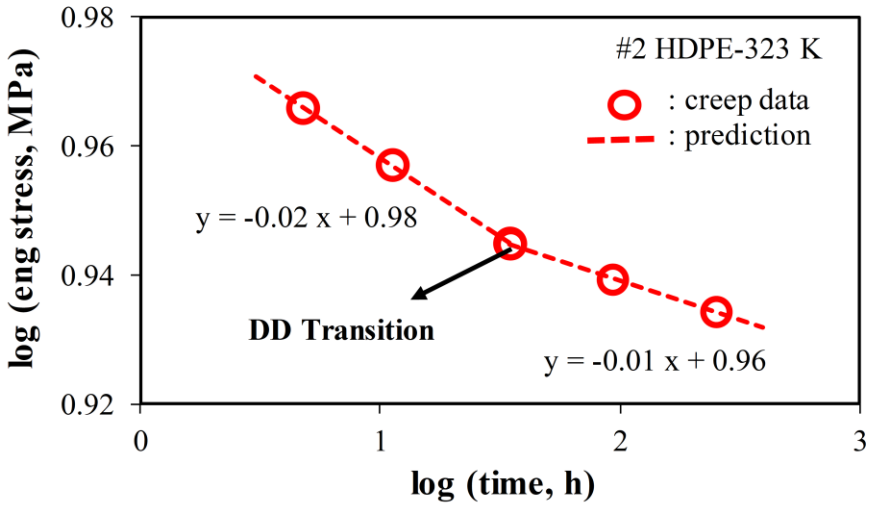

Fig. 2.11 Creep test results for #2 HDPE at 323 K.

A transitional phenomenon similar to that shown in Fig. 2.11 was reported by Crissman [37] on an ethylene-hexene copolymer for natural gas piping systems. Difference of the transitional phenomenon reported by Crissman and the DD transition is that for the former, slope in the double logarithmic plot of applied stress versus failure time is not affected by the temperature change on both sides of the transition, but for the DD transition, the slope is not affected by the temperature change only after the DD transition. Before the DD transition, the slope shows a linear function of 1/T, as depicted in Fig. 2.7(b) for #2 HDPE.

Fig. 2.12 summarizes slope and intercept values from all creep test data for #2 HDPE, by combining data in Figs. 2.6(b) and 2.11. Trend lines in Fig. 2.12 were generated using the same expressions for #2 HDPE in Fig. 2.7. Fig. 2.12 shows that even with two slopes and intercept values at 323 K, the trend lines given in Fig. 2.7 still fit pretty well with data obtained from the experimental testing. This suggests that occurrence of the DD transition does not generate significant change in the slope or intercept values. Therefore, the best way to detect the DD transition is through the trend line change in the plot of slope versus $1/T$, as shown in Fig. 2.7(b) for #2 HDPE. The DB transition, on the other hand, can be detected using either the trend line change in the double logarithmic plot of applied stress versus failure time at a given temperature, such as those master curves shown in Fig. 2.10, or the significant change in slope and intercept values in their plot versus 1/T, as shown in Fig. 2.7 for #3 HDPE.

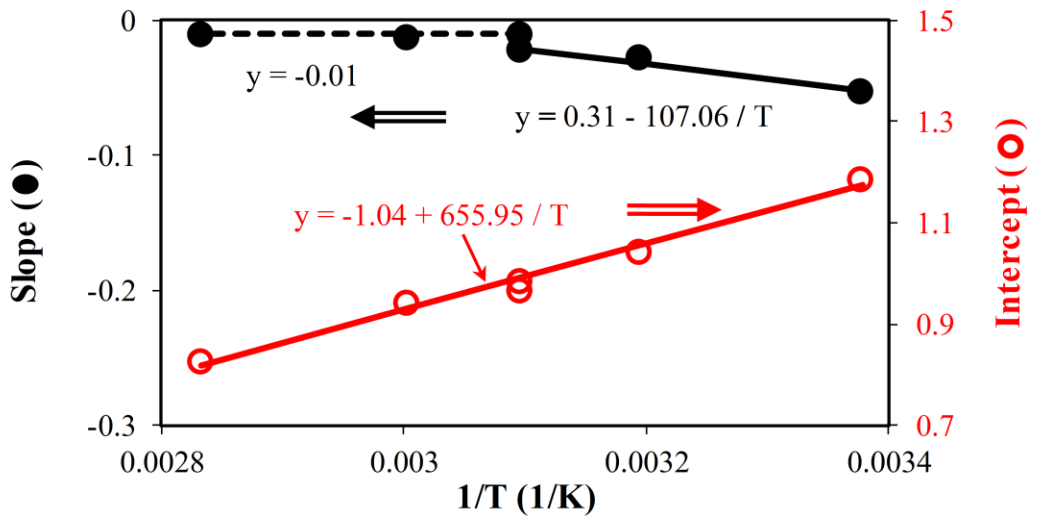

Fig. 2.12 Summary of slope and intercept values for #2 HDPE, including those presented in Figs. 2.6(b) and 2.11. The trend lines are based on the same expressions as those for #2 HDPE in Fig. 2.7.

Another interesting point about the data for #2 HDPE is that based on its solid trend line in Fig. 2.7(b), slope for #2 HDPE is expected to reach zero at 346 K above which the slope would become positive which is an impossible scenario for the creep testing. Therefore, if the DB transition could occur in #2 HDPE under the creep loading, brittle failure should have been generated below 346 K. But the ductile failure was still generated at 353 K, as shown in Fig. 2.6(b). Therefore, rather than the DB transition, the DD transition must occur in #2 HDPE before 346 K to keep the slope to be negative.

It should be noted that although DD and DB transitions were detected in #2 HDPE and #3 HDPE, respectively, the study did not detect any transition in #1 LLDPE. Based on the trend line for #1 LLDPE in Fig. 2.7(b), the slope should reach zero at about 361 K. Therefore, either DD or DB transition is expected to occur at a temperature between 353 and 361 K, in order to avoid the slope becoming positive. However, creep tests could not be conducted on #1 LLDPE in this

temperature range, as these tests would require a force resolution that is beyond the capability of the test machine used in this study. For example, creep test on #1 LLDPE at 358 K would require a force resolution that should be better than 0.1 N in order to establish the trend line for the double logarithmic plot of applied stress versus failure time, but maintaining a loading level with resolution better than 0.1 N during the creep test is not possible for our test machine.

Although it is yet to clarify the underlying factor that is responsible for the occurrence of DB and DD transitions, as observed in #3 HDPE and #2 HDPE, respectively, results presented in this work indicate that change of PE's mass density (or degree of crystallinity) affects the dependence of failure time on the applied stress level. Occurrence of the DD and DB transition is speculated to be caused by the difference in mechanisms involved in the deformation process. As a semi-crystalline polymer, PE's deformation generally involves both crystalline and amorphous phases. The DD and DB transitions could be caused by changes in the interaction between the two phases. The amorphous phase is expected to be more compliant than the crystalline phase, even with the constraints of the molecular motion introduced by the adjacent crystalline phase. When subjected to a relatively high stress level at a sufficiently fast loading rate, which in this study is at a stress level above the point for the DD or DB transition, deformation introduced to the crystalline phase is sufficient to start disintegrating the crystalline structure at an early stage of the creep deformation, thus causing ductile failure in a relatively short test period. For #2 HDPE, by reducing the applied stress to a level below the critical value for the DD transition, stress is still sufficient to introduce plastic deformation to the crystalline phase, but initially only enough for localized deformation such as intra-lamellar shearing. Accumulation of the localized deformation eventually leads to a large-scaled lamellar disintegration to generate ductile failure. For #1 LLDPE, its low degree of crystallinity suggests that difference between the stress for the localized

deformation and the stress for a large-scaled lamella disintegration could be very small, and thus difficult to detect. As a result, the creep test could yield either short-term failure or no failure at all (i.e., taking a very long time to fail which could not be detected in a short-term creep test). For #3 HDPE which is the PE used with the highest mass density, stress required to introduce plastic deformation in the crystalline phase is expected to be the highest. At a low strain rate, the amorphous phase may not be able to transfer the required stress level to disintegrate the crystalline phase before cavitation is initiated in the amorphous phase, thus causing crack growth between the crystalline layers to form a brittle-like failure surface. This generates the DB transition. Increase of temperature enhances molecular disentanglement in the amorphous phase, thus encouraging cavitation and crack growth in the amorphous phase.

The above suggestion for the change of deformation mechanisms to cause DD or DB transition could provide a reasonable explanation for the observation presented in this work, but the concept is simply a speculation at this stage. Further investigation, possibly through molecular dynamics simulation, is needed to provide supporting evidence for the above suggestion.

2.4.2 Relationship between stroke rate and failure time under creep loading

After the successful detection of DD and DB transitions from the experimental data, we then proceeded to investigate potential influence of the two transitions on the relationship between stroke rate and failure time which at the secondary creep stage, is known to be linear in a double logarithmic plot. The linear relationship is commonly known as the Monkman-Grant (MG) relationship [38], as given in the expression below, which was developed for metallic materials, but has recently been applied to polymers [39-41].

$$\log(t) + m \log\left(\dot{\delta}\right) = C_{MG} \tag{2.2}$$

where t is creep failure time, $\dot{\delta}$ stroke rate, and C_{MG} and m constants that are assumed to be independent of applied stress and temperature [42]. Note that stroke rate is used here to represent the rate of deformation in the original MG relationship. This is for consistency of information presented here, especially for the plots presented in Fig. 2.5. Besides, the measured stroke values were found to follow a linear relationship with the measured strain values before the necking started.

Figs. 2.13 presents a double logarithmic plot of failure time in hour (h) versus stroke rate in mm/h at the secondary creep stage, for all data obtained from the study. The figure suggests that for ductile failure, regardless of the difference in PE type, applied stress, and test temperature, Eq. (2.2) can provide a reasonable linear regression function to fit all data points. A similar phenomenon was reported by Vakili-Tahami and Adibeig [40], but only for small deformation. Fig. 2.13 also suggests that the occurrence of DD transition in #2 HDPE does not affect the trend line for the MG relationship. On the other hand, data for brittle failure, i.e., for #3 HDPE after the DB transition, Fig. 2.13 suggests that failure time and stroke rate show a poor correlation, even for the same material and in a relatively narrow temperature range from 333 to 358 K. Although data points for brittle failure at the same temperature do show some linear relationship, the number of points is too small to draw a meaningful conclusion. Therefore, the analysis concludes that the MG relationship is valid for PEs that show ductile failure under the creep loading and that the existence of the DD transition does not affect the MG relationship.

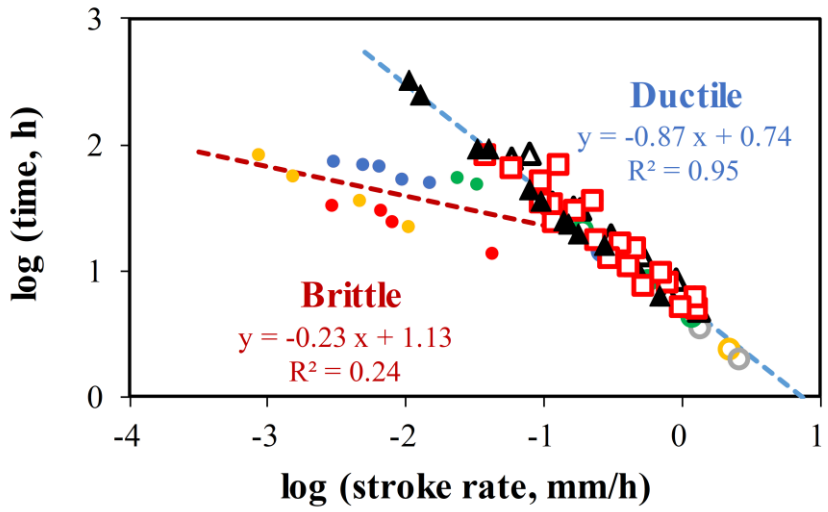

Fig. 2.13 Double logarithmic plot of failure time versus stroke rate for ductile and brittle failures for all specimens used in the study, that is, #1 LLDPE (□), #2 HDPE (△ and ▲), and #3 HDPE (○ and ●). Open and solid symbols represent before and after DD and DB transitions, respectively (DD transition for #2 HDPE and DB transition for #3 HDPE). Different colours for #3 HDPE in the electronic version represent results from different temperatures.

2.5 Conclusions

In this work, notch-free specimens of three PEs, all being ethylene-hexene copolymers but with different mass density, were tested under creep loading. A stress-time-temperature (StT) parametric method, similar to that introduced in ISO 9080, is used to express applied stress used for the testing in terms of time for creep failure and test temperature. Master curves of applied stress versus time to creep failure are successfully established using the StT parametric method, which are also verified using data from additional creep tests. The well-known ductile-brittle (DB) transition is detected in #3 HDPE, and a less known ductile-ductile (DD) transition in #2 HDPE. For #1 LLDPE, based on the trend line of the temperature dependence of the slope in the double

logarithmic plot of applied stress versus failure time, as shown in Fig. 2.7(b), DB transition is unlikely to occur without additional influence from aging or environmental degradation.

Using test data obtained from the study, the Monkman-Grant (MG) relationship was evaluated for its applicability to ductile and brittle failures of PE. The analysis suggests that the MG relationship is applicable to ductile failure of PE, even with the DD transition, but cannot be applied to data for brittle failure.

References

[1] A. Peacock, Handbook of polyethylene: structures, properties, and applications, CRC press, New York, 2000. doi:10.1201/9781482295467.

[2] Y. Zhang, P.Y. Ben Jar, Phenomenological modelling of tensile fracture in PE pipe by considering damage evolution, Mater. Des. 77 (2015) 72–82. doi:10.1016/j.matdes.2015.04.011.

[3] Z. Qi, N. Hu, G. Li, D. Zeng, X. Su, Constitutive modeling for the elastic-viscoplastic behavior of high density polyethylene under cyclic loading, Int. J. Plast. 113 (2019) 125–144. doi:10.1016/j.ijplas.2018.09.010.

[4] ISO 9080, Plastics piping and ducting systems—Determination of the long-term hydrostatic strength of thermoplastics materials in pipe form by extrapolation, Int. Organ. Stand. (2012). doi:10.31030/1908468.

[5] P.A. O'Connell, R.A. Duckett, I.M. Ward, Brittle-ductile transitions in polyethylene, Polym. Eng. Sci. 42 (2002) 1493–1508. doi:10.1002/pen.11046.

[6] X. Lu, N. Brown, The ductile-brittle transition in a polyethylene copolymer, J. Mater. Sci. 25 (1990) 29–34. doi:10.1007/BF00544180.

[7] H.B.H. Hamouda, M. Simoes-betbeder, F. Grillon, P. Blouet, N. Billon, R. Piques, Creep damage mechanisms in polyethylene gas pipes, Polymer (Guildf). 42 (2001) 5425–5437. doi:10.1016/S0032-3861(00)00490-0.

[8] R.W. Lang, A. Stern, G. Doerner, Applicability and limitations of current lifetime prediction models for thermoplastics pipes under internal pressure, Angew. Makromol. Chemie. 247 (1997) 131–145. doi:10.1002/apmc.1997.052470109.

[9] R.K. Krishnaswamy, Analysis of ductile and brittle failures from creep rupture testing of high-density polyethylene (HDPE) pipes, Polymer (Guildf). 46 (2005) 11664–11672. doi:10.1016/j.polymer.2005.09.084.

[10] J. Poduška, P. Hutař, J. Kučera, A. Frank, J. Sadílek, G. Pinter, L. Náhlík, Residual stress in polyethylene pipes, Polym. Test. 54 (2016) 288–295. doi:10.1016/j.polymertesting.2016.07.017.

[11] A. Frank, G. Pinter, R.W. Lang, Prediction of the remaining lifetime of polyethylene pipes after up to 30 years in use, Polym. Test. 28 (2009) 737–745. doi:10.1016/j.polymertesting.2009.06.004.

[12] A. Frank, G. Pinter, Evaluation of the applicability of the cracked round bar test as standardized PE-pipe ranking tool, Polym. Test. 33 (2014) 161–171. doi:10.1016/j.polymertesting.2013.11.013.

[13] P. Hutař, M. Ševčík, L. Náhlík, G. Pinter, A. Frank, I. Mitev, A numerical methodology for lifetime estimation of HDPE pressure pipes, Eng. Fract. Mech. 78 (2011) 3049–3058. doi:10.1016/j.engfracmech.2011.09.001.

[14] C. Tischler, T.R. Kratochvilla, H. Muschik, H. Dragaun, Notched ring test for measuring slow cracking resistance in plastics pipes and fittings, Macromol. Symp. 296 (2010) 626–631. doi:10.1002/masy.201051082.

[15] E. Nezbedová, G. Pinter, A. Frank, P. Hutař, J. Poduška, J. Hodan, Accelerated tests for lifetime prediction of PE-HD pipe grades, Macromol. Symp. 373 (2017) 1600096. doi:10.1002/masy.201600096.

[16] N. Brown, J. Donofrio, X. Lu, The transition between ductile and slow-crack-growth failure in polyethylene, Polymer (Guildf). 28 (1987) 1326–1330. doi:10.1016/0032-3861(87)90446-0.

[17] X. Lu, X. Wang, N. Brown, Slow fracture in a homopolymer and copolymer of polyethylene, J. Mater. Sci. 23 (1988) 643–648. doi:10.1007/BF01174699.

[18] X. Lu, N. Brown, The transition from ductile to slow crack growth failure in a copolymer of polyethylene, J. Mater. Sci. 25 (1990) 411–416. doi:10.1007/BF00714048.

[19] A.L. Ward, X. Lu, Y. Huang, N. Brown, The mechanism of slow crack growth in polyethylene by an environmental stress cracking agent, Polymer (Guildf). 32 (1991) 2172–2178. doi:10.1016/0032-3861(91)90043-I.

[20] X. Lu, N. Brown, Effect of thermal history on the initiation of slow crack growth in linear polyethylene, Polymer (Guildf). 28 (1987) 1505–1511. doi:10.1016/0032-3861(87)90350-8.

[21] X. Lu, N. Brown, A test for slow crack growth failure in polyethylene under a constant load, Polym. Test. 11 (1992) 309–319. doi:10.1016/0142-9418(92)90025-7.

[22] ASTM F1473, Standard test method for notch tensile test to measure the resistance to slow crack growth of polyethylene pipes and resins, ASTM Int. (2016). doi:10.1520/F1473-16.2.

[23] E. Nezbedová, P. Hutař, M. Zouhar, Z. Knésl, J. Sadílek, L. Náhlík, The applicability of the Pennsylvania Notch Test for a new generation of PE pipe grades, Polym. Test. 32 (2013) 106–114. doi:10.1016/j.polymertesting.2012.09.009.

[24] Y. Zhao, B.H. Choi, A. Chudnovsky, Characterization of the fatigue crack behavior of pipe grade polyethylene using circular notched specimens, Int. J. Fatigue. 51 (2013) 26–35. doi:10.1016/j.ijfatigue.2013.01.016.

[25] A. Frank, G. Pinter, Lifetime prediction of polyethylene pipes based on an accelerated extrapolation concept for creep crack growth with fatigue tests on cracked round bar specimens, in: Antec, Chicago, 2009: pp. 2169–2174. doi:10.13140/RG.2.1.3718.1845.

[26] S.H. Beech, E.Q. Clutton, Interpretation of results of full notch creep test and comparison with notched pipe test, Plast. Rubber Compos. 34 (2005) 294–300. doi:10.1179/174328905x59791.

[27] S. Choi, S. Pyo, Y.S. Suh, Y. Seo, Development of notched ring test for measuring slow cracking resistance in plastics pipes and fittings, Plast. Rubber Compos. 36 (2007) 219–225. doi:10.1179/174328907x191314.

[28] G. Pinter, M. Haager, W. Balika, R.W. Lang, Fatigue crack growth in PE-HD pipe grades, Plast. Rubber Compos. 34 (2005) 25–33. doi:10.1179/174328905x29758.

[29] E. Nezbedova, A. Zahradnickova, Z. Salajka, Brittle failure versus structure of HDPE pipe resins, J. Macromol. Sci. Part B. 40 (2001) 507–515. doi:10.1081/MB-100106173.

[30] A. Adib, C. Domínguez, R.A. García, M.A. Garrido, J. Rodríguez, Influence of specimen geometry on the slow crack growth testing of HDPE for pipe applications, Polym. Test. 48 (2015) 104–110. doi:10.1016/j.polymertesting.2015.09.012.

[31] ASTM D4703-16, Standard practice for compression molding thermoplastic materials into test specimens, plaques or sheets, ASTM Int. (2016). https://doi.org/10.1520/D4703-16.

[32] K.D. Pae, S.K. Bhateja, The effects of hydrostatic pressure on the mechanical behavior of polymers, J. Macromol. Sci. Macromol. Chem. 13 (1975) 1–75. doi:10.1080/15321797508068145.

[33] P. Y. Ben Jar, Transition of neck appearance in polyethylene and effect of the associated strain rate on the damage generation, Polym. Eng. Sci. 54 (2014) 1871–1878. doi:10.1002/pen.23735.

[34] J.M. Crissman, L.J. Zapas, Creep failure and fracture of polyethylene in uniaxial extension, Polym. Eng. Sci. 19 (1979) 99–103. doi:10.1002/pen.760190208.

[35] S. Boros, Long-term hydrostatic strength and design of thermoplastic piping compounds, J. ASTM Int. 8 (2011) 1–11. doi:10.1520/JAI102850.

[36] J. Moon, H. Bae, J. Song, S. Choi, Algorithmic methods of reference-line construction for estimating long-term strength of plastic pipe system, Polym. Test. 56 (2016) 58–64. doi:10.1016/j.polymertesting.2016.09.011.

[37] J.M. Crissman, On the long time creep and lifetime behavior in uniaxial extension of a linear low density polyethylene, Polym. Eng. Sci. 31 (1991) 541–547. doi:10.1002/pen.760310802.

[38] G. Sundararajan, The monkman-grant relationship, Mater. Sci. Eng. A. 112 (1989) 205–214. doi:10.1016/0921-5093(89)90360-2.

[39] Z. Gao, W. Liu, Q. Li, Z. Yue, Creep life assessment craze damage evolution of polyethylene methacrylate, Adv. Polym. Technol. 37 (2018) 3619–3628. doi:10.1002/adv.22146.

[40] F. Vakili-tahami, M.R. Adibeig, Using developed creep constitutive model for optimum design of HDPE pipes, Polym. Test. 63 (2017) 392–397. doi:10.1016/j.polymertesting.2017.08.040.

[41] M. Eftekhari, A. Fatemi, Creep behavior and modeling of neat, talc-filled, and short glass fiber reinforced thermoplastics, Compos. Part B Eng. 97 (2016) 68–83. doi:10.1016/j.compositesb.2016.04.043.

[42] F. Povolo, Comments on the Monkman-Grant and the modified Monkman-Grant relationships, J. Mater. Sci. 20 (1985) 2005–2010. doi:10.1007/BF01112283.

Chapter 3 Creep deformation and failure behaviour of polyethylene and its copolymers

Creep tests were conducted on four types of polyethylene (PE), one homo-polymer and three ethylene-hexene copolymers, at temperatures from 296 to 358 K. Three failure modes were observed, i.e., low- and high-temperature brittle failures and ductile failure, but the Monkman-Grant relationship was only applicable to ductile and low-temperature brittle failures. The test results were also analyzed using the Norton Power Law and the Eyring's Law. The analysis indicates that the former cannot provide a proper description of the creep deformation for all PEs, but the latter can if two processes acting in parallel are considered. Activation energy for the Eying's model also shows a strong correlation with the transition from ductile to high-temperature brittle failures. Therefore, short-term creep test should have the potential for predicting the ductile-brittle transition that has long been a major concern about PE for load–carrying applications.

3.1 Introduction

The use of polyethylene (PE) as a structural material requires the assurance of its long-term durability. However, PE's strong viscoelastic behaviour [1-2] has been a barrier for material evaluation for this purpose, which requires time-consuming experiments to evaluate and often uses tests at elevated temperatures to shorten the test time [3-4]. To ensure validity of the high-temperature test results, a comprehensive understanding of the creep deformation behaviour, including the influences of temperature and stress levels on the PE failure, is needed.

In general, PE exhibits ductile failure in the laboratory testing at room temperature [5]. But by decreasing the stress below a critical level, the failure may change to a brittle mode [6]. The change is known as the ductile-brittle (DB) transition which plays a significant role in evaluating long-term durability of PE [7]. The brittle failure is also known as slow crack growth (SCG) which often emanates from a defect in the material [6, 8]. Hence, artificial notches are used in the test specimens to encourage the SCG development, and to shorten the time required to generate the DB transition [9]. For the new generation of PE, however, improvement of the SCG resistance has required the tests to be conducted at elevated temperatures in order to shorten the test time for identifying the critical stress level for the DB transition [10]. Brittle failure generated in such tests is thus referred to as the high-temperature brittle failure (HTBF) in this work.

When conducting creep tests at elevated temperatures, influence of temperature on the failure behaviour should be carefully considered, as more than one failure mode could be detected even using fully notched specimens, such as brittle failure at low temperature which is referred to as low-temperature brittle failure (LTBF) and ductile failure. Transitions from LTBF to ductile failure and then to HTBF have been reported by O'Connell et al. [7] using monotonic tensile tests

on fully-notched specimens, by increasing temperature and decreasing loading rate. Since the ductile failure occurs between LTBF and HTBF, it is believed that different mechanisms are involved in the two brittle failure modes which compete with the mechanism for the ductile failure. In general, LTBF is believed to be dominated by chain scission which is enhanced by the increase of loading rate to prevent disentanglement of the interlocking molecules [7]. The HTBF, on the other hand, is believed to be a disentanglement-controlled deformation process that occurs in a confined space, followed by crack initiation and SCG development. Ductile failure that occurs in-between is a result of bulk yielding, which requires a sufficiently high stress level to involve both amorphous and crystalline phases, but at a relatively low loading rate to prevent the interlocking of the molecules. Such a competition among the three mechanisms for the failure has been schematically described by Deblieck et al. [11].

Over the last few decades, many researchers have shown considerable interests in HTBF-related creep behaviours of PE. For example, Brown and his co-workers investigated the effects of molecular side chains [6], crack tip blunting [8], environmental stress cracking agent [12] and thermal history [13] on the initiation of HTBF of PE. Nezbedová et al. [14] studied HTBF behaviour of different pipe-grade high-density PE (HDPE) using Pennsylvania notch test (PENT) [15] and full notch creep test (FNCT) [16]. However, Krishnaswamy, by firstly comparing the occurrence of HTBF in two HDPE pipes using PENT test and hydrostatic pressure test [17] and then investigating the influence of wall thickness on the occurrence of HTBF of an HDPE pipe [18], suggests that even at low stress levels, PE can show very diverse mechanical behaviours. Therefore, it is of great importance to fully characterize the long-term behaviour of PE before its large-scaled production.

To our knowledge, only limited work is available in the literature [7, 11, 19] which paid attention to the relationship among LTBF, HTBF and ductile failure. This has served as the motivation for the current work. Considering that deformation at the secondary creep stage can best reflect the load-carrying performance of PE in the long-term applications [20], creep tests were used in this study, and the analysis was based on test results at the secondary creep stage.

3.2 Experiments

3.2.1 Materials and specimens

Four commercial PEs in compression-molded plaques were provided by Imperial Oil and used in this study. Commercial names of the PEs and their basic properties are given in Tab. 3.1. For convenience, the four PEs are referred to as #1 LLDPE, #2 HDPE, #3 HDPE and #4 HDPE, respectively. The former three PEs are ethylene-hexene copolymers, while #4 HDPE is a homopolymer. Specimen geometry and preparation are same as those reported in Ref. [21].

Tab. 3.1 Summary of characteristics for PEs used in this study.

Material	Commercial name	Density (g/cc)	Crystallinity (%)	Yield strength (MPa)	Melt index (g/10 min) at 190ºC/2.16 Kg	Peak melting temperature (ºC)
#1 LLDPE	LL 8460.29	0.938	63	17	3.3	126
#2 HDPE	HD 8660.29	0.941	64	19	2.0	129
#3 HDPE	HD 6706.17	0.952	71	26	6.7	132
#4 HDPE	HD 6908.19	0.965	79	30	8.2	135

3.2.2 Mechanical testing

All tests were performed using a universal testing machine (Qualitest Quasar 100, Lauderdale, FL, USA), with the test program and data acquisition controlled by a personal computer. An extensometer was used to record changes of the width in the gauge section during the test. The recorded width change was then used to determine the strain (ε) development during the creep test, based on the following expression [22]:

$$\varepsilon = 2 \times \ln\left(\frac{w_0}{w}\right) \tag{3.13}$$

where w_0 and w are original and deformed widths in the gauge section, respectively. Creep tests at 296, 315, 333 and 353 K were conducted on all PEs, but for #3 HDPE creep tests were also conducted at 358 K to obtain one additional set of data for HTBF that was needed in the analysis. In this study, at least four creep tests were conducted for each PE at each temperature. Totally, 76 creep tests were conducted. The test conditions are identical to those used previously [21], thus not detailed here.

3.2.3 Scanning electron microscopy (SEM)

Surfaces generated from brittle failure were examined using a Zeiss Sigma field emission scanning electron microscope (SEM). Note that these specimens were not coated with a conductive layer. Rather, the SEM chamber was back-filled with nitrogen gas to minimize charging of the surface, and a backscattering detector was used to collect signals for the imaging.

3.3 Results

3.3.1 Creep test

Typical curves from creep tests to cover the full temperature range used in the study are shown in Fig. 3.1. In total, three failure behaviours are observed, LTBF, HTBF and ductile failure (denoted as DF in the figure). As shown in the figure, all curves have similar profiles, with the main difference being the transition from the secondary to the tertiary creep stages. Transitions in the curves for ductile failure and LTBF are relatively smooth, while those for HTBF are sharp. For #1 LLDPE and #2 HDPE, only ductile failure was detected in the test conditions, with neck being well developed in the gauge section at the tertiary creep stage. The same phononmenon was observed for #3 HDPE up to 333 K above which HTBF occurs, indicating that failure mode has changed from ductile to brittle. For #4 HDPE, LTBF was observed at room temperature (296 K), but occurred only in a very narrow stress window. By further reducing the applied stress, creep failure would become ductile. At 315 K, ductile deformation dominated the failure behaviour with a total creep stroke larger than that for the brittle failure. But the failure behaviour changed to brittle again with a further increase of temperature, to 333 and 353 K, indicating that both brittle-ductile (BD) and ductile-brittle (DB) transitions can occur in #4 HDPE by increase of the test temperature. Such a phenomenon was also observed under simple tensile loading, as reported by O'Connell et al. [7]. In our results, the BD transition corresponds to the change from LTBF to ductile failure, while the DB transition from ductile failure to HTBF.

Using strain to quantify the creep deformation, typical creep curves for the three failure modes in Fig. 3.1 are shown in Fig. 3.2. The critical point for the onset of failure is defined as the intersection of trend lines in the secondary and tertiary creep stages, as indicated by red dots in

Fig. 3.2. Noted that the tertiary creep stage for LTBF is too short to draw a trend line. Therefore, a vertical line was used to replace the trend line at the tertiary creep stage. The corresponding critical failure strains as a function of applied stress are plotted in Fig. 3.3, with unfilled symbols for ductile failure and filled symbols for brittle failure. Overall, Fig. 3.3 indicates that the failure strain varies appreciably. For ductile failure, the failure strain increases by decreasing the applied stress. The counterpart for brittle failure shows a different trend. As shown by brittle failure of #3 HDPE and #4 HDPE in Fig. 3.3, in filled symbols, the strain is lower than the corresponding ductile failure strain. Furthermore, failure strain for HTBF decreases with the decrease of the applied stress level. However, it should be pointed out that the data set for LTBF, for #4 HDPE only, covers only a limited stress range which is too narrow to draw a clear conclusion.

In view that deformation at the secondary creep stage reflects closely performance of PE in the load-carrying applications [20], special attention was paid to modeling of PE deformation at this stage, with the corresponding strain rate ($\dot{\varepsilon}_s$) determined by the slopes of the fitting lines as shown in Fig. 3.2. The modeling considers thermally activated rate process based on the Norton Power Law (NPL) and the Eyring's Law.

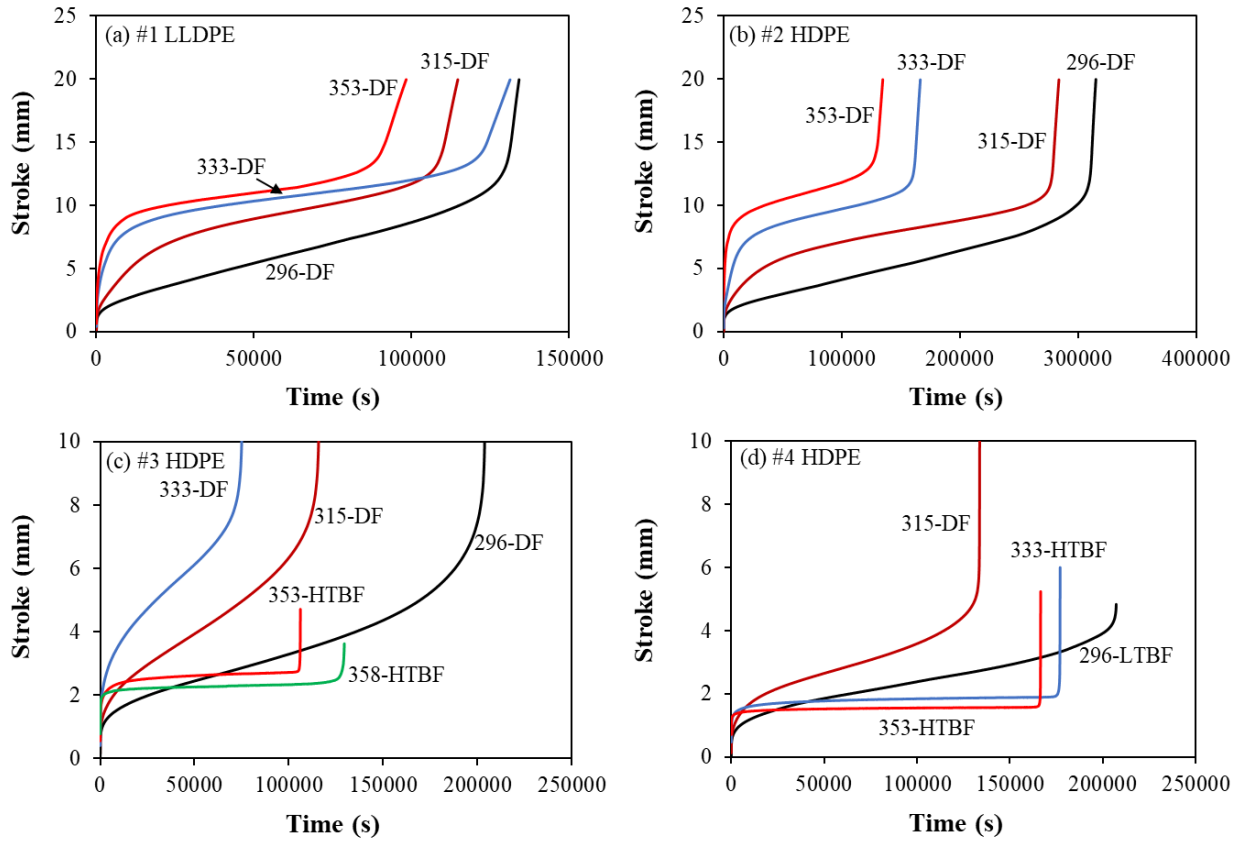

Fig. 3.1 Typical creep curves for four PEs used in the study, with temperatures indicated by the numbers next to each curve, followed by DF (ductile failure), LTBF (low-temperature brittle failure) and HTBF (high-temperature brittle failure).

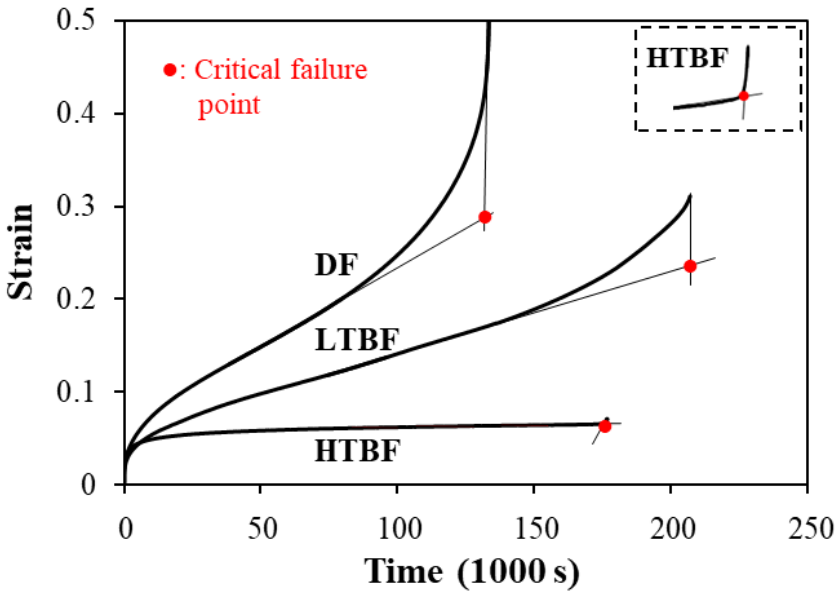

Fig. 3.2 Typical strain-time curves to demonstrate the determination of the critical failure point and the corresponding secondary creep strain rate.

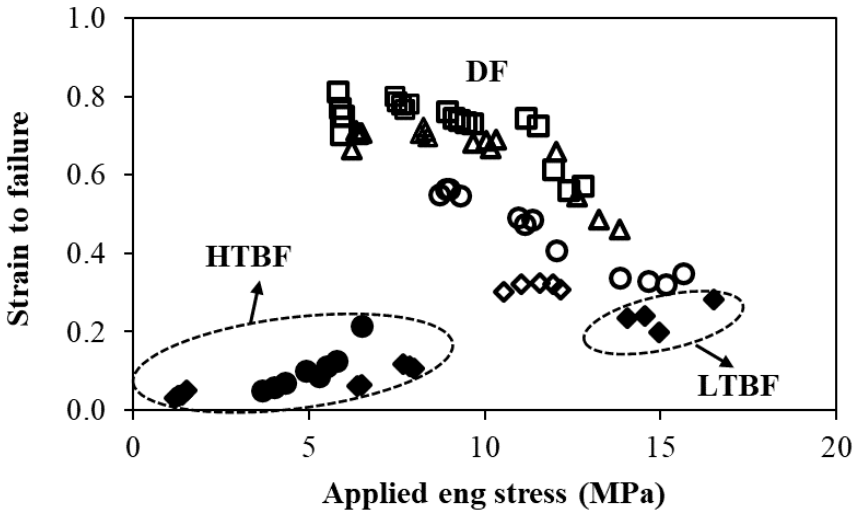

Fig. 3.3 Summary of strains to failure as a function of the applied stress for the four PEs. #1 LLDPE (□), #2 HDPE (△), #3 HDPE (○ and ●), and #4 HDPE (◇ and ◆), in which unfilled and filled symbols represent ductile and brittle failures, respectively.

3.3.1.1 Norton Power Law

The NPL which is widely used for modeling creep behaviour at the secondary stage [20, 23], describes a linear natural logarithmic relationship between $\dot{\varepsilon}_s$ and the applied engineering stress (σ), as expressed below:

$$\ln\dot{\varepsilon}_s = n\ln\sigma - \frac{E_N}{RT} + \ln A_1 \tag{3.2}$$

where n is the power law exponent, E_N the activation energy obtained from NPL, R the Boltzmann constant and A_1 the material constant. Values for n in Eq. (3.2) were determined using Fig. 3.4 which summarizes plots of $\dot{\varepsilon}_s$ versus σ in a natural logarithmic scale. In spite of some differences in the fitting quality, Fig. 3.4 indicates that each set of data can be fitted using a linear function, with slope of the fitting functions representing the n values that are also summarized in Fig. 3.5(a). Fig. 3.5(a) indicates that the n values for ductile failure (in unfilled symbols) show a remarkable dependence on temperature, that is, n increases with the increase of temperature. The dependence of n with temperature was also reported by Fatemi and his co-workers [23-24] for thermoplastic composites and HDPE. However, their results do not show any clear correlation between n and temperature. On the other hand, n values in Fig. 3.5(a) for brittle failure show little dependency on temperature. This temperature-independence is consistent with that reported before [20] in which HDPE used for the study has mass density comparable to those for #3 HDPE and #4 HDPE used here.

Activation energy for NPL, E_N, is embodied in the last two terms of Eq. (3.2), and can be determined from the intercepts of the expressions in Fig. 3.4 plotted as a function of reciprocal

temperature, as shown in Fig. 3.5(b). Note that in spite of three failure modes involved in #4 HDPE, its four points in Fig. 3.5(b) show a good linear relationship, suggesting that a single E_N value can be used for #4 HDPE for the secondary creep stage, regardless of the difference in failure mode. The curves of the best fit in Fig. 3.5(b) for #4 HDPE give E_N and A_1 values of 240 kJ/mol and 1.5×10^{21} $MPa^{-n}\,s^{-1}$, respectively. For #3 HDPE, data for ductile failure and HTBF require different trend lines, for which the expressions are also given in Fig. 3.5(b). The expression for HTBF leads to E_N of 385 kJ/mol and A_1 of 3.4×10^{39} $MPa^{-n}\,s^{-1}$. But for the ductile failure, the expression results in a negative E_N value. The trend lines for #1 LLDPE and #2 HDPE also yield negative E_N values. Considering that Eq. (3.2) cannot provide positive E_N values for #1 LLDPE, #2 HDPE and ductile failure for #3 HDPE, it seems that the NPL is merely a mathematical fitting function for characterizing the secondary creep behaviour of HDPE, without much of the physical meaning. A similar conclusion was drawn from other studies [25-26] which suggest that due to change of mechanisms for creep deformation at different temperatures, the NPL does not provide a good fit to data from creep tests for ceramics. Therefore, NPL is just an empirical-based model for characterizing creep deformation of PE.

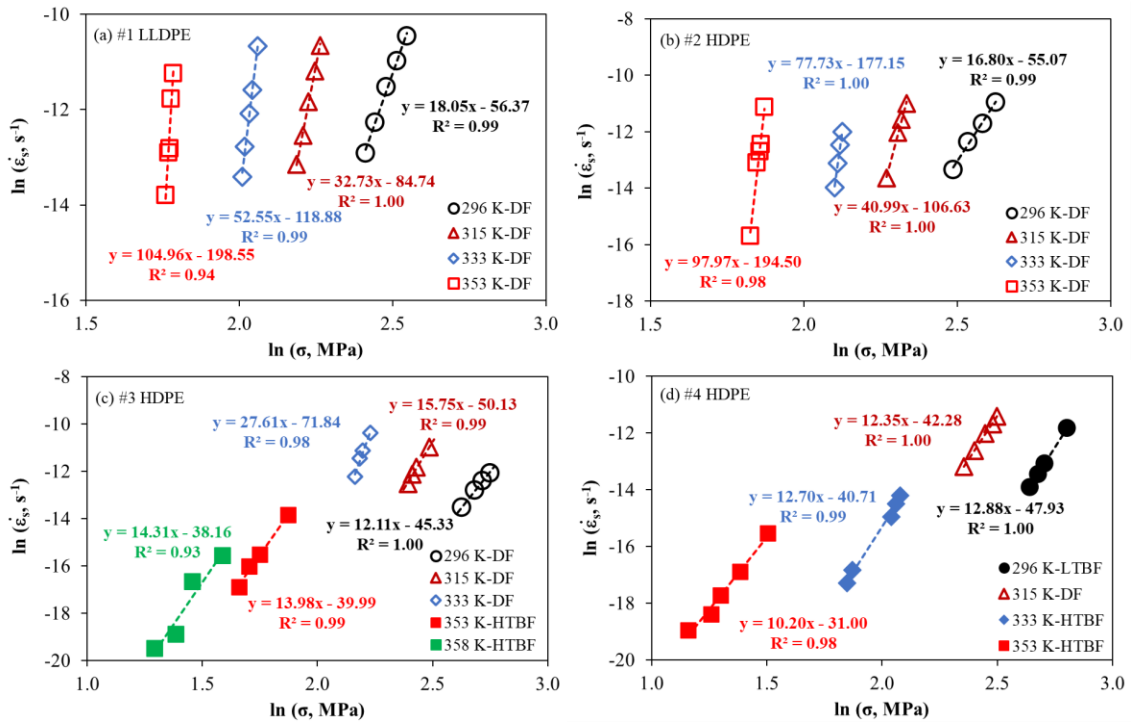

Fig. 3.4 Natural logarithmic plots of strain rate at the secondary creep stage versus the applied stress.

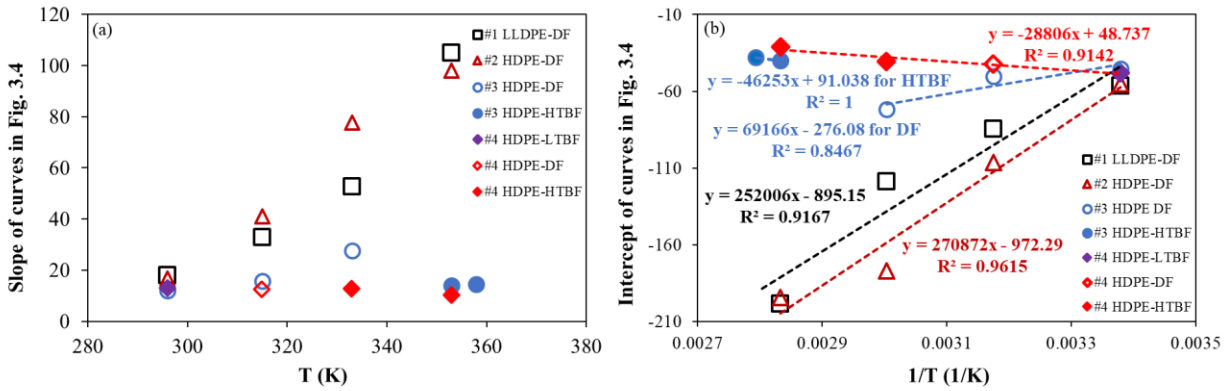

Fig. 3.5 Summary of the NPL-based analysis: (a) slopes (n) of the expressions in Fig. 3.4 versus T, and (b) intercepts of expressions in Fig. 3.4 versus $1/T$. Unfilled symbols are for ductile failure and filled symbols for brittle failure.

3.3.1.2 Eyring's Law

The Eyring's Law, which likes NPL, is based on the Arrhenius equation, and has also been used to describe the temperature- and stress-dependence of the creep behaviour at the secondary creep stage. The Eyring's Law takes the following form:

$$\frac{\sigma}{T} = \frac{R}{V}\sinh^{-1}\left(\frac{\dot{\varepsilon}_s}{\dot{\varepsilon}_0}\exp\left(\frac{E}{RT}\right)\right) \tag{3.3}$$

where V is the activation volume, E the activation energy and $\dot{\varepsilon}_0$ the reference strain rate. Plots of σ/T versus ln ($\dot{\varepsilon}_s$) at different temperatures are constructed to determine V, as shown in Fig. 3.6. Linear trend lines and the corresponding expressions are listed next to each curve. As suggested by Liu and Truss [27], if slopes for the expressions in each figure of Fig. 3.6 can be set to have a common value, then the slope is equal to R/V under the condition of $\frac{\dot{\varepsilon}_s}{\dot{\varepsilon}_0}\exp\left(\frac{E}{RT}\right) \gg 1$. As shown in Fig. 3.6, however, it is not possible to have a common slope for all trend lines in each figure, especially for those data at lower temperatures. Some studies [27-30] have suggested that a significant change of slopes for the trend lines in Fig. 3.6 could be characterized using two Eyring's processes acting in parallel, as shown in the expression below:

$$\frac{\sigma}{T} = \frac{\sigma_1}{T} + \frac{\sigma_2}{T} = \frac{R}{V_1}\sinh^{-1}\left(\frac{\dot{\varepsilon}_s}{\dot{\varepsilon}_{01}}\exp\left(\frac{E_1}{RT}\right)\right) + \frac{R}{V_2}\sinh^{-1}\left(\frac{\dot{\varepsilon}_s}{\dot{\varepsilon}_{02}}\exp\left(\frac{E_2}{RT}\right)\right) \tag{3.4}$$

where the subscripts '1' and '2' denote processes 1 and 2, respectively. Process 1 is active for all test conditions, while process 2 is active only at high stresses. To determine values for the Eyring's parameters in each process of Eq. (3.4), the following approximations are used:

$$\frac{\sigma}{T} = \begin{cases} \dfrac{R\dot{\varepsilon}_s}{V\dot{\varepsilon}_0}\exp\left(\dfrac{E}{RT}\right) & \text{for } 0 < \dfrac{\dot{\varepsilon}_s}{\dot{\varepsilon}_0}\exp\left(\dfrac{E}{RT}\right) \ll 1 \quad (3.5a) \\ \dfrac{R}{V}\ln(\dot{\varepsilon}_s) - \dfrac{R}{V}\ln\dfrac{\dot{\varepsilon}_0}{2} + \dfrac{E}{VT} & \text{for } \dfrac{\dot{\varepsilon}_s}{\dot{\varepsilon}_0}\exp\left(\dfrac{E}{RT}\right) \gg 1 \quad (3.5b) \end{cases}$$

For #1 LLDPE and #2 HDPE, in view that their slopes for the trend lines at 333 and 353 K have small difference, it is reasonable to assume that data points at these temperatures can be fit using trend lines of the same slope, i.e., based on the same Eyring's process (process 1). On the other hand, process 2 which is an additional process is active only for results at 296 and 315 K. A similar concept is applied to #3 HDPE and #4 HDPE. That is, process 1 is active at all temperatures, but process 2 is active only before the DB transition, i.e., at and below 333 K for #3 HDPE and at and below 315 K for #4 HDPE. The fitting procedure used to determine parameters in Eq. (3.4) is described as follows.

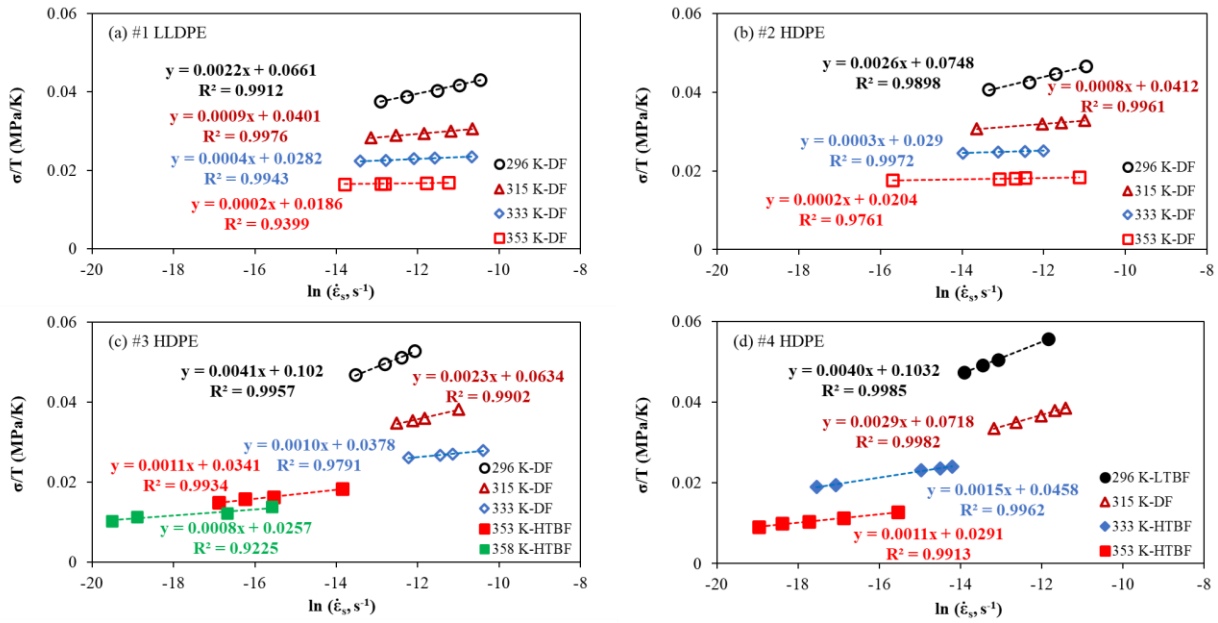

Fig. 3.6 Plots of σ/T versus ln ($\dot{\varepsilon}_s$) for the four PEs used in the study.

In the fitting procedure, value for V_1 was determined first using Eq. (3.5b), i.e. by fitting the plot of σ/T versus ln ($\dot{\varepsilon}_s$) for data collected at two highest temperatures from the experimental testing, as presented in Fig. 3.7. Each data set in Fig. 3.7 was fit using two trend lines. The dashed trend lines with the expressions on the left were based on the best R^2, and the solid trend lines with the expressions on the right using a slope that is same at both temperatures. Values for the common slopes were taken to be close to the average of the two slopes for the dashed trend lines, except #1 LLDPE for which the common slope was taken to be the same as that for #2 HDPE. This is because data in Figs. 3.7(a) and (b) have very flat trend lines, with their R^2 values showing little sensitivity to the change of the slope. Therefore, the same value was used for their slopes. The corresponding V_1 values determined using the common slope are given on the top right corner in each figure.

With Eq. (3.5b), values for E_1 and $\dot{\varepsilon}_{01}$ were determined by plotting intercepts of the solid trend lines in Fig. 3.7 as a function of reciprocal temperature, as shown in Fig. 3.8(a). Ideally, three

or more data points should be used to ensure linearity of the trend line, but due to four temperatures used for the testing and only one trend line was obtained for creep data at each temperature, each trend line in Fig. 3.8(a) could only be established using two data points. Nevertheless, as to be shown later, E values so determined could still distinguish the different creep behaviours, as to be presented below.

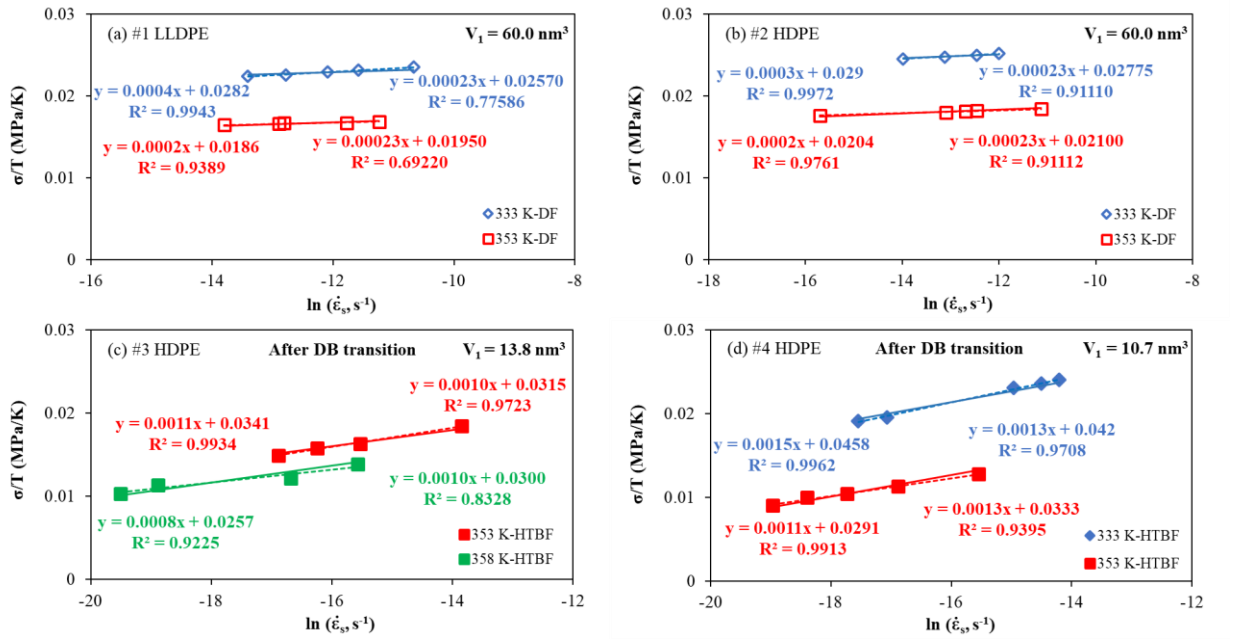

Fig. 3.7 Plots of σ/T versus ln ($\dot{\varepsilon}_s$) at two highest temperatures used in the experimental testing, for determining the V_1 values.

To examine validity of the assumption for Eq. (3.5b), values for $\frac{\dot{\varepsilon}_S}{\dot{\varepsilon}_{01}}\exp\left(\frac{E_1}{RT}\right)$ for all PEs used in this study are summarized in Fig. 3.8(b). The figure indicates that the condition $\frac{\dot{\varepsilon}_S}{\dot{\varepsilon}_{01}}\exp\left(\frac{E_1}{RT}\right) \gg 1$ holds for all E_1 and $\dot{\varepsilon}_{01}$ values determined from Fig. 3.8(a). Therefore, these values and the corresponding V_1 values are listed in Tab. 3.2, under 'Process 1.'

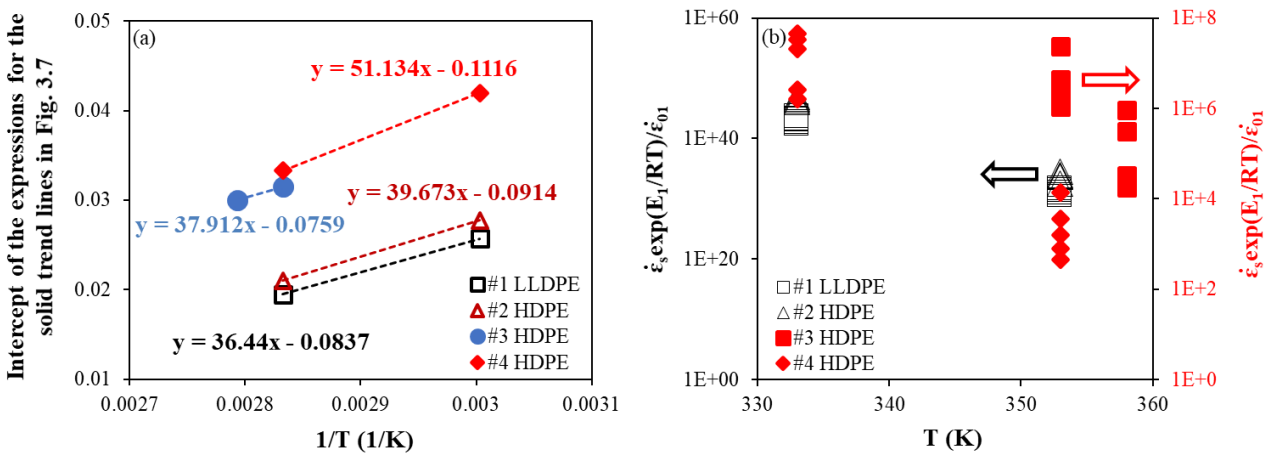

Fig. 3.8 Summary of analysis for process 1 based on the Eyring's model: (a) The intercept values for the solid trend lines in Fig. 3.7, and (b) values for $\frac{\dot{\varepsilon}_s}{\dot{\varepsilon}_{01}} \exp\left(\frac{E_1}{RT}\right)$ versus T.

Tab. 3.2 Fitting parameters of the Eyring's Law for the four PEs.

Material	Process 1			Process 2		
	$\dot{\varepsilon}_{01}$ (s^{-1})	E_1 (kJ/mol)	V_1 (nm^3)	$\dot{\varepsilon}_{02}$ (s^{-1})	E_2 (kJ/mol)	V_2 (nm^3)
#1 LLDPE	2.2E+158	1317	60.0	2.3E+15	118	6.9
#2 HDPE	7.7E+172	1433	60.0	1.4E+19	140	6.0
#3 HDPE	1.8E+33	315	13.8	5.5E+16	133	4.5
#4 HDPE	7.5E+37	329	10.7	2.4E+17	135	5.1

In order to determine values for the parameters in the Eyring's Law for process 2, Eq. (3.4) was rearranged to become

$$\frac{\sigma_2}{T} = \frac{1}{T}(\sigma - \sigma_1) = \frac{R}{V_2}\sinh^{-1}\left(\frac{\dot{\varepsilon}_s}{\dot{\varepsilon}_{02}}\exp\left(\frac{E_2}{RT}\right)\right) \tag{3.6}$$

That is,

$$\frac{1}{\dot{\varepsilon}_s}\sinh\left[\frac{V_2}{RT}(\sigma - \sigma_1)\right] = \frac{1}{\dot{\varepsilon}_{02}}\exp\left(\frac{E_2}{RT}\right) \tag{3.7}$$

where σ_1 was obtained from Eq. (3.3) using $\dot{\varepsilon}_s$ measured from the experimental testing and parameters for process 1, as listed in Tab. 3.2. By taking natural logarithm on both sides of Eq. (3.7), we have:

$$\ln\left\{\frac{1}{\dot{\varepsilon}_s}\sinh\left[\frac{V_2}{RT}(\sigma - \sigma_1)\right]\right\} = \frac{E_2}{RT} - \ln(\dot{\varepsilon}_{02}) \tag{3.8}$$

Although determination of the V_2 value could be based on a procedure similar to that for process 1, it was not clear whether the assumption of $\frac{\dot{\varepsilon}_s}{\dot{\varepsilon}_{02}}\exp\left(\frac{E_2}{RT}\right) \gg 1$ could be satisfied for all data points. Therefore, an alternative approach was used, in which a preliminary analysis was carried out to determine a temporary values for V_2, E_2 and $\dot{\varepsilon}_{02}$. Then, the assumption of $\frac{\dot{\varepsilon}_s}{\dot{\varepsilon}_{02}}\exp\left(\frac{E_2}{RT}\right) \gg 1$ was examined using these temporary values to identify data points that could satisfy the assumption of $\frac{\dot{\varepsilon}_s}{\dot{\varepsilon}_{02}}\exp\left(\frac{E_2}{RT}\right) \gg 1$. The data points that satisfied the assumption were then

used to carry out the same analysis the second time to determine the true V_2, E_2 and $\dot{\varepsilon}_{02}$ values. Details of the analysis are described as follows.

First of all, using data points at 296 and 315 K for #1 LLDPE, #2 HDPE and #4 HDPE, and at 296, 315 and 333 K for #3 HDPE, a common slope in the plot of $(\sigma - \sigma_1)/T$ versus ln $(\dot{\varepsilon}_s)$ was determined for each PE using an approach similar to that applied to Fig. 3.7. These slope values were then used to determine the temporary V_2 value based on Eq. 3.5(b). With the experimentally measured $\dot{\varepsilon}_s$ and σ values and σ_1 determined from Eq. (3.3), values for the left-hand side (LHS) of Eq. (3.8) were determined and plotted as a function of reciprocal temperature in Fig. 3.9(a) in which the trend line expressions are also given. Slope and intercept values for the expressions in Fig. 3.9(a) were then used to determine the temporary values for E_2 and $\dot{\varepsilon}_{02}$, based on Eq. (3.8), in the same way as that used earlier to determine E_1 and $\dot{\varepsilon}_{01}$.

The temporary E_2 and $\dot{\varepsilon}_{02}$ values were then used to determine values for $\frac{\dot{\varepsilon}_S}{\dot{\varepsilon}_{02}} \exp\left(\frac{E_2}{RT}\right)$ which are summarised in Fig. 3.9(b) as a function of temperature. Fig. 3.9(b) suggests that only data points at room temperature met the condition of $\frac{\dot{\varepsilon}_S}{\dot{\varepsilon}_{02}} \exp\left(\frac{E_2}{RT}\right) \gg 1$. Therefore, values for $(\sigma - \sigma_1)/T$ at the room temperature were plotted as a function of ln $(\dot{\varepsilon}_s)$ in Fig. 3.10(a) to determine the V_2 values based on Eq. (3.5b). These V_2 values, along with the experimentally measured $\dot{\varepsilon}_s$ and σ values and σ_1 determined from Eq. (3.3), were then used to calculate values for the LHS of Eq. (3.8), referred to as 'true LHS of Eq. (3.8),' which are presented in Fig. 3.10(b). Slope and intercept for the trend lines expressions in Fig. 3.10(b) were then used to determine E_2 and $\dot{\varepsilon}_{02}$ values, based on Eq. (3.8), as listed in Tab. 3.2 under 'Process 2.'

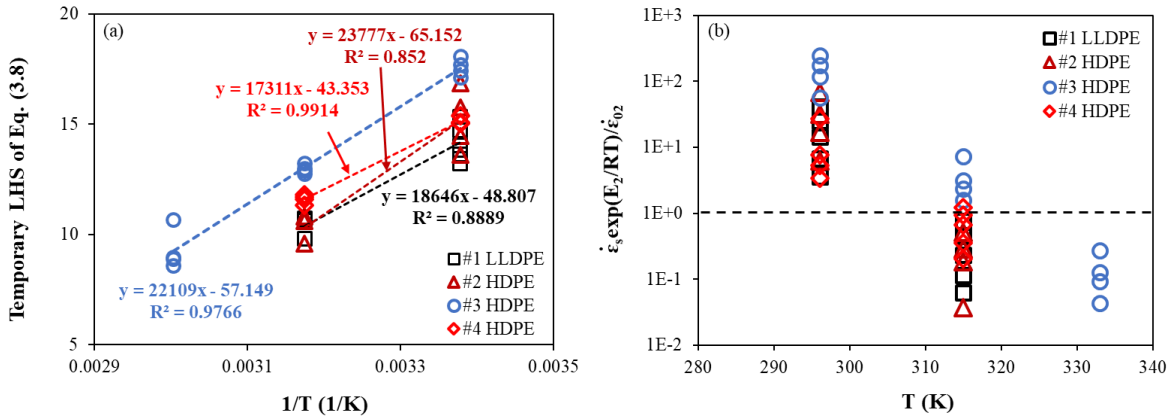

Fig. 3.9 (a) The left-hand side (LHS) of Eq. (3.8) generated using the temporary V_2 values, and (b) plots of $\frac{\dot{\varepsilon}_S}{\dot{\varepsilon}_{02}} \exp\left(\frac{E_2}{RT}\right)$ versus T, using temporary E_2 and $\dot{\varepsilon}_{02}$ values based on the temporary V_2 values.

Note that for #4 HDPE, although three failure behaviours were observed, i.e. LTBF, ductile failure and HTBF, a third Eyring's process was not needed to regenerate results from the creep tests.

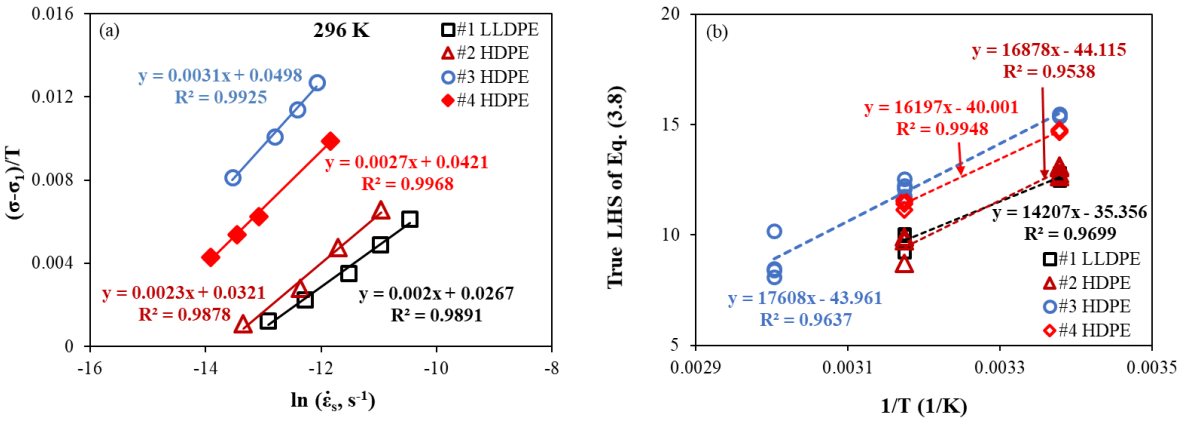

Fig. 3.10 Summary of results for determining V_2, E_2 and $\dot{\varepsilon}_{02}$: (a) creep data at room temperature to determine V_2 based on Eq. (3.5b), and (b) plot of values from the LHS of Eq. (3.8) generated using the true V_2 values, as a function of $1/T$.

3.3.2 Fractographic analysis

Fig. 3.11 presents SEM images for #4 HDPE on the initiation site of the fracture surfaces. Fig. 3.11(a) is from LTBF at 296 K, and Figs. 3.11(b) and (c) from HTBF at 333 K and 353 K, respectively. The micrographs on the right-hand side of Fig. 3.11 are the enlarged views of the boxed regions on the left. These SEM images depict drawn fibrils and relatively brittle surface in between. In addition, the left image of Fig. 3.11(a), from LTBF, shows evidence of fracture behaviour that resulted in multiple 'islands,' which suggests that the fracture might be initiated from multiple sites that were on slightly different cross sections. In Figs. 3.11(b) and (c), from HTBF, number for such islands is much reduced and the fibrils were drawn to a less extent. The initiation site becomes quite smooth, though the enlarged views on the right-hand side suggest that microfibrils were still involved in the fracture process, but the stretch was less extensive. Apart from the above features, the initiation site generated by the brittle failure does not show much difference between LTBF and HTBF.

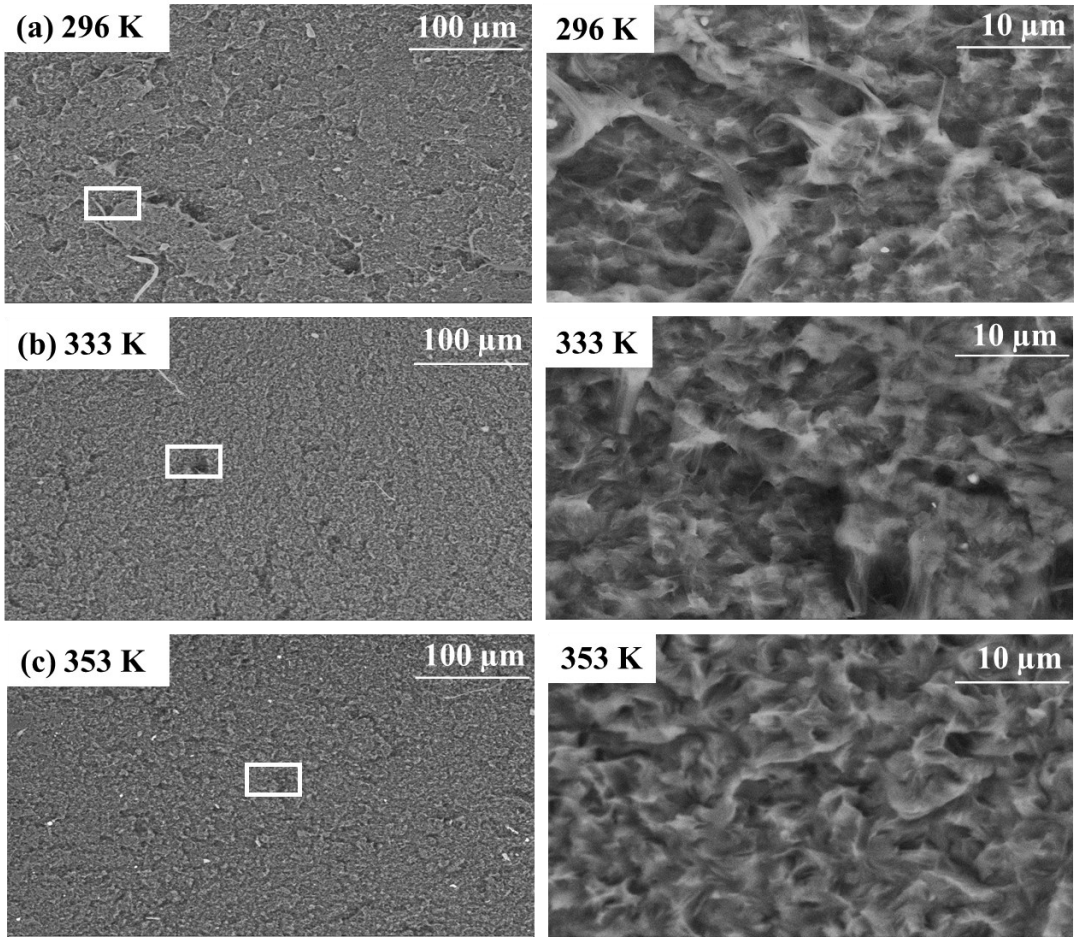

Fig. 3.11 SEM micrographs of surfaces generated by brittle failure of #4 HDPE: (a) LTBF at 296 K, (b) HTBF at 333 K and (c) HTBF at 353 K.

3.4 Discussion

3.4.1 Applicability of the Monkman-Grant relationship

It has recently been demonstrated [21] that the Monkman-Grant (MG) relationship, as described in Eq. (3.9), is applicable to data for the three copolymers failed in a ductile manner, i.e. #1 LLDPE, #2 HDPE and #3 HDPE, regardless of the difference in mass density, applied stress and test temperature.

$$\log(t) + m\log(\dot{\varepsilon}_s) = C_{MG} \tag{3.9}$$

where t is the failure time, and m and C_{MG} constants that should be independent of applied stress and temperature [31]. Fig. 3.12 presents a double-logarithmic plot of t versus $\dot{\varepsilon}_s$ for all data obtained from the study, with data for ductile failure represented by unfilled symbols and brittle failure (both LTBF and HTBF) using filled symbols.

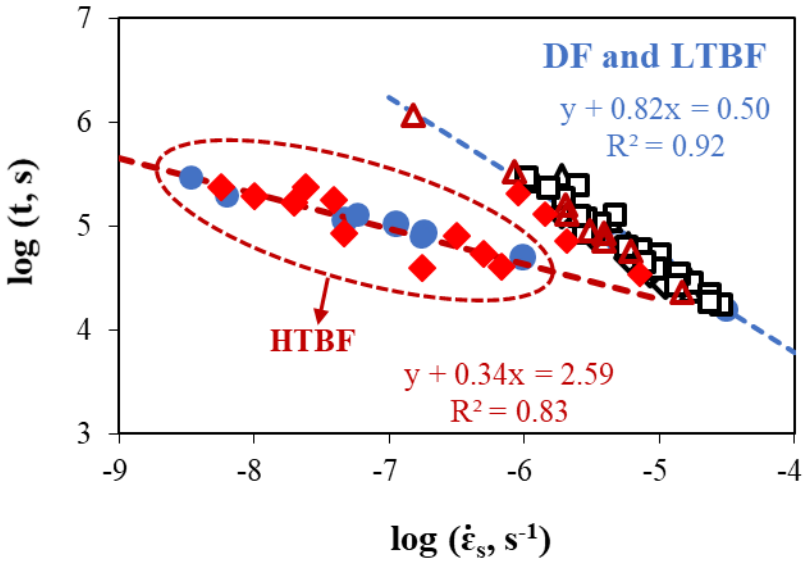

Fig. 3.12 The Monkman-Grant (MG) plot for all data reported here: #1 LLDPE (□), #2 HDPE (△), #3 HDPE (○ and ●) and #4 HDPE (◇ and ◆) in which unfilled symbols represent ductile failure and filled symbols brittle failure.

Fig. 3.12 suggests that the MG relationship is applicable to data for LTBF and ductile failure. Therefore, LTBF might be generated by deformation that is similar to the deformation that led to ductile failure. Data for HTBF, on the other hand, lie on a different trend line which suggests

that at a given strain rate, HTBF occurred in a much shorter time frame than that for the ductile failure or LTBF. In view that HTBF occurred after a sharp transition from the secondary to the tertiary creep stages, in contrast to the relatively smooth transition before the occurrence of ductile failure or LTBF, HTBF might be caused by a premature failure. This is consistent with the failure mode proposed in a previous work, suggesting that the appeared brittle behaviour for HTBF is possibly due to the fracture being confined in the amorphous phase, constrained by the neighboring lamellae [32].

3.4.2 Mechanisms and comparison of Eyring's parameters for the four PEs

Fig. 3.13 compares the experimentally measured applied stress and failure time with those predicted using the Eyring's model based on parameters listed in Tab. 3.2. The figure shows a fairly good agreement between the experimental measurements and the model predictions. The Eyring's processes (1 or 1+2) that were used to regenerate the experimental measurements are also given next to each data set. Furthermore, Fig. 3.13(d) indicates that for #4 HDPE, the relationship between the applied stress and strain rate at the secondary creep stage for both LTBF at 296 K and ductile failure at 315 K can be predicted using the same two Eyring's processes. With Fig. 3.12 that shows the same kinematic relationship between strain rate and failure time for the two failure modes, it is possible that the same deformation mechanisms are involved in the generation of LTBF and ductile failure for #4 HDPE. However, the final failure behaviours are very different, and factors that cause such different failure behaviours require further investigation.

Fig. 3.13 also suggests that mechanisms that govern creep deformation in #1 LLDPE and #2 HDPE might have changed when test temperature increased from 315 to 333 K, as process 2 that was involved at 315 K was no longer involved at 333 K, though the failure behaviour remained

ductile. In a previous study [21], a transition named ductile-ductile (DD) transition was detected for #2 HDPE through the change of the trend line slope in a double logarithmic plot of creep stress versus failure time, by decreasing the creep stress to below a critical level. However, such a change was not detected in #1 LLDPE. Therefore, the DD transition may have also occurred in #1 LLDPE, but not detectable using the change of the trend line between creep stress and failure time. Results presented here suggest that the DD transition can also be detected by the change of the Eyring's processes needed to simulate the creep test results.

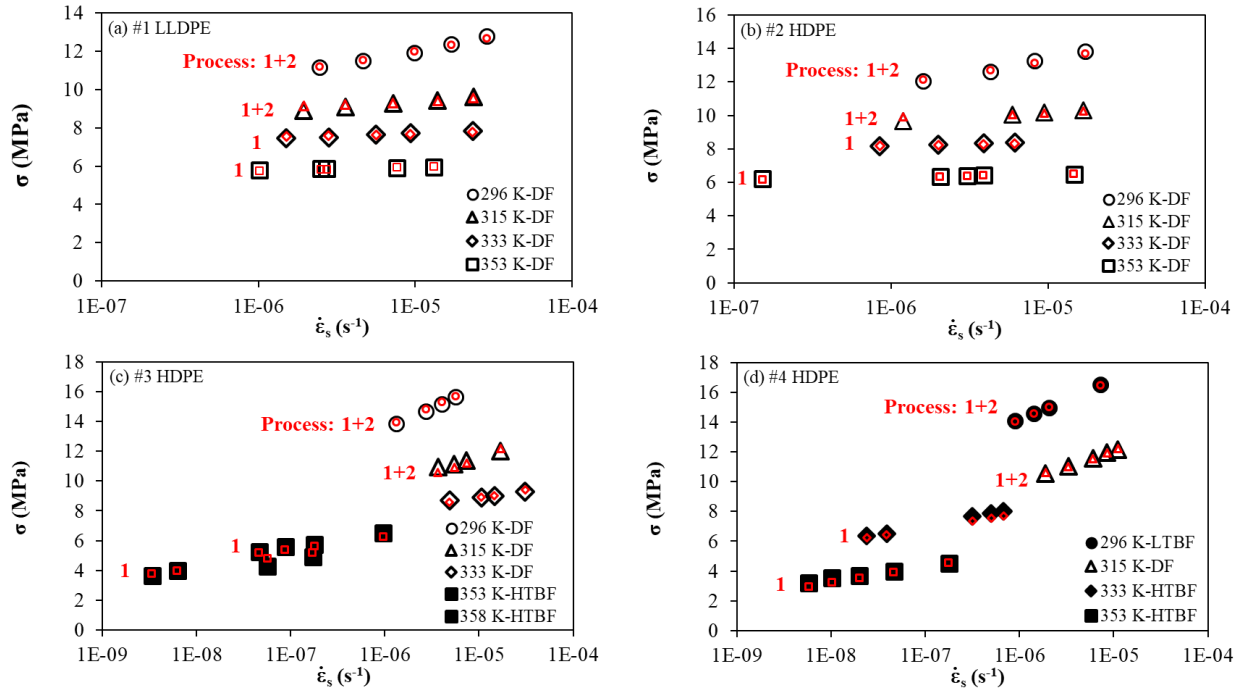

Fig. 3.13 Comparison of experimental measurements (unfilled and filled symbols of large size in black) with predictions based on the Eyring's Law using parameters listed in Tab. 3.2 (unfilled symbols of small size in red).

Occurrence of LTBF, ductile failure and HTBF is believed to be caused by difference in mechanisms involved in the deformation process. As a semi-crystalline polymer, under a high creep stress, both amorphous and crystalline phases are involved at the beginning of creep deformation, but it is the extensive disintegration of the crystalline phase before the crack development that results in the ductile failure. If strength for the amorphous phase is not high enough to survive from the disintegration process, fracture occurs before the extensive deformation is generated. On the other hand, if the applied stress is sufficiently low that limits the deformation and the eventual fracture in the amorphous phase without much involvement of the crystalline phase, brittle-like failure occurs. The former is believed to be responsible for LTBF in #4 HDPE, and the latter for HTBF in #3 HDPE and #4 HDPE. Therefore, the occurrence of LTBF should be due to the sufficiently high stress used for deformation which could occur in all PEs as long as crack is generated before complete disintegration of the crystalline phase. The occurrence of HTBF, on the other hand, is due to weak amorphous phase in PE. When the applied stress is sufficiently low to avoid the crystalline phase involved in the deformation process, fracture is expected to occur eventually in the amorphous phase to result in a brittle-like failure, due to the limited space available for the fracture development.

Activation energy in the Eyring's model is defined as the energy barrier that needs to be overcome for molecular motions [33], and involvement of the two Eyring's processes should be able to distinguish the mechanisms involved in the deformation process. Work by Ward and Wilding [29] has suggested that the process 1 is related to the amorphous phase and process 2 to the involvement of the crystalline phase. Some of the activation energy values reported for PE in the literature are listed in Tab. 3.3, which show the similar order of magnitudes as those listed in Tab. 3.2.

In view that #1 LLDPE and #2 HDPE has significantly larger values of E_1 than the counterpart for #3 HDPE and #4 HDPE, it is believed that the former two PEs have a stronger amorphous phase than the latter two PEs to resist crack development in the amorphous phase before disintegration of the crystalline phase occurs. For E_2 which represents the additional activation energy needed to involve the crystalline phase in the deformation process, Tab. 3.2 suggests that E_2 values for all PEs used in this study are similar, especially for the three co-polymers, and thus resistance of their crystalline phase to deformation should be similar.

Tab. 3.3 Activation energy (in kJ/mol) in literature for deformation of PE using two Eyring's processes.

Reference	Materials	Specimen geometry	Process 1	Process 2
Truss et al. [30]	Linear PE	Dumbbell and cylindrical specimens	146–285	46–180
Truss et al. [34]	HDPE and MDPE	Notched cylindrical specimens	243	100
Sedighiamiri et al. [35]	PE100	Dog-bone and cylindrical specimens	560–1293	110
Taherzadehboroujeni et al. [36]	PE100	Pipe segments and pipe rings	903	108
Jar [32]	PE4710	Notched-pipe-ring specimens	1140	82

3.5 Conclusions

Creep tests were performed on one ethylene homopolymer and three ethylene-hexene copolymers with different mass density. Three failure modes were observed from the creep testing, two brittle failures, LTBF and HTBF, and one ductile failure. Fractographic analysis on the crack initiation sites for the two brittle failures shows micro-fibrillation which is slightly more extensive

for LTBF than for HTBF. The results also suggest that in addition to ductile failure, the Monkman-Grant (MG) relationship is also applicable to LTBF, but not to HTBF.

Norton Power Law (NPL) and Eyring's Law were used to characterize creep behaviour at the secondary stage. The study shows that the NPL cannot fully describe the temperature-independence of activation energy and thus, may not be suitable for modeling creep behaviour of PE. On the other hand, two Eyring's processes that are connected in parallel can provide good characterization of the creep data, indicating three transitions that were observed in this study, i.e. DD transition for #1 LLPDE and #2 HDPE, DB transition for #3 HDPE, and BD and DB transitions for #4 HDPE. In addition, activation energy for process 1 (E_1) of the Eyring's model was found to be significantly higher for #1 LLDPE and #2 HDPE than for #3 HDPE and #4 HDPE, while the activation energy for process 2 (E_2) is similar among the four PEs. Value for E_1 is believed to be related to the strength in the amorphous phase. Since the latter is known to plays a significant role for the occurrence of DB transition, the Eyring's model with two processes could be used to fit the creep test data, and its E_1 value be used to characterize the likelihood of the occurrence of DB transition that has long been a concern for load-carrying application for PE.

References

[1] J. Raghavan, M. Meshii, Creep of polymer composites, Compos. Sci. Technol. 57 (1998) 1673–1688. doi:10.1016/S0266-3538(97)00104-8.

[2] G. Spathis, E. Kontou, Creep failure time prediction of polymers and polymer composites, Compos. Sci. Technol. 72 (2012) 959–964. doi:10.1016/j.compscitech.2012.03.018.

[3] F. Schwarzl, A.J. Staverman, Time-temperature dependence of linear viscoelastic behavior, J. Appl. Phys. 23 (1952) 838–843. doi:10.1063/1.1702316.

[4] A. Frank, W. Freimann, G. Pinter, R.W. Lang, A fracture mechanics concept for the accelerated characterization of creep crack growth in PE-HD pipe grades, Eng. Fract. Mech. 76 (2009) 2780–2787. doi:10.1016/j.engfracmech.2009.06.009.

[5] X. Lu, N. Brown, The ductile-brittle transition in a polyethylene copolymer, J. Mater. Sci. 25 (1990) 29–34. doi:10.1007/BF00544180.

[6] X. Lu, X. Wang, N. Brown, Slow fracture in a homopolymer and copolymer of polyethylene, J. Mater. Sci. 23 (1988) 643–648. doi:10.1007/BF01174699.

[7] P.A. O'Connell, R.A. Duckett, I.M. Ward, Brittle-ductile transitions in polyethylene, Polym. Eng. Sci. 42 (2002) 1493–1508. doi:10.1002/pen.11046.

[8] X. Lu, N. Brown, The transition from ductile to slow crack growth failure in a copolymer of polyethylene, J. Mater. Sci. 25 (1990) 411–416. doi:10.1007/BF00714048.

[9] M. Fleissner, Experience with a full notch creep test in determining the stress crack performance of polyethylenes, Polym. Eng. Sci. 38 (1998) 330–340. doi:10.1002/pen.10194.

[10] M. Parsons, E. V. Stepanov, A. Hiltner, E. Baer, Effect of strain rate on stepwise fatigue and creep slow crack growth in high density polyethylene, J. Mater. Sci. 35 (2000) 1857–1866. doi:10.1023/A:1004741713514.

[11] R.A.C. Deblieck, D.J.M. Van Beek, K. Remerie, I.M. Ward, Failure mechanisms in polyolefines: The role of crazing, shear yielding and the entanglement network, Polymer (Guildf). 52 (2011) 2979–2990. doi:10.1016/j.polymer.2011.03.055.

[12] A.L. Ward, X. Lu, Y. Huang, N. Brown, The mechanism of slow crack growth in polyethylene by an environmental stress cracking agent, Polymer (Guildf). 32 (1991) 2172–2178. doi:10.1016/0032-3861(91)90043-I.

[13] X. Lu, N. Brown, Effect of thermal history on the initiation of slow crack growth in linear polyethylene, Polymer (Guildf). 28 (1987) 1505–1511. doi:10.1016/0032-3861(87)90350-8.

[14] E. Nezbedova, A. Zahradnickova, Z. Salajka, Brittle failure versus structure of HDPE pipe resins, J. Macromol. Sci. Part B. 40 (2001) 507–515. doi:10.1081/MB-100106173.

[15] ISO 16421, Notch tensile test to measure the resistance to slow crack growth of polyethylene materials for pipe and fitting products (PENT), Int. Organ. Stand. (2015).

[16] ISO 16770, Plastics-determination of the environmental stress cracking (ESC) of polyethylene-full-notch creep test (FNCT), Int. Organ. Stand. (2004).

[17] R.K. Krishnaswamy, Analysis of ductile and brittle failures from creep rupture testing of high-density polyethylene (HDPE) pipes, Polymer (Guildf). 46 (2005) 11664–11672. doi:10.1016/j.polymer.2005.09.084.

[18] R.K. Krishnaswamy, Influence of wall thickness on the creep rupture performance of polyethylene pipe, Polym. Eng. Sci. 47 (2007) 516–521. doi:10.1002/pen.20729.

[19] N. Brown, I.M. Ward, The influence of morphology and molecular weight on ductile-brittle transitions in linear polyethylene, J. Mater. Sci. 18 (1983) 1405–1420. doi:10.1007/BF01111960.

[20] F. Vakili-Tahami, M.R. Adibeig, Using developed creep constitutive model for optimum design of HDPE pipes, Polym. Test. 63 (2017) 392–397. doi:10.1016/j.polymertesting.2017.08.040.

[21] N. Tan, P.Y. Ben Jar, Deformation transitions of ethylene-hexene copolymers under creep loading, Polymer (Guildf). 208 (2020) 122905. doi:10.1016/j.polymer.2020.122905.

[22] Y. Zhang, P.Y. Ben Jar, Comparison of mechanical properties between PE80 and PE100 pipe materials, J. Mater. Eng. Perform. 25 (2016) 4326–4332. doi:10.1007/s11665-016-2274-2.

[23] M. Eftekhari, A. Fatemi, Creep behavior and modeling of neat, talc-filled, and short glass fiber reinforced thermoplastics, Compos. Part B Eng. 97 (2016) 68–83. doi:10.1016/j.compositesb.2016.04.043.

[24] M. Amjadi, A. Fatemi, Creep behavior and modeling of high-density polyethylene (HDPE), Polym. Test. 94 (2020) 107031. doi:10.1016/j.polymertesting.2020.107031.

[25] W.E. Luecke, S.M. Wiederhorn, A new model for tensile creep of silicon nitride, J. Am. Ceram. Soc. 82 (1999) 2769–2778. doi:10.1111/j.1151-2916.1999.tb02154.x.

[26] C.J. Gasdaska, Tensilec creep in an in situ reinforced silicon nitride, J. Am. Ceram. Soc. 77 (1994) 2408–2418. doi:10.1111/j.1151-2916.1994.tb04612.x.

[27] Y. Liu, R.W. Truss, A study of tensile yielding of isotactic polypropylene, J. Polym. Sci. Part B Polym. Phys. 32 (1994) 2037–2047. doi:10.1002/polb.1994.090321210.

[28] J.S. Foot, R.W. Truss, I.M. Ward, R.A. Duckett, The yield behaviour of amorphous polyethylene terephthalate: an activated rate theory approach, J. Mater. Sci. 22 (1987) 1437–1442. doi:10.1007/BF01233145.

[29] I.M. Ward, M.A. Wilding, Creep behavior of ultrahigh-modulus polyethylene: influence of draw ratio and polymer composition, J. Polym. Sci. Polym. Phys. Ed. 22 (1984) 561–575. doi:10.1002/pol.1984.180220403.

[30] R.W. Truss, P. L. Clarke, R. A. Duckett, I. M. Ward, The dependence of yield behavior on temperature, pressure, and strain rate for linear polyethylenes of different molecular weight and morphology, J. Polym. Sci. Polym. Phys. Ed. 22 (1984) 191–209. doi:10.1002/pol.1984.180220205.

[31] F. Povolo, Comments on the monkman-grant and the modified monkman-grant relationships, J. Mater. Sci. 20 (1985) 2005–2010. doi:10.1007/BF01112283.

[32] P.Y. Ben Jar, Revisiting creep test on polyethylene pipe—Data analysis and deformation mechanisms, Polym. Eng. Sci. 61 (2021) 586-599. doi:10.1002/pen.25603.

[33] S.S. Yeo, Y.G. Hsuan, Evaluation of creep behavior of high density polyethylene and polyethylene-terephthalate geogrids, Geotext. Geomembr. 28 (2010) 409–421. doi:10.1016/j.geotexmem.2009.12.003.

[34] R.W. Truss, R.A. Duckett, I.M. Ward, Effect of hydrostatic pressure on the yield and fracture of polyethylene in torsion, J. Mater. Sci. 16 (1981) 1689–1699. doi:10.1007/BF02396889.

[35] A. Sedighiamiri, L.E. Govaert, M.J.W. Kanters, J.A.W. Van Dommelen, Micromechanics of semicrystalline polymers: yield kinetics and long-term failure, J. Polym. Sci. Part B Polym. Phys. 50 (2012) 1664–1679. doi:10.1002/polb.23136.

[36] M. Taherzadehboroujeni, R. Kalhor, G.B. Fahs, R.B. Moore, S.W. Case, Accelerated testing method to estimate the long-term hydrostatic strength of semi-crystalline plastic pipes, Polym. Eng. Sci. 60 (2020) 879–888. doi:10.1002/pen.25087.

Chapter 4 Determining deformation transition in polyethylene under tensile loading

In this chapter, a multi-relaxation (MR) test is developed based on the concept that stress relaxation behaviour can be used to reflect the material state of polyethylene (PE) under tension. Based on this concept, critical stroke for the onset of plastic deformation in the crystalline phase, named the 1st critical stroke, is determined using the MR test. Results from wide angle X-ray scattering suggest that phase transformation occurs in the crystalline phase of PE after the specimen is stretched beyond the 1st critical stroke. In this work, the MR test is applied to six PEs of different mass densities to determine their 1st critical strokes and the corresponding total and quasi-static (QS) stress values. The results show that the 1st critical stroke has very similar values among the six PEs. More interestingly, ratio of the QS stress at the 1st critical stroke to the yield stress from the standard tensile test shows little dependence on PE density. Therefore, it is possible to use the popular short-term tensile test to characterize the critical QS component of the applied stress to initiate plastic deformation in the crystalline phase, which is expected to play a significant role on the long-term, load-carrying applications of PE.

4.1 Introduction

Polyethylene (PE) is a family of commodity polymers with excellent durability, light weight [1-3], and relatively low cost. These advantages have attracted applications in many areas, ranging from plastic pipes for water and gas transportation to containers and film for materials packaging. For PE used in load-bearing applications, the main concern is about PE's time-, temperature- and strain-rate-dependent mechanical properties [4-6]. This issue is further complicated by the semi-crystalline nature of PE's microstructure which has crystalline and amorphous phases mingled in a lamellar arrangement. Although both phases are involved from the beginning of the deformation process, their role of involvement varies with the applied stress level [5]. A widely accepted concept is that deformation of PE is initially dominated by the amorphous phase, due to its relatively low resistance to deformation [7]. The crystalline phase is involved at this stage through inter-lamellar shear, inter-lamellar separation and lamellar stack rotation [7-10], of which the contribution depends on the loading mode and the stress level. In an engineering stress-stroke curve from tensile loading, PE is known to yield at the peak point, at which the lamellar structure starts to disintegrate. Necking occurs after the yielding, which from the microstructural viewpoint, is a process that transforms lamellae to fibril clusters.

Strobl and co-workers have characterized the mechanism transition in the above deformation process using four critical strains, of which the first two occur before the drastic disintegration of the lamellae [5, 11-14]. The first critical strain is suggested to have a value of around 0.04, at which local yielding starts in the crystalline phase. In other words, the first critical point for deformation transition is for the onset of plastic deformation in the crystalline phase. The second critical point, defined by the Strobl's group as the point with the maximum curvature on

the true stress-strain curve, represents the onset of the collective slipping in the crystalline phase, which is dominated in PE by the slip system of (100) plane in [001] direction [15-19]. Note that the corresponding point in the standard tensile test, which is usually conducted at a constant crosshead speed, is the peak point on the engineering stress-stroke curve.

Following the above work, a mechanical test, named multi-relaxation (MR) test, is developed to detect transition from the amorphous-phase-dominant deformation to the involvement of the crystalline phase in PE. The MR test contains multiple stress relaxation stages at different strokes. In view that a relatively small stroke is required to reach the critical point for the above mechanism transition and that for a given specimen geometry stroke and strain at such a small deformation level should follow a one-to-one relationship, stroke is used here, rather than strain, to quantify the deformation level introduced to the specimen. This paper gives details of analysis used to determine the critical stroke for the mechanism transition. Since transition from amorphous-phase-dominant deformation to that involving plastic deformation in the crystalline phase is the 1st transition detectable by the MR test, this point is denoted as the 1st critical point hereafter. Analysis presented here is based on a standard viscoelastic model in which the applied stress (named total stress) is divided into the time-independent, quasi-static (QS) component and the time-dependent, viscous component. In addition, this paper compares six PEs of different mass density for their stress and stroke for the 1st critical point. Wide-angle X-ray scattering (WAXS) is used to examine the change of the crystalline phase in the six PEs, before and after the stroke for the 1st critical point is reached.

4.2 Multi-relaxation (MR) test

Concept for the MR test is similar to that proposed by Hong et al. [14], which is to use the stress relaxation behaviour to characterize material state of PE during the tensile deformation. Transition of deformation mechanisms is detected through the change of stress relaxation behaviour. The main difference between MR test and that used by Hong et al. is that the former uses single specimen for all stress relaxation stages, while the latter uses multiple specimens, one for each stress relaxation stage. The latter approach was also used in our previous work on PE pipe specimens [20], from which critical deformation for the mechanism transition was found to be consistent with that using MR test on single specimen [21]. However, the use of single specimen has the advantage of avoiding inconsistency in the stress decay during stress relaxation which can be caused by for example, dimensional inconsistency among specimens. Note that our preliminary study has found that even through waterjet cutting, specimen width may vary up to 3% along the gauge section, and the width variation profile may not be consistent among specimens from the same batch. Moreover, the MR test takes the advantage of the computer control function that is available in the test machine. Therefore, all stress relaxation stages can be conducted with the minimum interference from the operator.

Analysis of the MR test results is based on a standard, viscoelastic model shown in Fig. 4.1, in which the upper branch represents the time-dependent viscous stress response to deformation and consists of a spring and a damper. The lower branch, on the other hand, represents the QS stress response and contains only a spring. As expressed in Eq. (4.1), the applied stress (σ_A), also referred to as the total stress (σ_t), is summation of the viscous stress component ($\sigma_r(t)$) and the QS stress component (σ_{st}):

$$\sigma_{\mathrm{A}} = \sigma_{\mathrm{r}}(t) + \sigma_{\mathrm{st}} \tag{4.1}$$

According to the model in Fig. 4.1, decay of total stress ($\Delta\sigma_{\mathrm{t}}$) comes from the change of viscous stress ($\Delta\sigma_{\mathrm{r}}$) which is equal to the change of the applied stress during the stress relaxation, as shown in the expression below:

$$\Delta\sigma_{\mathrm{t}} = \Delta\sigma_{\mathrm{r}} = \sigma_{\mathrm{r}}(0) - \sigma_{\mathrm{r}}(t) = \sigma_{\mathrm{A}}(0) - \sigma_{\mathrm{A}}(\mathrm{t}) \tag{4.2}$$

where *t* is time measured from the beginning of each stress relaxation stage.

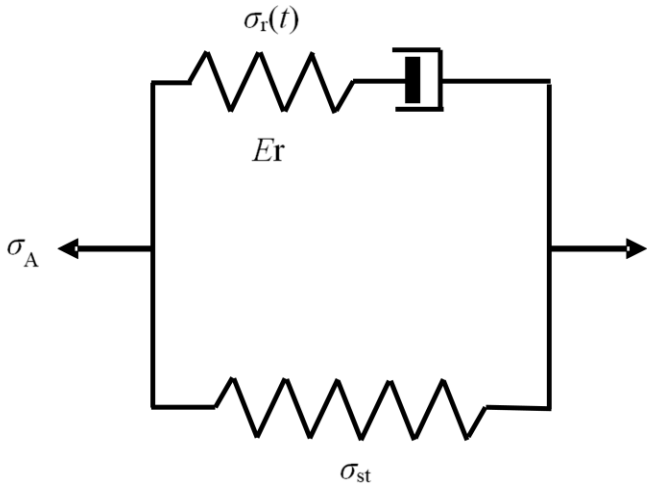

Fig. 4.1 Schematic diagram of the standard, visco-elastic model used in this work.

Following the assumption given in Ref. [14], the Eyring's Law of viscosity [22-24] is adopted to govern the stress response to deformation of the damper:

$$\frac{\sigma_{\mathrm{r}}}{\sigma_0} = \sinh^{-1}\frac{\dot{\varepsilon}_{\mathrm{D}}}{\dot{\varepsilon}_0} \tag{4.3}$$

with

$$\sigma_0 = \frac{RT}{V} \tag{4.4}$$

where σ_{r} is the stress applied to the damper, $\dot{\varepsilon}_0$ the reference strain rate, $\dot{\varepsilon}_{\mathrm{D}}$ the strain rate of the damper, σ_0 the reference stress, R the Boltzmann constant, T the absolute temperature, and V the activation volume. Since two branches of the model in Fig. 4.1 have the same strain and their value should remain constant during the stress relaxation, based on interaction between spring and damper in the viscous branch we have:

$$\dot{\varepsilon}_0 \sinh\frac{\sigma_{\mathrm{r}}}{\sigma_0} + \frac{1}{E_{\mathrm{r}}}\frac{\mathrm{d}\sigma_{\mathrm{r}}}{\mathrm{d}t} = 0 \tag{4.5}$$

where E_{r} is modulus for the spring in the viscous branch.

The above expression can also be expressed as:

$$\frac{1}{\sigma_0}\frac{\mathrm{d}\sigma_\mathrm{r}}{\mathrm{d}t} = -\frac{1}{\tau_\mathrm{r}}\sinh\frac{\sigma_\mathrm{r}}{\sigma_0} \tag{4.6}$$

with

$$\frac{1}{\tau_\mathrm{r}} = \dot{\varepsilon}_0\frac{E_\mathrm{r}}{\sigma_0} \tag{4.7}$$

where τ_r is the relaxation time, which following the work by Hong et al. [14], is given a constant value of 16,000 seconds for all stress relaxation stages. Stress decay ($\Delta\sigma_\mathrm{r}$) during the stress relaxation can be derived from Eq. (4.6), as shown in the following expression:

$$\Delta\sigma_\mathrm{r} = \sigma_\mathrm{r}(0) - 2\sigma_0\tanh^{-1}\left[\tanh\left(\frac{\sigma_\mathrm{r}(0)}{2\sigma_0}\right)\exp\left(-\frac{t}{\tau_\mathrm{r}}\right)\right] \tag{4.8}$$

Values for $\sigma_\mathrm{r}(0)$ and σ_0 in Eq. (4.8) are chosen so that curve generated from the equation matches the stress decay determined from the MR test. Once $\sigma_\mathrm{r}(0)$ and σ_0 values are determined, σ_st value can then be calculated from Eq. (4.1). Note that in this work, σ_st value is simply an approximation of the real QS stress at a given stroke, since the stress drop did not show any plateau at the end of each stress relaxation stage. Similarly, the corresponding $\sigma_\mathrm{r}(0)$ value is different from that determined from specimens subjected to single stress relaxation stage, in view that the $\sigma_\mathrm{r}(0)$

value is dependent on the deformation history. Nevertheless, $\sigma_r(0)$ and σ_{st} values determined from these MR tests can be used to indicate the trend of change of these values as functions of stroke.

Fig. 4.2 presents examples of the best match between the experimental measurements from different stress relaxation stages and the corresponding curves generated from Eq. (4.8). Fig. 4.2(a) is a plot based on the linear time scale, and Fig. 4.2(b) on the logarithmic time scale. The legends represent strokes used for the stress relaxation stages. As shown in Fig. 4.2, the curves generated from Eq. (4.8) do not match the experimental measurements for the entire stress relaxation period. Bartczak [25] has suggested to use at least two sets of Eyring's parameters to fit the experimental measurements for the entire stress relaxation period. In this work, however, only one set of Eyring's parameters was used for the curve fitting, to match the stress drop mainly in the timeframe above 1,000 seconds, as shown in Fig. 4.2(b). This is because, firstly, such a curve-fitting process is simple and can be used to determine σ_{st} values close to the real QS stresses. Secondly, using one set of Eyring's parameter has no effects on the relative change of σ_0 which is used to identify the stroke for the 1st critical point. Through this curve-fitting process, variations of σ_0 and σ_{st} are established as functions of stroke. It is worth to point out that as shown in Eq. (4.4), variation of σ_0 is independent of τ_r value used for the curve fitting. Therefore, the use of σ_0 to determine the stroke for the 1st critical point can avoid any unwanted influence from the assumption of constant relaxation time on the characterization of stress relaxation behaviour at all stages.

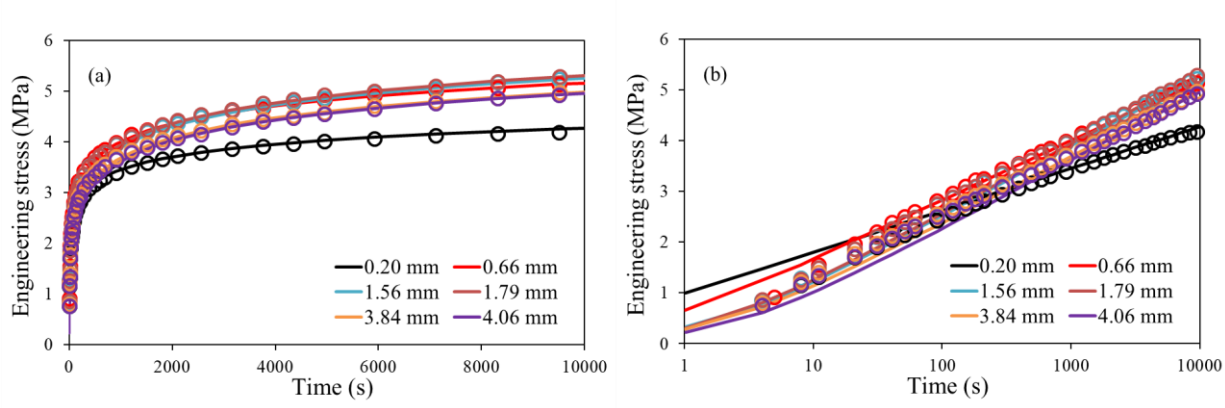

Fig. 4.2 Examples of stress drop obtained from the MR tests (open circles) and generated based on Eq. (4.8) (solid lines) for all stress relaxation stages: (a) with time in the linear scale, and (b) with time in the logarithmic scale.

4.3 Experimental details

4.3.1 Materials and specimen dimensions

Six types of PE are used in the study. As shown in Table 1, these PEs include one linear low-density PE (LLDPE) (#1), and five high-density PEs (HDPE) (#2 to #6) among which density for #2 is close to the lower end of HDPE, #4 close to the upper end, and #3, #5 and #6 in between. Tab. 4.1 also provides their yield strength from standard tests, melt index, and co-monomer type. All PEs are in the form of compression-molded plaques of 17.5 × 17.5 cm^2 in size and 3 mm in the nominal thickness, all from ExxonMobil Chemical provided by Imperial Oil. As commercial resins, their molecular weight and molecular weight distribution are not available. Specimens used for the mechanical testing have a modified dog-bone geometry, as depicted in Fig. 4.3, machined from the PE plaques. Choosing such geometry and dimensions in the gauge section is because of the limited space available in the sample holder of the X-ray diffraction system used for the WAXS

experiments. The sufficiently large end tabs are required to maintain the deformation in the gauge section after removing the specimen from the universal test machine. An in-house-designed insert is applied in the gauge section to maintain the deformation during the WAXS experiments, as to be described in Section 4.3.3.

Tab. 4.1 Material characteristics of PEs used in the study.

Material	Density (g/cc)	Yield strength (MPa)	Melt Index (g/10 min) at 190 °C/2.16 Kg	Molecular weight distribution	Co-monomer
#1 LLDPE	0.938	19.0	3.3	Unimodal	Hexene
#2 HDPE	0.941	22.0	2.0	Unimodal	Hexene
#3 HDPE	0.952	27.1	6.7	Unimodal	Hexene
#4 HDPE	0.965	31.4	8.2	Unimodal	-
#5 HDPE	0.954	27.7	0.3	Unimodal	Butene
#6 HDPE	0.957	29.2	0.46	Bimodal	Hexene

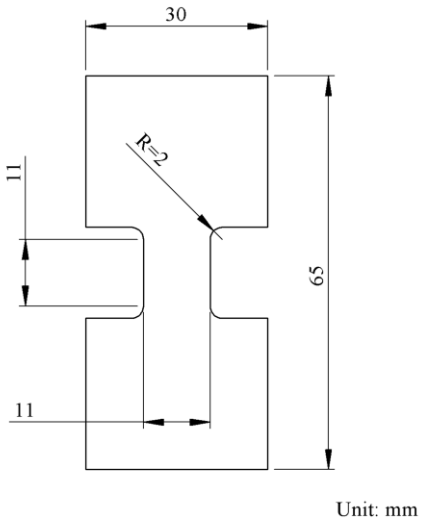

Fig. 4.3 Geometry and dimensions of the modified dog-bone specimens.

4.3.2 Multi-relaxation (MR) test

MR tests were conducted at room temperature using a universal test machine (Qualitest Quasar 100), with the test program and data acquisition controlled by a personal computer. Crosshead speed for the loading stages was 5 mm/min, to introduce a stroke increment of around 0.22 mm, followed by a stress relaxation stage with the stroke fixed. Each stress relaxation stage lasted for 10,800 seconds (3 hours) during which load was recorded as a function of time. Specimens of #4 HDPE fractured at a stroke around 3 mm. All other PEs showed no sign of fracture initiation at strokes above 7 mm, around which the tests were ended. Two specimens were tested for each PE, to ensure repeatability of the test results.

4.3.3 Wide-angle X-ray scattering (WAXS)

One dimensional (1D) WAXS experiments were conducted using a Bruker D8 Discover Diffraction System with Cu-source. Data were collected using a LynxEYE 1-D detector at a scanning speed of 0.8 deg/min, and in the angular range (2θ) from 10 to 64 degrees to cover most of the detectable peaks for PE. Fig. 4.4 gives a schematic diagram of the sample setup for the WAXS experiments.

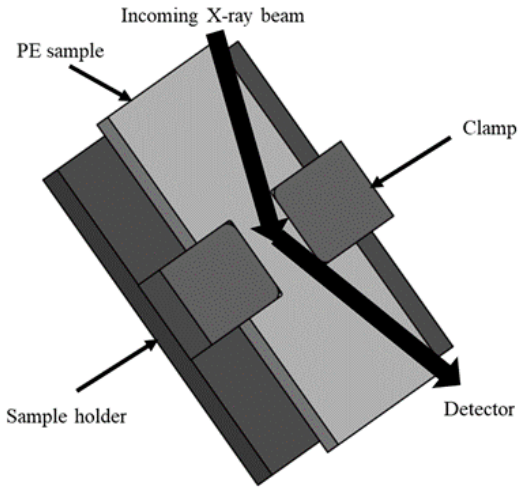

Fig. 4.4 Schematic description of the set-up for the WAXS experiment.

Each of the specimens for the WAXS experiments was firstly stretched to a pre-determined stroke using the same test set-up as that used for the MR test, except that at the end of the stretch, an in-house-designed and 3D-printed insert was used to maintain the stretch in the gauge section before the specimen was removed from the universal test machine. The assembly of specimen and insert, as shown in Fig. 4.4, was then scanned using X-ray within 20 minutes after the removal of the specimen from the test machine. Note that as suggested in Refs. [26, 27], deformation of PE could cause conversion of its lamellar crystals from orthorhombic to monoclinic structures, and the conversion could be reversed if the deformation was removed. Therefore, the insert was used to maintain the deformation level during the X-ray scanning. In this study, the stroke range used in MR tests for the WAXS experiments was to cover the stroke for the 1st critical point, so that the X-ray spectrum could confirm whether change of the crystalline structure occurred around the 1st critical point.

It should be noted that penetration depth of X-ray beam varies with diffraction angle, especially in the reflection mode shown in Fig. 4.4. The depth variation, in return, affects the collected peak intensity [28]. However, such variation is minimized by comparison of intensity from the diffraction peak at the same angle.

Two specimens from each type of PE were used for the WAXS experiments. Each specimen was used to obtain WAXS spectra at 3 different strokes, for totally 7 strokes (including the undeformed state). Total time to complete all WAXS spectra for one type of PE was about 9 hours. Therefore, all WAXS tests for each type of PE could be completed in one day. Note that all WAXS spectra presented here have already had the machine background removed, which was carried out following the procedure recommended for the machine.

4.4 Results and discussion

4.4.1 MR test

Fig. 4.5 presents typical results from the MR test for the six PEs. Fig. 4.5 summarizes plots of total stress at the beginning of each stress relaxation stage, as a function of stroke used for the stress relaxation. The peak point, corresponding to yielding of the specimen, is highlighted in the figure using open blue boxes, all in the range from 2 to 2.7 mm. Some curves, such as that for #2 HDPE, contain a secondary, relatively shallow peak at a stroke above 3 mm. Such a peak is quite common for PEs with side chain branches in the PE molecules. Work in Refs. [29, 30], based on dynamic mechanical analysis, has suggested that higher the branch density in the PE molecules, more significant the secondary peak appears. Significance of such a peak is also affected by the cooling process when making plaques from PE pellets.

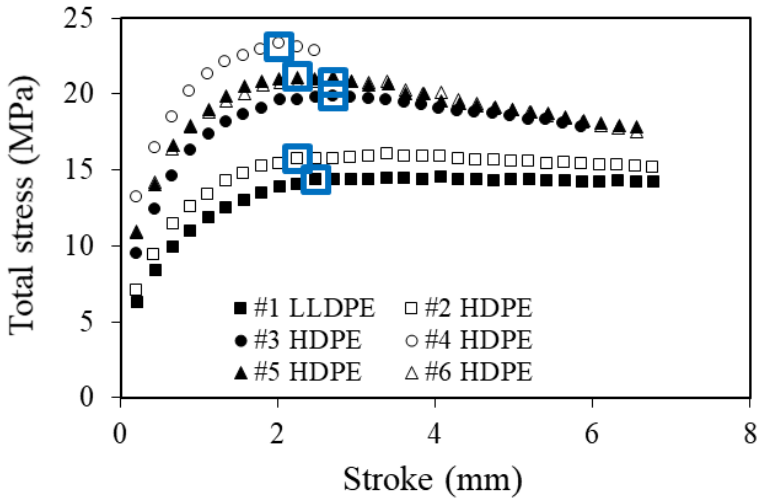

Fig. 4.5 Typical curves from the MR test, of total stress versus stroke with the total stress measured at the beginning of each stress relaxation stage, in which peak points are highlighted using open blue boxes.

Note that all PE specimens, except those of #4 HDPE, showed a clear necking behaviour at the end of the MR test, at a stroke around 7 mm. As mentioned earlier, specimens of #4 HDPE had a premature fracture at a stroke around 3 mm, without any indication of neck development.

Data from the stress relaxation stages were analyzed following the curve-fitting process described in section 2, in which $\sigma_r(0)$ and σ_0 values were used as fitting parameters to generate a curve based on Eq. (4.8), with $\tau_r = 16{,}000$ seconds, to fit the experimentally measured time function of the stress decay, $\Delta\sigma_r$. Critical point for the change of trend line in the σ_0-stroke curve was then used to determine the stroke for the 1st critical point. Fig. 4.6(a) presents two examples of the σ_0-stroke curves obtained from this study, both from #2 HDPE. The top curve shows a gradual increase of σ_0 with the increase of stroke till a plateau is reached. This is a typical curve for all PEs used in the study. Occasionally, a small drop of σ_0 appeared after its initial linear increase with the increase of stroke, as shown in the bottom curve of Fig. 4.6(a). Cause for such a small drop of σ_0

is not clear at this stage, but its appearance did not affect the general trend line of σ_0 versus stroke afterwards. Therefore, stroke for the 1st critical point was determined based on the intersection of two trend lines, one for the initial, linear increase of σ_0 with stroke and the other the horizontal line which represents the σ_0 value in the plateau region. In this way, possible inconsistency of the critical stroke values due to the presence of a small drop of σ_0 could be avoided. As depicted in Fig. 4.6(a), critical strokes from the two curves have very similar values.

Fig. 4.6(b) summaries σ_0-stroke plots, one for each PE used in the study. The 1st critical points are highlighted using open red circles, determined based on the approach depicted in Fig. 4.6(a). For comparison, the points corresponding to specimen yielding are also highlighted in Fig. 4.6(b) using open blue boxes. The data suggest that among the six PEs, strokes for the 1st critical point have better consistency than those for the yield point. The corresponding σ_{st} values at the beginning of each stress relaxation stages are summarized in Fig. 4.6(c). Similarly, the 1st critical points and yield points are highlighted in this figure using open red circles and open blue squares, respectively. It is interesting to point out that as shown in Fig. 4.6(c), peak σ_{st} values are only about 50-60% of the peak values of total stress shown in Fig. 4.5, suggesting that even with several stress relaxation stages before reaching the peak point, the applied stress still has a significant viscous stress component.

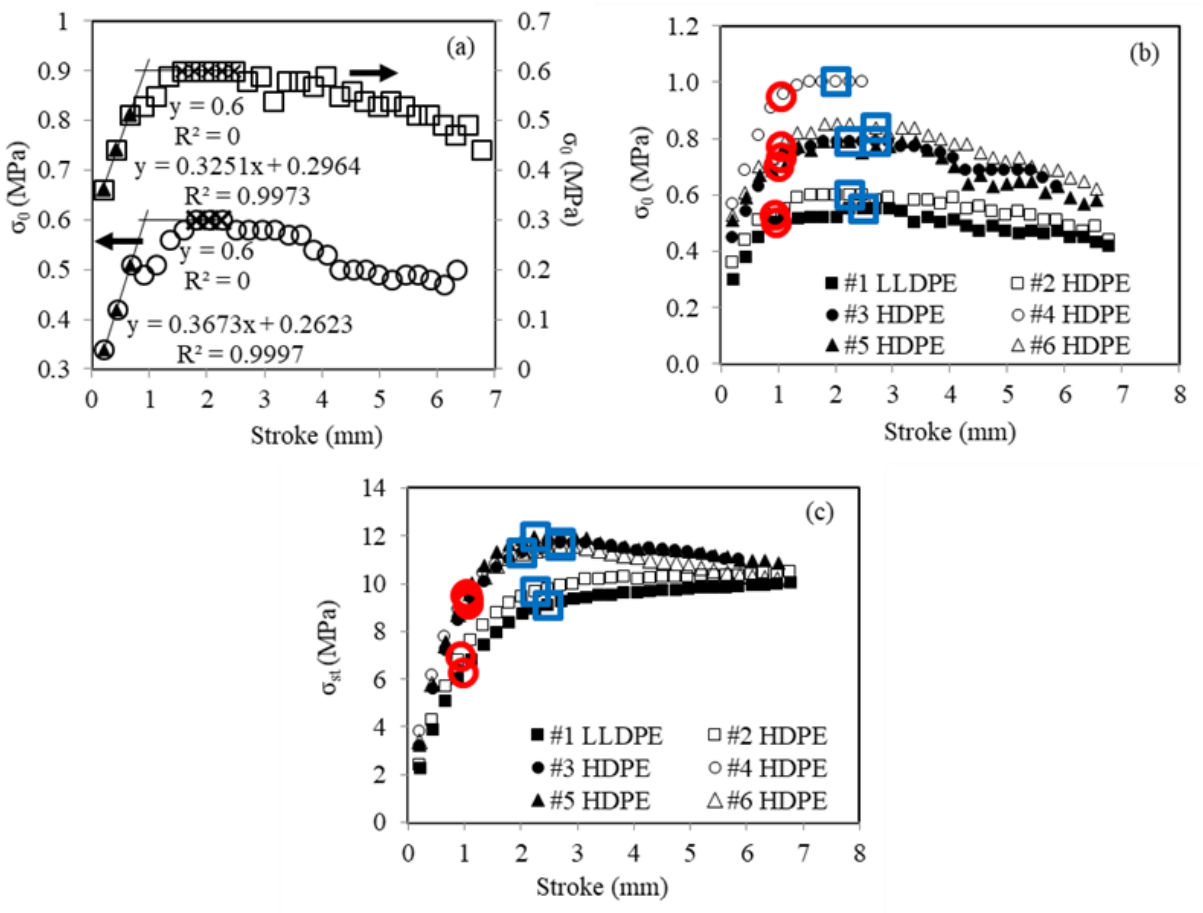

Fig. 4.6 Summary of MR test results: (a) sample curves showing the approach used to determine the stroke for the 1st critical point, (b) typical variation of σ_0 with stroke, (c) typical variation of σ_{st} with stroke (highlighted open red circles and open blue boxes indicate the 1st critical point and the yield point, respectively).

4.4.2 WAXS

Fig. 4.7 presents typical WAXS spectra obtained from PE specimens used in the study. Spectra in the figure are all from #2 HDPE, stretched to different strokes. Two major peaks, labelled (110) and (200), at 2θ of 21.6° and 24.0°, respectively, are from the orthorhombic structure [31, 32]. Stroke for each spectrum is not provided in the figure in order to maintain clarity of the

curves. The general trend of change among the curves in Fig. 4.7 is that peak intensity for (110) decreases with the increase of stroke, but the opposite trend for (200) (i.e., increase with the increase of stroke). In addition, a minor peak, as indicated by an arrow on the right shoulder of (200) peak, has peak intensity increase with increase of the stroke above a critical value which will be discussed later in this section. As suggested in Refs. [8, 27, 33-35], growth of this small peak is due to the development of a monoclinic structure which is known to exist in PE under tensile deformation.

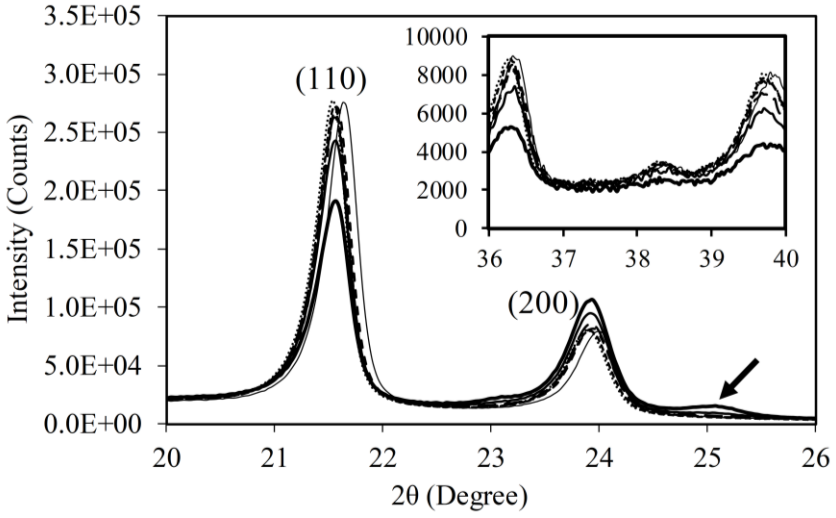

Fig. 4.7 Typical WAXS spectra with different strokes (from #2 HDPE) (Peak intensity for (110) decreases with increase of stroke applied to specimens).

The insert in Fig. 4.7 presents collection of spectra in the 2θ range from 36° to 40°, in which the peak intensity also decreases with the increase of stroke. However, intensity level for spectra in the insert of Fig. 4.7 is much lower than that for the two major peaks. Furthermore, change of the intensity for peak (200) is less significant than that for peak (110), and work reported

in Refs. [8, 36], for PEs different from those used here, shows little sensitivity of the intensity for peak (200) to the deformation change. Therefore, the following discussion is based on the change of intensity for peak (110), at 2θ of 21.6°.

Fig. 4.8 summarizes the intensity variation for peak (110) as a function of stroke used to stretch the specimens. At small strokes, the peak intensity is relatively constant, showing little dependence on the stroke, but when the stroke is sufficiently large, the peak intensity decreases noticeably with the increase of stroke. As a result, Fig. 4.8 indicates that the change of peak intensity goes through a transition. Critical stroke for the transition was determined based on the assumption that the peak intensity remains constant below the critical stroke, but above it, decreases linearly with the increase of stroke. The critical stroke for each PE is presented in Fig. 4.8 using an open circle, with the corresponding stroke value given under an arrow that points to the open circle. Fig. 4.8 suggests that the critical stroke for the onset of degradation in the orthorhombic crystalline structure can be detected using change in intensity of peak (110), and the extent of degradation increases with the increase of stroke. However, Fig. 4.8 suggests significant variation of the critical stroke values for the six PEs, which is different from that shown in Fig. 4.6 (represented by open red circles).

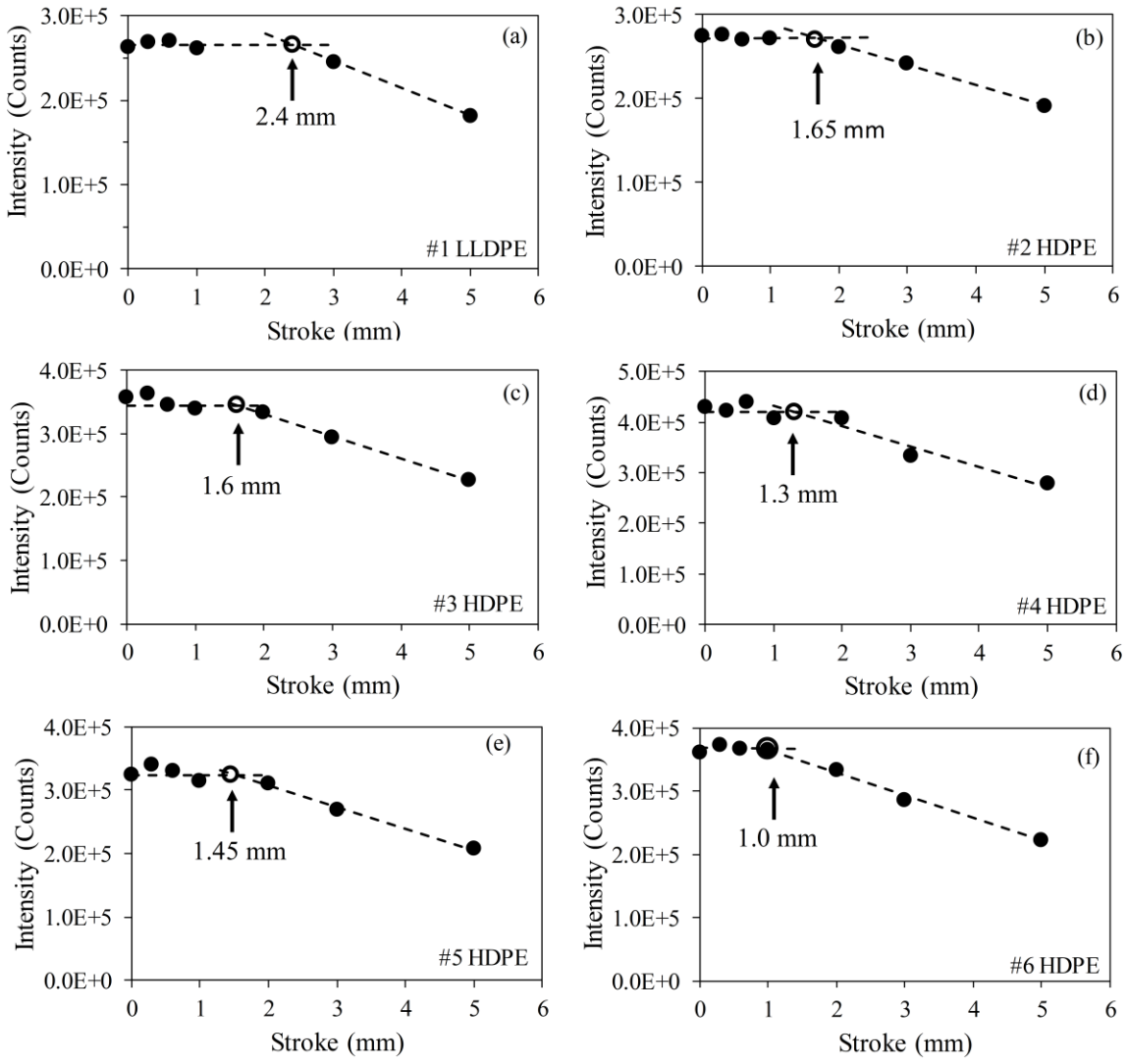

Fig. 4.8 Absolute intensity of peak (110) from the orthorhombic structure of PE, as a function of stroke used to stretch the specimens.

To resolve the issue of different critical stroke values given in Figs. 4.6 and 4.8, critical strokes determined from the WAXS spectra and those from the MR tests are summarized in Fig. 4.9, plotted as a function of PE density. Note that PE density is used here as a material parameter for convenience. Other parameters, such as degree of crystallinity from WAXS spectra [7, 37],

could also be used to represent material characteristics. However, our analysis has shown that values for the degree of crystallinity are linearly proportional to the values for PE density. Therefore, trend line of the dependence of test results on PE density should be the same as that on degree of crystallinity. In the following discussion, the former parameter is selected as the material parameter.

Fig. 4.9 suggests that the critical strokes from the WAXS experiment are either larger than or equal to (for #6 HDPE, with PE density of 0.957 g/cc) the stroke for the 1st critical point from the MR test. Note that stroke used in Fig. 4.8 represents dimension of the insert used to maintain the specimen deformation during the WAXS experiments. However, the maximum stroke required to place the insert in the specimen was always larger than the insert dimension, and the amount of extra stroke required varied among the PE specimens. Therefore, critical stroke values determined from Fig. 4.9 may have a bigger uncertainty than that determined from the MR test for which single specimen was used, with stroke resolution of the test machine being better than 0.01 mm. Since Fig. 4.9 suggests that none of the critical stroke values from WAXS spectrum is smaller than that determined from the MR test, it is believed that critical stroke values determined from the MR test represent the lower bound of the possible critical stroke values determined from the WAXS spectrum, and that the critical stroke values from the MR test are more reliable than those from the WAXS spectrum for quantifying the deformation level required to start plastic deformation in the crystalline phase of PE. Nevertheless, the WAXS experiments provide a plausible evidence to support that the stroke for the 1st critical point, determined from the MR test, represents the onset of plastic deformation in the crystalline phase of PE.

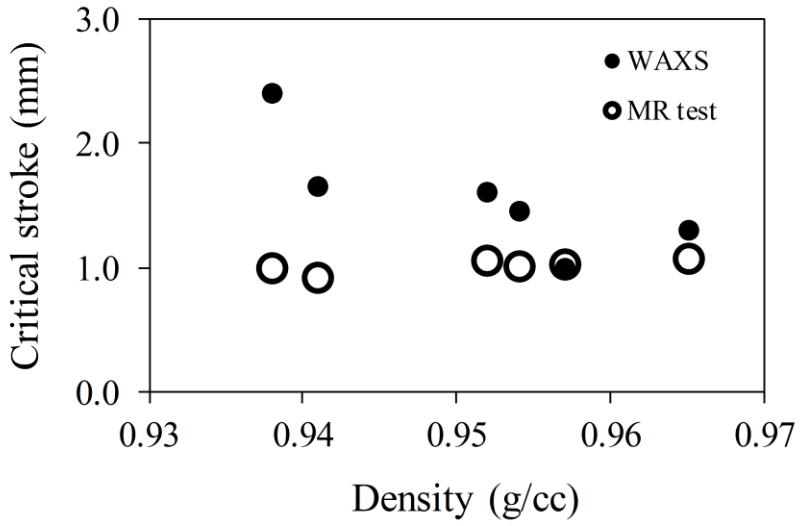

Fig. 4.9 Comparison of critical strokes in Fig. 4.8 and those for the 1st critical point from the MR test.

4.4.3 Discussion

Using the standard visco-elastic model shown in Fig. 4.1, total stress, σ_t, applied to PE in the MR test can be divided into the time-independent component, σ_{st}, and the time-dependent component, $\sigma_r(t)$. Based on change of the trend line for σ_0, critical strokes for the local and global plastic deformation of the crystalline phase, i.e., the 1st critical point and the yield point, respectively, were identified, and their corresponding σ_{st} values determined.

Fig. 4.10 depicts plots of σ_t (squares) and σ_{st} (circles) at the 1st critical point (solid symbols) and yield point (open symbols) determined from the MR tests, and yield strength values listed in Tab. 4.1 (σ_{yld}-mono, open diamonds) which were determined using standard test. The figure shows that all stress values that include viscous and quasi-static components, i.e., σ_{yld}-mono, σ_t-yield, and σ_t-1st, show a relatively linear relationship with PE density. However, the corresponding σ_{st} values

determined from the MR test, i.e., σ_{st}-yield and σ_{st}-1st, show a nonlinear relationship with PE density.

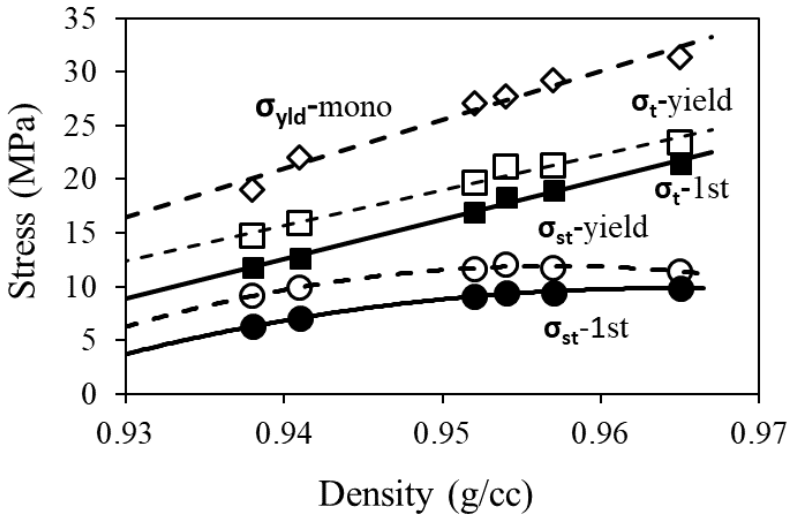

Fig. 4.10 Summary of σ_{st} and σ_t values at the 1st critical point and yield point from the MR tests (σ_{st}-1st, σ_{st}-yield, σ_t-1st, and σ_t-yield), and yield strength listed in Tab. 4.1 (σ_{yld}-mono), plotted as functions of PE density.

As shown in Fig. 4.10, the linear relationship between σ_t at the yield point and PE density is similar to that for σ_{yld}-mono, which is consistent with the common belief that yield strength for PE follows a close to linear relationship with PE density [38]. Such a linear relationship also exists for σ_t at the 1st critical point, as shown by the curve of σ_t-1st in Fig. 4.10. However, the figure also suggests that the relationship between σ_{st} and PE density is non-linear, at both the 1st critical point and the yield point. This could be caused by the assumption of constant τ_r value of 16000 sec in the Eyring's model for the entire deformation process, as σ_{st} value required for Eq. (4.8) to fit the experimental curve is known to vary with the τ_r value. Therefore, further investigation to allow τ_r

to vary with stroke is needed to verify whether the relationship between σ_{st} and PE density is indeed non-linear, as suggested by Fig. 4.10. Nevertheless, using constant τ_r is sufficient for our purpose at this stage. Our on-going study is to find a way to make τ_r as a free parameter in the curve fitting process.

In addition to the nonlinear relationship between σ_{st} and PE density, this study also discovered a possible linear relationship between stress ratio and PE density. Fig. 4.11 presents the stress ratio of σ_{st} at the 1st critical point (σ_{st}-1st) to the yield strength listed in Tab. 4.1 (σ_{yld}-mono), plotted as a function of PE density. The figure suggests that this stress ratio is nearly constant among six PEs used in the study, showing little dependence on the PE density. This phenomenon sheds a light on the possibility of using short-term test to determine the time-independent stress component, σ_{st}, which at this stage cannot be correctly measured using any standard test.

In view that σ_{st}-1st represents the critical QS stress to initiate local plastic deformation in the crystalline phase of PE, its value could play a significant role on the long-term performance of PE, especially for load-carrying applications. The possibility of using a short-term test to determine σ_{st}-1st value, as indicated in Fig. 4.11, will greatly benefit the industry for a quick evaluation of the long-term performance of PE. Study to address the above issues is important to confirm such a possibility, and is planned when this manuscript is prepared.

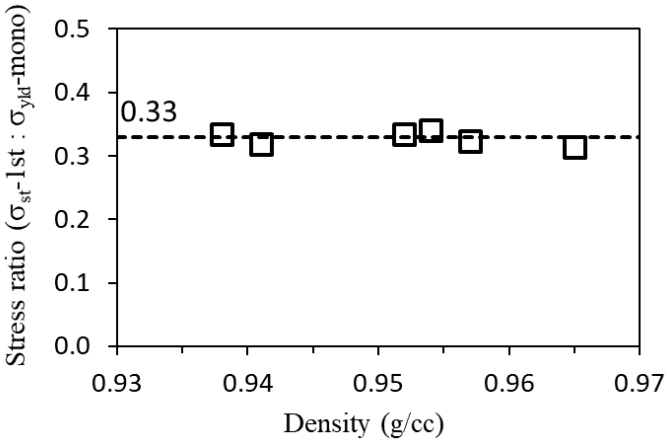

Fig. 4.11 Ratio of σ_{st} at the 1st critical point from the MR test (σ_{st}-1st) to yield stress from the standard tensile test (σ_{yld}-mono) listed in Tab. 4.1, plotted as a function of PE density.

4.5 Conclusions

A new, multi-relaxation (MR) test method is developed and applied to six PEs of different densities, to determine their critical points for the transition from the amorphous-phase-dominant deformation to the involvement of the crystalline phase. The critical stroke level for the onset of local plastic deformation in the crystalline phase, named the 1st critical point, has been identified for the six PEs. These critical stroke values were found to be nearly constant and independent of the PE density. All of these phenomena are consistent with those reported in the past, using similar analysis but based on test results from multiple specimens [14, 20]. WAXS experiments were conducted to examine change of the crystal structure at the 1st critical point. The WAXS spectra confirmed that after reaching the stroke for the 1st critical point, intensity for the (110) peak shows a significant decrease with the increase of stroke.

Through the study on six PEs, it was discovered that the σ_{st} component for the 1st critical point does not show a linear relationship with PE density, in contrast to the yield stress measured from the standard test.

This study also discovered that the stress ratio of σ_{st}-1st to σ_{yld}-mono from the standard test shows a nearly constant value, independent of PE density. Since the long-term, load-carrying performance of PE should be based on its σ_{st} value, the nearly constant ratio of σ_{st}-1st to σ_{yld}-mono indicates the possibility of using short-term test to evaluate PE's long-term performance, but further investigation is needed.

Overall, the study provides some insights on the time-independent mechanical properties of PE and the associated mechanisms for deformation. We intend to apply the information to evaluation of PE, in order to explore practical benefits of the MR test on characterization of PE's long-term, load-carrying performance.

References

[1] A. Peacock, Handbook of polyethylene: structures, properties, and applications, CRC press, New York, 2000. doi:10.1201/9781482295467.

[2] D. Li, H. Garmestani, S.R. Kalidindi, R. Alamo, Crystallographic texture evolution in high-density polyethylene during uniaxial tension, Polymer (Guildf). 42 (2001) 4903–4913. doi:10.1016/S0032-3861(00)00829-6.

[3] Y. Zhang, P.Y. Ben Jar, Phenomenological modelling of tensile fracture in PE pipe by considering damage evolution, Mater. Des. 77 (2015) 72–82. doi:10.1016/j.matdes.2015.04.011.

[4] S. Humbert, O. Lame, J.M. Chenal, C. Rochas, G. Vigier, New insight on initiation of cavitation in semicrystalline polymers: in-situ SAXS measurements, Macromolecules. 43 (2010) 7212–7221. doi:10.1021/ma101042d.

[5] R. Hiss, S. Hobeika, C. Lynn, G. Strobl, Network stretching, slip processes, and fragmentation of crystallites during uniaxial drawing of polyethylene and related copolymers. A comparative study, Macromolecules. 32 (1999) 4390–4403. doi:10.1021/ma981776b.

[6] Y. Zhang, P.Y. Ben Jar, S. Xue, L. Li, Quantification of strain-induced damage in semi-crystalline polymers: a review, J. Mater. Sci. 54 (2019) 62–82. doi:10.1007/s10853-018-2859-2.

[7] L. Farge, J. Boisse, J. Dillet, S. André, P.A. Albouy, F. Meneau, Wide-angle X-ray scattering study of the lamellar/fibrillar transition for a semi-crystalline polymer deformed in tension in relation with the evolution of volume strain, J. Polym. Sci. Part B Polym. Phys. 53 (2015) 1470–1480. doi:10.1002/polb.23790.

[8] M.F. Butler, A.M. Donald, W. Bras, G.R. Mant, G.E. Derbyshire, A.J. Ryan, A real-time simultaneous small- and wide-angle X-ray scattering study of in-situ deformation of isotropic polyethylene, Macromolecules. 28 (1995) 6383–6393. doi:10.1021/ma00123a001.

[9] R. Hiss, S. Hobeika, C. Lynn, G. Strobl, General scheme derived from video-controlled stretching tests and WAXS for describing tensile deformations of polyethylenes, J. Macromol. Sci. Part B. 38 (1999) 37–41. doi:10.1080/00222349908248143.

[10] D.J. Louse, R.J. Gaylord, The amorphous contribution to the modulus of a semi-crystalline

polymer, Polym. Eng. Sci. 18 (1978) 512–517. doi:10.1002/pen.760180614.

[11] Q. Fu, Y. Men, G. Strobl, Understanding of the tensile deformation in HDPE/LDPE blends based on their crystal structure and phase morphology, Polymer (Guildf). 44 (2003) 1927–1933. doi:10.1016/S0032-3861(02)00940-0.

[12] Y. Men, G. Strobl, Critical strains in poly(ε-caprolactone) and blends with poly(vinyl methyl ether) and poly(styrene-co-acrylonitrile), Macromolecules. 36 (2003) 1889–1898. doi:10.1021/ma025955b.

[13] S. Hobeika, Y. Men, G. Strobl, Temperature and strain rate independence of critical strains in polyethylene and poly (ethylene-co-vinyl acetate), Macromolecules. 33 (2000) 1827–1833. doi:10.1021/ma9910484.

[14] K. Hong, A. Rastogi, G. Strobl, A model treating tensile deformation of semicrystalline polymers: Quasi-static stress-strain relationship and viscous stress determined for a sample of polyethylene, Macromolecules. 37 (2004) 10165–10173. doi:10.1021/ma049174h.

[15] Z. Wang, Y. Liu, C. Liu, J. Yang, L. Li, Understanding structure-mechanics relationship of high density polyethylene based on stress induced lattice distortion, Polymer (Guildf). 160 (2019) 170–180. doi:10.1016/j.polymer.2018.11.054.

[16] M. Kuriyagawa, K.H. Nitta, Structural explanation on natural draw ratio of metallocene-catalyzed high density polyethylene, Polymer (Guildf). 52 (2011) 3469–3477. doi:10.1016/j.polymer.2011.05.028.

[17] C.J.G. Plummer, A. Goldberg, A. Ghanem, Micromechanisms of slow crack growth in

polyethylene, In European Structural Integrity Society. 32 (2003) 3-14. doi:10.1016/S1566-1369(03)80079-1.

[18] A. Pawlak, A. Galeski, A. Rozanski, Cavitation during deformation of semicrystalline polymers, Prog. Polym. Sci. 39 (2014) 921–958. doi:10.1016/j.progpolymsci.2013.10.007.

[19] B. Na, Q. Zhang, Q. Fu, Y. Men, K. Hong, G. Strobl, Viscous-force-dominated tensile deformation behavior of oriented polyethylene, Macromolecules. 39 (2006) 2584–2591. doi:10.1021/ma052496g.

[20] Y. Zhang, P.Y. Ben Jar, Effects of crosshead speed on the quasi-static stress–strain relationship of polyethylene pipes, J. Press. Vessel Technol. 139 (2016) 021402. doi:10.1115/1.4033777.

[21] N. Tan, P.Y.B. Jar, Multi-relaxation test to characterize PE pipe performance, Plast. Eng. 75 (2019) 40–45. doi:10.1002/peng.20184.

[22] H. Eyring, Viscosity, plasticity, and diffusion as examples of absolute reaction rates, J. Chem. Phys. 4 (1936) 283–291. doi:10.1063/1.1749836.

[23] I.M. Ward, The yield behaviour of polymers, J. Mater. Sci. 6 (1971) 1397–1417. doi:10.1007/BF00549685.

[24] T.A. Tervoort, R.J.M. Smit, W.A.M. Brekelmans, L.E. Govaert, A constitutive equation for the elasto-viscoplastic deformation of glassy polymers, Mech. Time-Dependent Mater. 1 (1998) 269–291. doi:10.1126/science.146.3650.1458.

[25] Z. Bartczak, Effect of the molecular network on high-strain compression of cross-linked

polyethylene, Eur. Polym. J. 48 (2012) 2019–2030. doi:10.1016/j.eurpolymj.2012.09.006.

[26] A. Lustiger, R.L. Markham, Importance of tie molecules in preventing polyethylene fracture under long-term loading conditions, Polymer (Guildf). 24 (1983) 1647–1654. doi:10.1016/0032-3861(83)90187-8.

[27] P.B. Bowden, R.J. Young, Deformation mechanisms in crystalline polymers, J. Mater. Sci. 9 (1974) 2034–2051. doi:10.1007/BF00540553.

[28] W. Cao, M.P. Mullarney, B.C. Hancock, S. Bates, K.R. Morris, Modeling of transmitted X-ray intensity variation with sample thickness and solid fraction in glycine compacts, J. Pharm. Sci. 92 (2003) 2345–2353. doi:10.1002/jps.10480.

[29] S. Humbert, O. Lame, G. Vigier, Analysis of the effects of local stress transmission on yielding properties of the polyethylenes, Int. J. Mater. Form. 1 (2008) 611–614. doi:10.1007/s12289-008-0.

[30] S. Humbert, O. Lame, G. Vigier, Polyethylene yielding behaviour: What is behind the correlation between yield stress and crystallinity?, Polymer (Guildf). 50 (2009) 3755–3761. doi:10.1016/j.polymer.2009.05.017.

[31] K.H. Wang, I.J. Chung, M.C. Jang, J.K. Keum, H.H. Song, Deformation behavior of polyethylene/silicate nanocomposites as studied by real-time wide-angle X-ray scattering, Macromolecules. 35 (2002) 5529–5535. doi:10.1021/ma020165n.

[32] H.S. Jaggi, B.K. Satapathy, A.R. Ray, Viscoelastic properties correlations to morphological and mechanical response of HDPE/UHMWPE blends, J. Polym. Res. 21 (2014) 482.

doi:10.1007/s10965-014-0482-8.

[33] R.E. Cohen, Z. Bartczak, A.S. Argon, Evolution of the crystalline texture of high-density polyethylene during uniaxial compression, Macromolecules. 25 (1992) 4692–4704. doi:10.1021/ma00044a034.

[34] Z. Bartczak, A.S. Argon, R.E. Cohen, Deformation mechanisms and plastic resistance in single-crystal-textured high-density polyethylene, Macromolecules. 25 (1992) 5036–5053. doi:10.1021/ma00045a034.

[35] B. Xiong, O. Lame, C. Rochas, R. Seguela, G. Vigier, Temperature-microstructure mapping of the initiation of the plastic deformation processes in polyethylene via in situ WAXS and SAXS, Macromolecules. 48 (2015) 5267–5275. doi:10.1021/acs.macromol.5b01258.

[36] J.A.H.M. Moonen, W.A.C. Roovers, R.J. Meier, B.J. Kip, Crystal and molecular deformation in strained high-performance polyethylene fibers studied by wide-angle x-ray scattering and Raman spectroscopy, J. Polym. Sci. Part B Polym. Phys. 30 (1992) 361–372. doi:10.1002/polb.1992.090300406.

[37] P. Sajkiewicz, T. Hashimoto, K. Saijo, A. Gradys, “Intermediate phase” in poly(ethylene) as elucidated by the WAXS. Analysis of crystallization kinetics, Polymer (Guildf). 46 (2005) 513–521. doi:10.1016/j.polymer.2004.11.018.

[38] X. Lu, R. Qian, N. Brown, The effect of crystallinity on fracture and yielding of polyethylenes, Polymer (Guildf). 36 (1995) 4239–4244. doi:10.1016/0032-3861(95)92219-5.

Chapter 5 Multi-relaxation test to characterize the long-term performance of PE and its pressure pipe

A new concept is proposed, which uses results from a multi-relaxation test to characterize transition of deformation mechanisms in polyethylene (PE) pipes, from the amorphous phase only to the involvement of the crystalline phase. The former mechanism is believed to lead to brittle failure, while the latter ductile failure. The transition from ductile to brittle (DB) failure has been observed in creep tests of PE pipes by reducing the applied stress below a critical level. This paper presents results from six PE pipes of different density and molecular weight distribution. The results suggest that high-density PE pipes require a higher deformation level for the involvement of the crystalline phase than the medium-density PE pipes. The results also suggest that the trend of change in the critical stress level for the involvement of the crystalline phase is close to the trend of change in the hydrostatic design basis, but the former takes less than two weeks to complete, while the latter more than 1 year. Therefore, the multi-relaxation test can be used as an alternative method to characterize PE pipe performance, as a means for preliminary screening or in-service monitoring of pipe performance.

5.1 Introduction

Polyethylene (PE) is a semi-crystalline polymer with a microstructure of chain-folding crystalline lamellae and inter-lamellar amorphous phase. The material has long been an attractive option for pipe applications, due to its light weight and excellent ductility [1-4]. Many researchers have studied complex mechanisms involved in its deformation process, which induces changes in the microstructural morphology [5-6]. However, these studies are yet to provide evidence to clarify the mechanisms for the well-known unusual ductile-to-brittle (DB) transition that has been observed in laboratory testing of PE pipe sections when subjected to the creep loading. This DB transition is known to cause brittle failure at a low stress level, occurring often after a long incubation period [7-9]. Therefore, it is difficult to predict its occurrence in the short-term laboratory testing.

Over the last few decades, many researchers have shown considerable interests in predicting the long-term performance of PE using the short-term laboratory tests [10-12]. Most of these tests introduced notches to specimens to reduce time required to initiate slow crack growth (SCG), thus shortening the time for detecting the DB transition. However, the use of notches prevents the test results from prediction of critical stress and time for the DB transition in PE products that do not contain any notch [13]. To our knowledge, only a few groups have tried to use notch-free specimens to predict the DB transition, and apply the test results to prediction of service life of PE in service [14-15]. Therefore, it is of great significance to develop a new short-term test to characterize the long-term performance of PE using notch-free specimens.

At a sufficiently low strain rate, deformation in PE is known to start firstly in the amorphous phase, because of its relatively lower resistance to deformation than the crystalline

counterpart [1]. Based on this concept, we believe that the brittle-like failure behavior in PE at a low stress level is caused by the limited extent of deformation due to the constraint in the inter-lamellar, amorphous phase. Hong et al. [16] have proposed an approach to identify the deformation transition from the amorphous phase only to the involvement of the crystalline phase. Following their concept, a preliminary study [17] was conducted on one ethylene-hexene copolymer (PE plaque) to identify the critical quasi-static stress levels for deformation transition. It was found that a short-term multi-relation (MR) test is capable of detecting two critical points for deformation transition, one for the onset of plastic deformation in the crystalline phase and another for global yielding in the crystalline phase. Moreover, one of the two critical points correlates well with critical stress for the DB transition of the PE plaque. Such a phenomenon sheds a light on the possibility of using a short-term test to characterize DB transition of PE and this concept was transferred to PE pipes. In this study, creep tests were not conducted to determine critical stress for the DB transition in PE pipes used in the study. Instead, hydrostatic design basis (HDB) provided by the pipe supplier is used to compare with the critical quasi-static stress for transition determined from the MR test. This chapter summarizes the test results and discusses possible means to obtain additional evidence to support the conclusions.

5.2 Experiments

5.2.1 Materials and sample preparation

Materials used in the study are six 2-inch PE pipes of different categories, based on difference in density, medium- or high-density (MD or HD, respectively) and molecular weight distribution (bi- or uni-modal), denoted as u-MDPE, b-MDPE, u-HDPE and b-HDPE in which “u” stands for uni-modal molecular weight distribution and “b” bi-modal. In addition to the above

differences, pipes #1 to #4 used in this study were from manufacture A, while pipes #5 and #6 from manufacturer B. All pipes have the ratio of pipe outer diameter to wall thickness (SDR) of 11. Fundamental characteristics for these PE pipes are listed in Tab. 5.1.

Tab. 5.1 Material characteristics for pipes used in the study.

Material	**Pipe code**	**Density (g/cc)**	**Yield strength (MPa)**	**HDB[1] @23 ºC (MPa)**
#1 u-MDPE	PE2708	0.940	19.3	8.62
#2 u-HDPE	PE3408	0.944	22.8	11.03
#3 b-MDPE	PE2708	0.940	19.3	8.62
#4 b-HDPE	PE4710	0.949	24.8	11.03
#5 u-MDPE	PE2708	0.940	19.3	8.62
#6 b-HDPE	PE4710	0.949	>24.1	11.03

[1] Hydrostatic design basis

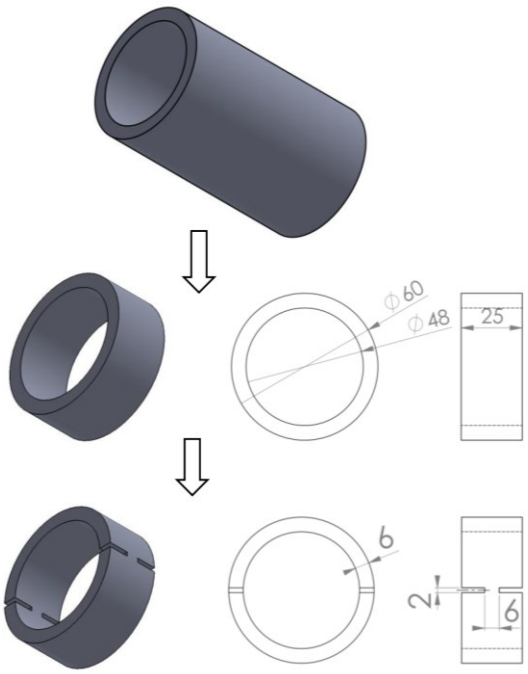

Fig. 5.1 Schematic description of specimen preparation.

Notched-pipe-ring (NPR) specimens, with the overall width of 25 mm and ligament length of nominally 6 mm, were machined from the above PE pipes. Instead of the conventional round notch, a flat notch profile is used to improve stress evenness across the ligament length [18]. Fig. 5.1 depicts the general machining process for NPR specimens. At least two tests were conducted for each type of PE pipes to ensure repeatability of the test results.

5.2.2 Multi-relaxation (MR) test

D-split tensile loading was applied to the NPR specimens using a universal test machine (Quasar 100), with test program and data acquisition controlled using a personal computer. Fig. 5.2 depicts the test setup. The tests were under displacement control, consisting of multiple relaxation stages each of which was for a relaxation period of 10,000 seconds. A constant

displacement increment of 0.33 mm, at a speed of 5 mm/min, was introduced between two adjacent relaxation stages. The maximum displacement for each multi-relaxation test was 10 mm, followed by unloading at the same crosshead speed. A home-made extensometer was mounted on each specimen before the test, to record changes of the gauge length during the test. All of the tests were conducted at room temperature.

In each multi-relaxation test, raw data of load, stroke and extensometer readings were recorded as functions of time, based on which engineering stress (σ_{eng}) and area strain ($\varepsilon_{\text{area}}$) were calculated using the following expressions.

$$\sigma_{\text{eng}} = \frac{F}{2T_0 W_0} \tag{5.1}$$

$$\varepsilon_{\text{area}} = 2 \ln \frac{W_0}{W} \tag{5.2}$$

where F is the applied load, W ligament length, and T_0 ligament thickness. Subscript "0" stands for the initial values of the parameters.

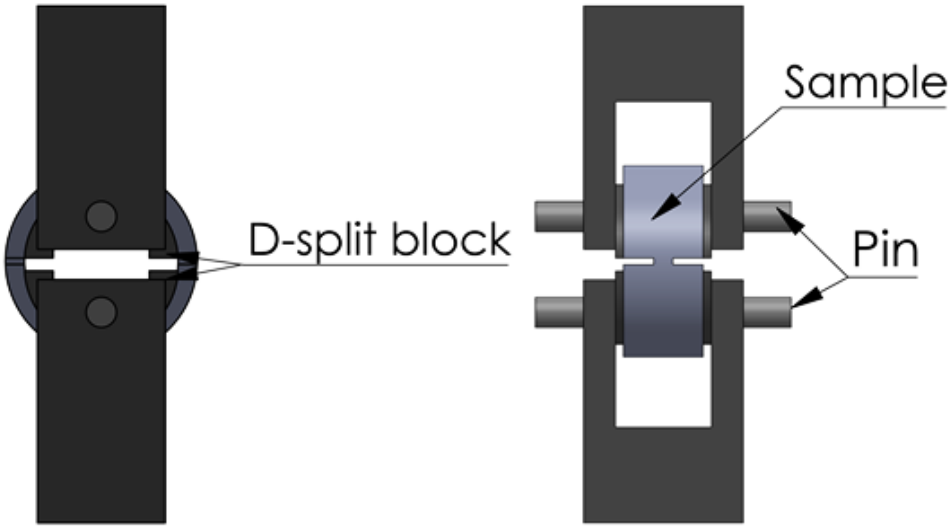

Fig. 5.2 Set-up of the D-split tensile test.

5.3 Idea of using MR test to predict critical stress for the DB transition

In a previous study [17], uniaxial creep tests were conducted on one ethylene-hexene copolymer (PE plaque) over a wide range of stress and temperature. A stress-time-temperature (StT) expression, following the procedure in Chapter 2, was established to construct the master curve of stress versus creep time to ductile (or brittle) failure at a given temperature, which contains the transition between the two behaviors (commonly known as the DB transition). For the PE plaque used in this study, examples of master curves of applied creep stress versus failure time are constructed for several temperatures, as shown in Fig. 5.3. Open circles in the figure are data obtained from the creep tests. In each master curve, intersection of two straight lines with different slopes is the location where DB transition is expected.

Fig. 5.4 summarizes critical stresses for the DB transition at different temperatures, determined based on the plots in Fig. 5.3. Fig. 5.4 indicates that at room temperature (296 K),

critical stress for the DB transition is 11.43 MPa, which is consistent with the previous expectation that stress for brittle failure to occur should be less than half of the yield stress (27.1 MPa) [19]. Fig. 5.4 also indicates that for this PE plaque, critical stress for the DB transition decreases significantly, to 6.50 MPa, by increasing temperature to 358 K.

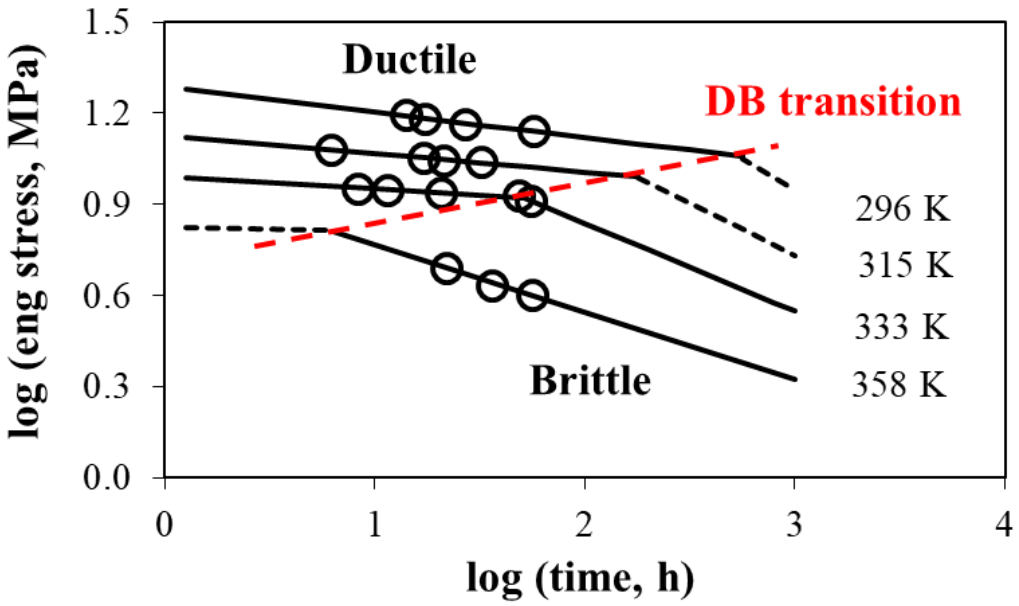

Fig. 5.3 Master curves of engineering stress versus time, including the DB transition and creep test results.

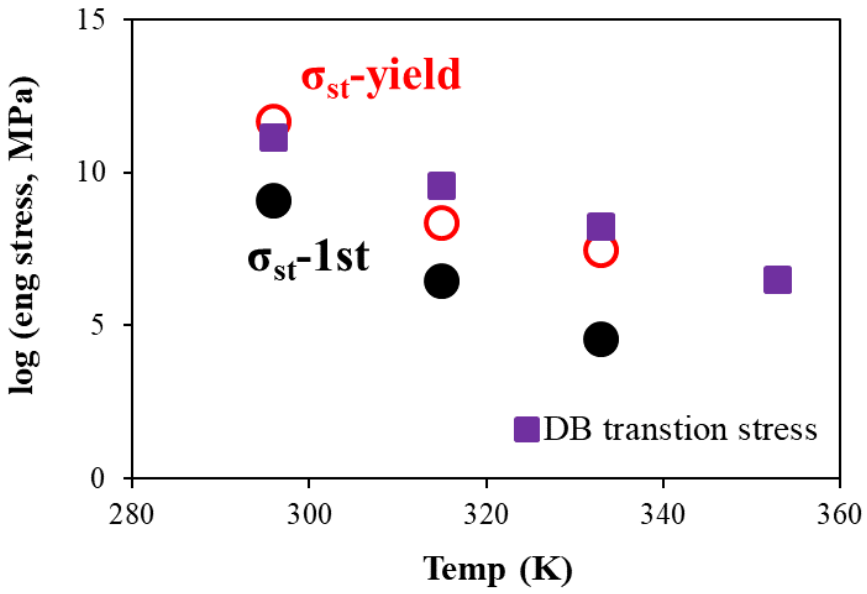

Fig. 5.4 Critical stresses for the DB transition (■) from creep tests, first critical quasi-static stresses (●) and critical quasi-static stress for global yielding (○) from short-term MR tests at different temperatures.

The short-term MR test were conducted at three temperatures of 296, 315 and 333 K, identical to the lower three temperatures selected for the creep test. This is to provide a more thorough comparison between results from short-term MR test and those from creep test. Following the analysis in Ref. [20], two critical quasi-static stresses were determined and listed in Fig. 5.4, which represent the quasi-static stress for the onset of plastic deformation in the crystalline phase (σ_{st}-1st) and for the global yielding of the crystalline phase (σ_{st}-yield). As indicated in Fig. 5.4, the critical stress for the DB transition and σ_{st}-yield have very similar values. Therefore, it is likely that σ_{st}-yield can be used to represent the critical stress for the DB transition. Although data presented here are limited, the phenomenon has shed a light on the possibility of using short-term test results to determine critical point for mechanism transition in the long-term performance of PE. Based on this phenomenon, MR tests were conducted on PE pipe to predict critical stresses

for the DB transition. Note that the creep tests on pipe specimens (NPR specimens) were conducted at room temperature only.

5.4 Results and discussions

Fig. 5.5 presents a typical engineering stress-stroke curve from the multi-relaxation test, while the line connecting the engineering stress at the beginning of each relaxation stage is used to represent the applied engineering stress-stroke curve for each specimen.

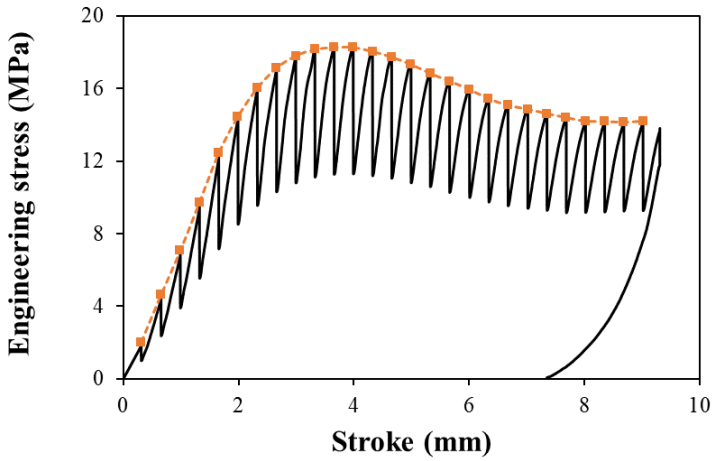

Fig. 5.5 A typical engineering stress-stroke curve (from #5 u-MDPE).

Fig. 5.6 summarizes curves of engineering stress versus stroke for the six PE pipes. The figure suggests that HDPE pipes exhibit higher yield strength than the MDPE pipes, for both uni-modal and bi-modal molecular weight distribution. Such a trend is also reflected in the curves of true stress versus area strain, as shown in Fig. 5.7. The results also show that the HDPE pipes has better mechanical strength than the MDPE counterparts, which is consistent with the well-known concept that strength for PE is mainly governed by the degree of crystallinity [21].

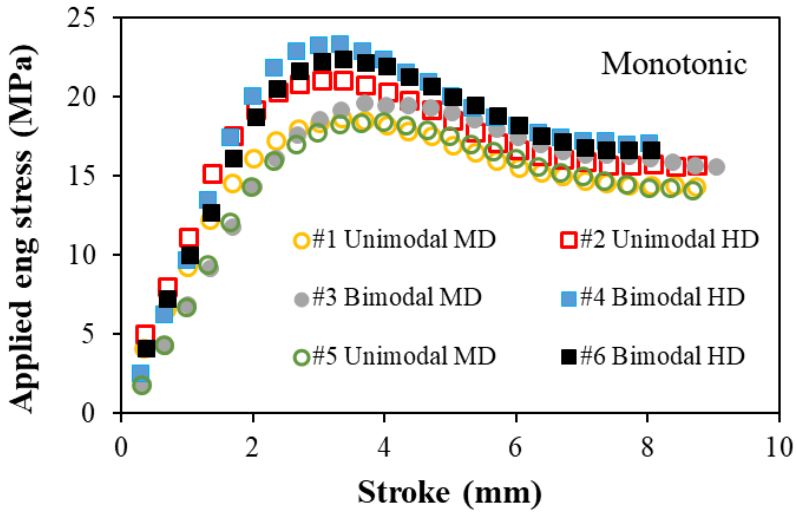

Fig. 5.6 Curves of applied engineering stress versus stroke for the six PE pipes.

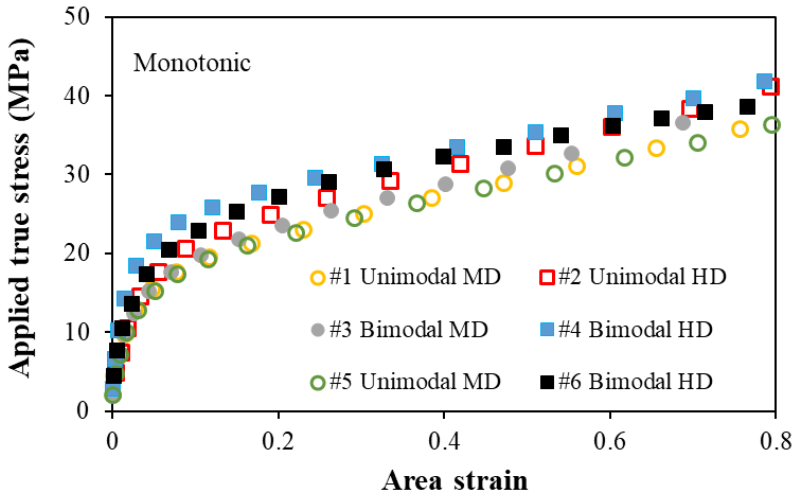

Fig. 5.7 Curves of applied true stress versus area strain for the six PE pipes.

The applied stress (σ_A) for the mechanical testing of PE can be decomposed into two components, i.e. the time-dependent viscous stress, $\sigma_r(t)$, and the time-independent quasi-static stress, σ_{st}, as shown in the following expression:

$$\sigma_{\mathrm{A}}(t) = \sigma_{\mathrm{st}} + \sigma_{\mathrm{r}}(t) \tag{5.3}$$

Based on the Eyring's Law, as suggested by Hong et al. [16], the drop of viscous stress during the relaxation stage ($\Delta\sigma_{\mathrm{r}}$) can be expressed as a function of relaxation time using the following equation.

$$\Delta\sigma_{\mathrm{r}} = \sigma_{\mathrm{r}}(0) - \sigma_{\mathrm{r}}(t) = \sigma_{\mathrm{r}}(0) - 2\sigma_0 \tanh^{-1}\left[\tanh\left(\frac{\sigma_{\mathrm{r}}(0)}{2\sigma_0}\right)\exp\left(-\frac{t}{\tau_{\mathrm{r}}}\right)\right] \tag{5.4}$$

where σ_0 is the reference stress, and τ_{r} the characteristic relaxation time which is fixed as 16000 seconds, following the work by Hong et al. [16]. Since σ_{st} is independent of time, $\Delta\sigma_{\mathrm{r}}$ is equivalent to the total stress decay in the relaxation stage. Therefore, by adjusting values for σ_0 and $\sigma_{\mathrm{r}}(0)$ in Eq. (5.4) so that the curve from the experimental measurements at each relaxation stage matches that from Eq. (5.4), the σ_0 and $\sigma_{\mathrm{r}}(0)$ values can be plotted as a function of stroke or area strain. As suggested by Hong et al. [16], the first change in the trend for σ_0 represents the transition in deformation from the amorphous phase only to the involvement of the crystalline phase, and is referred to as the first critical point. The second critical point, corresponding to the peak point on the engineering stress-stroke curve, represents the onset of the collective slipping in the crystalline phase.

Although the curve generated from Eq. (5.4) cannot fully match the curve obtained experimentally, in view that the current study is focused on the long-term performance of PE pipes, values for σ_0 and $\sigma_{\mathrm{r}}(0)$ were chosen so that the curve generated from Eq. (5.4) matches the linear part of the curve for stress drop versus logarithmic scale of time, in the time frame above 1000

seconds at the relaxation stage. Fig. 5.8 provides an example of such curve fitting. Two curves are presented in Fig. 5.8(a) as a linear function of time, one from the experimental testing and the other based on the Eyring's Law, and Fig. 5.8(b) as a logarithmic function of time.

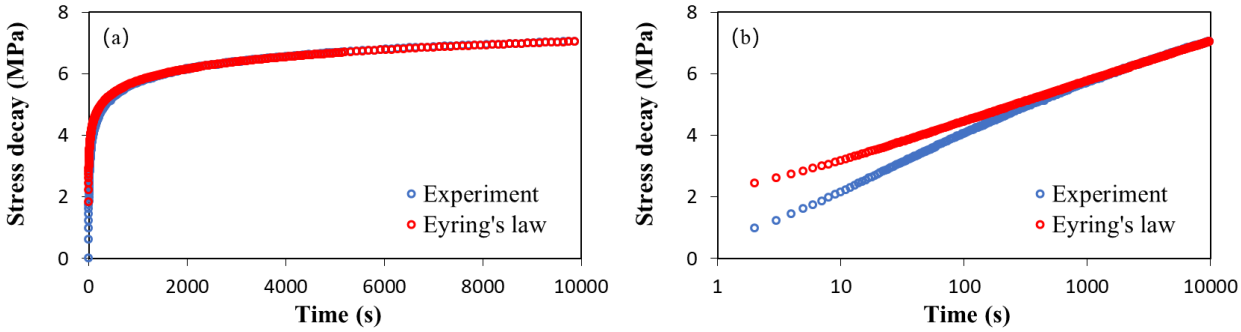

Fig. 5.8 Curve fitting of experimental data according to the Eyring's Law.

By applying the above curve fitting process to data measured at each relaxation stage, values for σ_0 were determined and plotted as a function of stroke. Fig. 5.9 gives an example of such plots for NPR specimens. Following the suggestion by Hong et al. [16], as mentioned earlier, the first critical point occurs when the trend line for σ_0 changes with the increase of deformation. Such a change is indicated in Fig. 5.9 using an arrow. It is worth mentioning that, different from Fig. 5.9, a small drop of σ_0 appeared after its initial linear increase with the increase of stroke for PE plaques, as shown in Fig. 4.6 (a). As a result, the ways used to determine the first critical point for PE plaques and for PE pipes are different.

Fig. 5.10 summarizes variation of σ_0 as a function of either stroke in (a) or area strain in (b). The solid triangles (▲) in the plots represent the critical stroke or area strain for the first critical point. In general, the two plots in Fig. 5.10 indicate that critical values of stroke and area

strain for the first critical point in the HDPE pipes are larger than the corresponding values for the MDPE pipes.

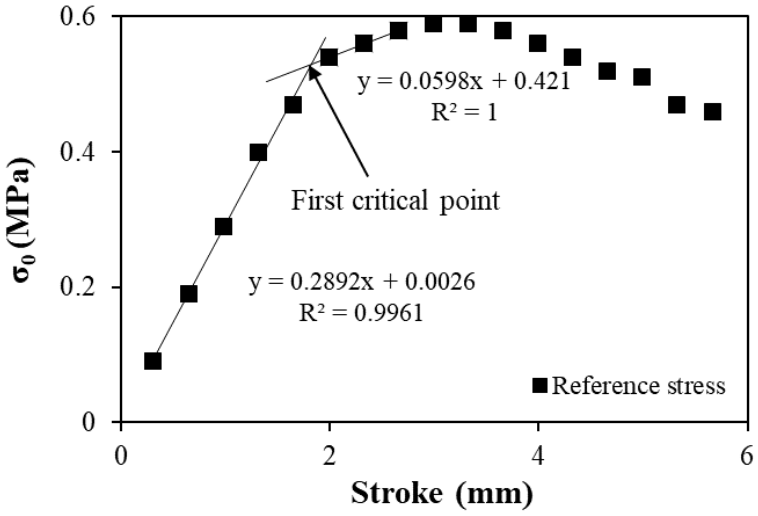

Fig. 5.9 Plot of reference stress (σ_0) as a function of stroke for a NPR specimen, and depiction of the process to determine the first critical point for deformation transition.

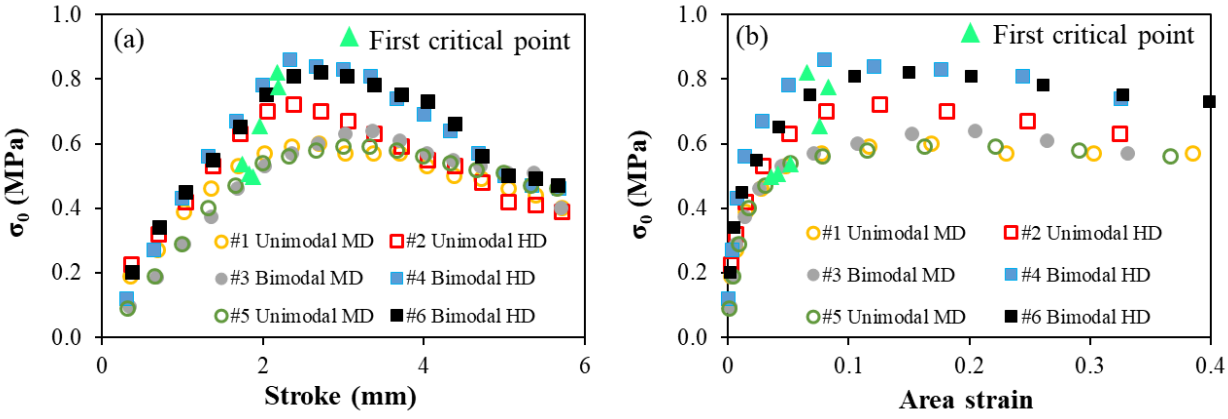

Fig. 5.10 Reference stress (σ_0) as a function of (a) stroke, and (b) area strain.

Fig. 5.11(a) presents the plot of maximum viscous stress component, $\sigma_r(0)$, as a function of stroke, and Fig. 5.11(b) the corresponding quasi-static stress component, σ_{st}. The figures suggest that $\sigma_r(0)$ and σ_{st} exhibit the same trend of difference among the six pipes, but the difference for $\sigma_r(0)$ is bigger than that for σ_{st}. In general, their maximum values for HDPE pipes are larger than those for MDPE pipes, and for pipes in the same density category, $\sigma_r(0)$ values for those with bi-modal molecular weight distribution are larger than those with the uni-modal counterpart, but the difference for the σ_{st} values are less.

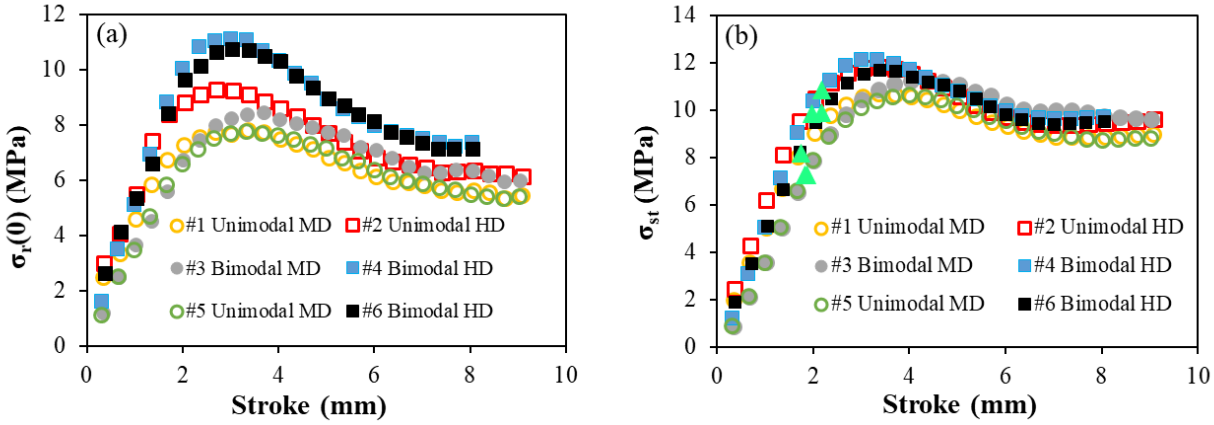

Fig. 5. 11 Two stress components determined from the multi-relaxation tests as a function of stroke for the six PE pipes: (a) $\sigma_r(0)$ and (b) σ_{st}.

In order to investigate the possibility of using the short-term MR test to characterize long-term performance, critical quasi-static stresses are compared with results from long-term hydrostatic pressure tests. The latter tests were conducted on pipe sections by the pipe supplier, following the procedure specified using ASTM D2837 [22].

Tab. 5.2 summarizes critical area strains for the first critical point and the corresponding σ_{st} values for the six PE pipes, and compares these values with their hydrostatic design basis (HDB) at 23ºC and long-term hydrostatic strength (LTHS) determined using ASTM D2837 [22]. As mentioned earlier, the critical area strain values for MDPE pipes are smaller than those for HDPE pipes, and consequently the corresponding σ_{st} values for MDPE are smaller than those for HDPE. It is interesting to point out that critical σ_{st} values for these PE pipes are quite close to their HDB values. Since HDB is determined from the measured values for LTHS which takes more than 10,000 hours (> 1 year) to complete, results from the multi-relaxation test, taking only about four days to complete, can serve as an alternative, time-saving approach to evaluation of long-term mechanical performance of PE pipes.

Tab. 5.2 Summary of results from the multi-relaxation tests and those from standard test methods (HDB and LTHS).

Material	**First critical area strain**	**First critical quasi-static stress (σ_{st}) (MPa)**	**HDB @23ºC (MPa)**	**LTHS[1] (MPa)**
#1 u-MDPE	0.05	8.18	8.62	8.27 -10.55
#2 u-HDPE	0.09	10.16	11.03	10.55 -11.93
#3 b-MDPE	0.04	7.25	8.62	8.27 -10.55
#4 b-HDPE	0.07	10.86	11.03	10.55 -11.93
#5 u-MDPE	0.04	7.25	8.62	8.27 -10.55
#6 b-HDPE	0.08	9.88	11.03	10.55 -11.93

[1] Long-term hydrostatic strength

5.5 Conclusions

Results from the study suggest that in general, HDPE pipes have better mechanical strength than MDPE pipes. For PE pipes with the same density, PE pipes of bi-modal molecule weight distribution are stronger than those of unimodal molecular weight distribution.

In the deformation process that starts in the amorphous phase and involves the crystalline phase, a short-term multi-relaxation (MR) test can be used to determine the critical quasi-static stress level for the deformation transition from the amorphous phase only to the involvement of the crystalline phase. Among the six pipes used in the study, the results show that the critical stroke and the corresponding area strain values for the involvement of the crystalline phase in the MDPE pipes are always smaller than those for the HDPE pipes. The results also suggest that the critical stress levels for the involvement of the crystalline phase are quite close to their HDB values. Therefore, the proposed MR test can be used as an alternative to ASTM D2837, for comparison of long-term performance of PE pipes in a very short timeframe.

References

[1] L. Farge, J. Boisse, J. Dillet, S. André, P.A. Albouy, F. Meneau, Wide-angle X-ray scattering study of the lamellar/fibrillar transition for a semi-crystalline polymer deformed in tension in relation with the evolution of volume strain, J. Polym. Sci. Part B Polym. Phys. 53 (2015) 1470–1480. doi:10.1002/polb.23790.

[2] R.E. Cohen, Z. Bartczak, A.S. Argon, Evolution of the crystalline texture of high-density polyethylene during uniaxial compression, Macromolecules. 25 (1992) 4692–4704. doi:10.1021/ma00044a034.

[3] Z. Bartczak, A.S. Argon, R.E. Cohen, Deformation mechanisms and plastic resistance in single-crystal-textured high-density polyethylene, Macromolecules. 25 (1992) 5036–5053. doi:10.1021/ma00045a034.

[4] B. Xiong, O. Lame, C. Rochas, R. Seguela, G. Vigier, Temperature-microstructure mapping of the initiation of the plastic deformation processes in polyethylene via in situ WAXS and SAXS, Macromolecules. 48 (2015) 5267-5275. doi:10.1021/acs.macromol.5b01258.

[5] M.F. Butler, A.M. Donald, W. Bras, G.R. Mant, G.E. Derbyshire, A.J. Ryan, A real-time simultaneous small- and wide-angle X-ray scattering study of in-situ deformation of isotropic polyethylene, Macromolecules. 28 (1995) 6383–6393. doi:10.1021/ma00123a001.

[6] P.B. Bowden, R.J. Young, Deformation mechanisms in crystalline polymers, J. Mater. Sci. 9 (1974) 2034–2051. doi:10.1007/BF00540553.

[7] P.A. O'Connell, R.A. Duckett, I.M. Ward, Brittle-ductile transitions in polyethylene, Polym. Eng. Sci. 42 (2002) 1493–1508. doi:10.1002/pen.11046.

[8] X. Lu, X. Wang, N. Brown, Slow fracture in a homopolymer and copolymer of polyethylene, J. Mater. Sci. 23 (1988) 643–648. doi:10.1007/BF01174699.

[9] M.J. Shirkavand, H. Azizi, I. Ghasemi, M. Karabi, Effect of molecular structure parameters on crystallinity and environmental stress cracking resistance of high-density polyethylene/TiO2 nanocomposites, Adv. Polym. Technol. 37 (2018) 770–777. doi:10.1002/adv.21719.

[10] A. Frank, G. Pinter, R.W. Lang, Prediction of the remaining lifetime of polyethylene pipes

after up to 30 years in use, Polym. Test. 28 (2009) 737–745. doi:10.1016/j.polymertesting.2009.06.004.

[11] C. Tischler, T.R. Kratochvilla, H. Muschik, H. Dragaun, Notched ring test for measuring slow cracking resistance in plastics pipes and fittings, Macromol. Symp. 296 (2010) 626–631. doi:10.1002/masy.201051082.

[12] E. Nezbedová, G. Pinter, A. Frank, P. Hutař, J. Poduška, J. Hodan, Accelerated tests for lifetime prediction of PE-HD pipe grades, Macromol. Symp. 373 (2017) 1–8. doi:10.1002/masy.201600096.

[13] P. Y. Ben Jar, Transition of neck appearance in polyethylene and effect of the associated strain rate on the damage generation, Polym. Eng. Sci. 54 (2014) 1871–1878. doi:10.1002/pen.23735.

[14] R.H. Carey, Creep and stress-rupture behavior of polyethylene resins, Ind. Eng. Chem. 50 (2005) 1045–1048. doi:10.1021/ie50583a040.

[15] L.J. Zapas, J.M. Crissman, An instability leading to failure of polyethylene in uniaxial creep, Polym. Eng. Sci. 19 (1979) 104–107. doi:10.1002/pen.760190209.

[16] K. Hong, A. Rastogi, G. Strobl, A model treating tensile deformation of semicrystalline polymers: quasi-static stress-strain relationship and viscous stress determined for a sample of polyethylene, Macromolecules. 37 (2004) 10165–10173. doi:10.1021/ma049174h.

[17] N. Tan, P.Y. Ben Jar, Establishing ductile-to-brittle transition of unimodal high density polyethylene under creep test. Annu. Tech. Conf.-ANTEC, Conf. Proc. 2020-April (2020)

[18] P.Y. Ben Jar, S. Muhammad, Cavitation-induced rupture in high-density polyethylene copolymers, Polym. Eng. Sci. 52 (2012) 1005–1014. doi:10.1002/pen.

[19] M. Schilling, U. Niebergall, M. Böhning, Full notch creep test (FNCT) of PE-HD–Characterization and differentiation of brittle and ductile fracture behavior during environmental stress cracking (ESC), Polym. Test. 64 (2017) 156–166. doi:10.1016/j.polymertesting.2017.09.043.

[20] N. Tan, P.Y. Ben Jar, Determining deformation transition in polyethylene under tensile loading, Polymers (Basel). 11 (2019) 1415. doi:10.3390/polym11091415.

[21] X. Lu, R. Qian, N. Brown, The effect of crystallinity on fracture and yielding of polyethylenes, Polymer (Guildf). 36 (1995) 4239–4244. doi:10.1016/0032-3861(95)92219-5.

[22] ASTM D2837-13, Standard test method for obtaining hydrostatic design basis for thermoplastic pipe materials or pressure design basis for thermoplastic pipe products, ASTM Int. (2013). doi:10.1520/D2837-13.cable.

Chapter 6 Conclusions and future work

Chapter 6, drawing from previous chapters, summarizes the main contributions of this research project. In addition, this chapter suggests possible work for the future investigation.

6.1 Main conclusions

The ultimate goal of this study is to develop a short-term test using notch-free specimens to detect critical points, as well as their strain and stress values, for deformation transitions of PE and to predict critical stress for the DB transition. In this study, determining the deformation transitions of PE under creep loading through the use of a stress-time-temperature (StT) parametric method, and interpreting the test data in terms of activation energy involved through the use of the Eyring's Law, have improved our understanding and knowledge of PE's long term performance. In addition, a short-term multi-relaxation (MR) test was proposed to determine deformation transitions under tensile loading. To achieve this ultimate goal, quantitative comparison was made between results from short-term MR test and creep test. The main contributions of this thesis are summarized as follows.

(1) Characterization of deformation transitions of PE under creep loading

The study of deformation transitions in PE has a great importance not only from the academic viewpoint, but also for the prediction of service life for load-carrying applications. In Chapter 2, creep tests were conducted on three ethylene-hexene copolymers differing mainly in mass density, using notch-free PE specimens. The master time-to-failure curves were constructed through the use of a stress-time-temperature (StT) parametric method similar to that introduced in ISO 9080, which are also verified using data from additional creep tests. The well-known ductile-brittle (DB) transition , including its critical time and stress level, is detected for PE with the highest mass density, and a less known ductile-ductile (DD) transition in PE with the medium mass density. With the creep test data, the analysis also suggests that the Monkman-Grant relationship

is applicable to ductile failure of PE, even with the DD transition, but cannot be applied to data for brittle failure after the DB transition.

(2) Characterization of creep deformation and failure behaviour in PE plaque

In chapter 3, creep tests were performed on four types of polyethylene (PE), one homo-polymer and three ethylene-hexene copolymers, at temperatures from 296 to 358 K. Three failure modes were observed, i.e., low- and high-temperature brittle failures and ductile failure, but the Monkman-Grant relationship is applicable to both ductile and low-temperature brittle failures. The test results were analyzed through the use of the Norton Power Law (NPL) and the Eyring's Law. The analysis suggests that the former cannot provide a proper description of the creep deformation for all PEs, but the latter can by considering two processes acting in parallel. The analysis also suggests a correlation between the failure mode transition and activation energy for deformation at the secondary creep stage. Therefore, rather than the use of creep tests with failure time up to 13 months, short-term creep tests have the potential for predicting the ductile-brittle transition that has been a major concern for long-term, load–carrying applications for PE.

(3) A short-term multi-relaxation test to characterize deformation transitions in PE plaque under tensile loading

A multi-relaxation (MR) test is developed based on the concept that stress relaxation behaviour can be used to reflect the material state. Based on this concept, two critical points, one for the onset of plastic deformation in the crystalline phase of PE, referred to as the 1st critical point, and another for global yielding, are determined for six PEs using the MR test. The corresponding critical quasi-static stresses are determined by removing the viscous stress component based on a standard visco-elastic model. The results show that the 1st critical stroke has

very similar values among the six PEs. More interestingly, ratio of the QS stress at the 1st critical stroke to the yield stress from the standard tensile test shows little dependence on PE density. Therefore, it is possible to use the short-term test to characterize the critical quasi-statics component of the applied stress to initiate plastic deformation in the crystalline phase, which is expected to play a significant role on the long-term, load-carrying applications of PE.

(4) Comparison of results from short-term multi-relaxation test and creep test in PE and its pressure pipe

To achieve the ultimate goal of this study, a quantitative comparison was made between the results from short-term MR test and creep test. For PE plaques, critical stress for the DB transition shows a good correlation with the critical quasi-static stress for the onset of global yielding in the crystalline phase. Such a phenomenon sheds a light on the possibility of using a short-term test to characterize long-term performance of PE pipe. Based on this observation, MR tests were conducted on six PE pipes to explore the possibility of using short-term test to predict the long-term behaviour. For the six PEs studied, as described in Chapter 5, the results suggest that the critical quasi-static stress for the involvement of the crystalline phase is close to the trend of change in the hydrostatic design basis (HDB), but the former takes less than two weeks to complete, while the latter more than 1 year. Therefore, the MR test can be used as an alternative method to characterize PE pipe performance, as a means for preliminary screening or in-service monitoring of pipe performance.

6.2 Future work

Overall, the research work presented in this thesis is a step toward developing a reliable short-term test for preliminary screening or in-service monitoring of PE. However, further research is needed before its application is realized in industry.

(1) Evaluating the effect of relaxation time on the determination of critical quasi-static stress in the MR test

The proposed short-term MR test has been successfully used to determine two points for deformation transitions in this thesis. In order to obtain the corresponding quasi-static stress component, the relaxation time in the Eyring's Law was fixed as 16000 seconds, following the work done by Strobl's group [1]. Using a constant relaxation time is sufficient for our purpose at this stage. However, to apply this new test method to engineering practices, it is necessary to evaluate the effect of relaxation time on the determination of critical quasi-static stress and find a way to make relaxation time as a free parameter in the curve-fitting process.

(2) Evaluating the crystallinity of PE under deformation using wide-angle X-ray scattering

In Chapter 4, wide-angle X-ray scattering (WAXS) was used to detect the involvement of the crystalline phase during deformation. We also conducted a preliminary study on the determination of the crystallinity of PE under deformation using WAXS. Fig. 6.1 shows typical WAXS spectra (from #1 LLDPE with stroke of 5 mm) after subtraction of machine background noise. A deconvolution procedure was carried out for the amorphous halo, (1 1 0), (2 0 0) and the monoclinic peak at 2θ of 19.7°, 21.6°, 24.0° and 25.0°, respectively. According to Ref. [2], the

individual contribution of each peak can be approximated by the Pearson VII function which takes the form:

$$f(2\theta) = \frac{G}{\left[1 + 4\left(\frac{2\theta - 2\theta_{\mathrm{hkl}}}{\Delta 2\theta_{\mathrm{hkl}}}\right)^2 (2^{1/e} - 1)\right]^e} \tag{6.1}$$

where $f(2\theta)$ is the peak profile, θ_{hkl} the Bragg angle, G the peak height, $\Delta(2\theta_{\mathrm{hkl}})$ the full width at half maximum and e the shape parameter of the function. For each peak, G, $\Delta(2\theta_{\mathrm{hkl}})$ and e are fitting parameters. In the preliminary study, for (1 1 0), (2 0 0) and the monoclinic peak, e was fixed as 1 and Pearson VII function reduces to the Cauchy function, while e was fixed as 1E+7 for the amorphous halo and Pearson VII function takes the Gaussian form. In Fig. 6.1, the fitting to the WAXS spectra was the sum of several Pearson VII functions, and contribution from each peak was also included. Integration under each individual peak has allowed estimate of the degree of crystallinity (X_c) using Eq. (6.2):

$$X_c = \frac{\sum F_c}{\sum F_c + F_a} \tag{6.2}$$

where F_c and F_a are areas of crystalline peak and amorphous halo, respectively [3]. Using such a technique, it is possible to estimate the crystallinity of polymers under deformation. It is worth mentioning that the technique used in the preliminary study only takes into account a few major peaks at 2θ from 10° to 30°, without considering the contribution from small peaks, such as the one indicated by an arrow in Fig. 6.1. If possible, this technique can be further investigated and optimized to evaluate the change of crystallinity of PE over the deformation process.

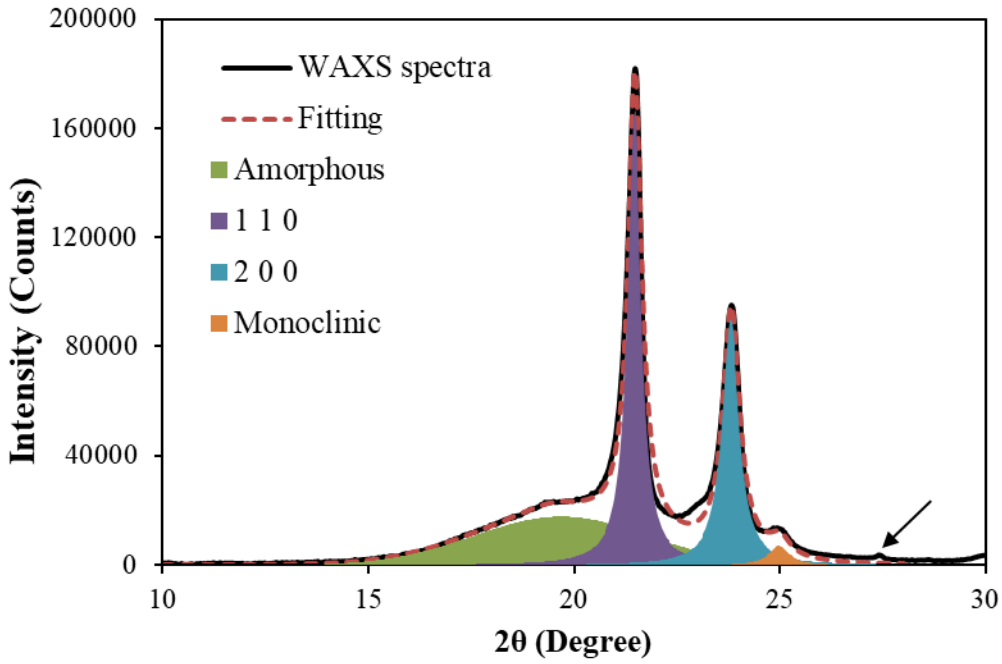

Fig. 6.1 Typical WAXS spectra (from #1 LLDPE with stroke of 5 mm) and the individual contribution of each peak from the deconvolution procedure.

(3) Evaluating the effect of residual stress on the occurrence of DB transition in PE pipes

Residual stresses are a consequence of thermal gradient along pipe wall thickness [4-8] due to difference in cooling rate introduced during the manufacturing processes. As pointed out by many investigators [4, 8-9], the presence of tensile residual stress within pipes can accelerate the fracture process when conducting a creep rupture test, resulting in the premature failure of PE pipes. Exploring the effect of residual stress on the occurrence of DB transition in PE pipes will definitely be beneficial to improvement of the manufacturing processes of PE pipe, to assure its long-term performance in service.

References

[1] K. Hong, A. Rastogi, G. Strobl, A model treating tensile deformation of semicrystalline polymers: quasi-static stress-strain relationship and viscous stress determined for a sample of polyethylene, Macromolecules. 37 (2004) 10165–10173. doi:10.1021/ma049174h.

[2] L. Farge, J. Boisse, J. Dillet, S. André, P.A. Albouy, F. Meneau, Wide-angle X-ray scattering study of the lamellar/fibrillar transition for a semi-crystalline polymer deformed in tension in relation with the evolution of volume strain, J. Polym. Sci. Part B Polym. Phys. 53 (2015) 1470–1480. doi:10.1002/polb.23790.

[3] L.D. Majdanac, D. Poleti, M.J. Teodorovic, Determination of the crystallinity of cellulose samples by x-ray diffraction, Acta Polym. 42 (1991) 351–357. doi:10.1002/actp.1991.010420802.

[4] R.K. Krishnaswamy, Analysis of ductile and brittle failures from creep rupture testing of high-density polyethylene (HDPE) pipes, Polymer (Guildf). 46 (2005) 11664–11672. doi:10.1016/j.polymer.2005.09.084.

[5] J. Poduška, P. Hutař, J. Kučera, A. Frank, J. Sadílek, G. Pinter, L. Náhlík, Residual stress in polyethylene pipes, Polym. Test. 54 (2016) 288–295. doi:10.1016/j.polymertesting.2016.07.017.

[6] P.J. Withers, H.K.D.H. Bhadeshia, Residual stress. Part 1–measurement techniques, Mater. Sci. Technol. 17 (2001) 355–365. doi:10.1179/026708301101509980.

[7] J.R. White, Origins and measurements of internal stress in plastics, Polym. Test. 4 (1984) 165–191. doi:10.1016/0142-9418(84)90010-2.

[8] J.G. Williams, J.M. Hodgkinson, A. Gray, The determination of residual stresses in plastic pipe and their role in fracture, Polym. Eng. Sci. 21 (1981) 822–828. doi:10.1002/pen.760211304.

[9] P. Hutař, M. Ševčík, A. Frank, L. Náhlík, J. Kučera, G. Pinter, The effect of residual stress on polymer pipe lifetime, Eng. Fract. Mech. 108 (2013) 98–108. doi:10.1016/j.engfracmech.2013.04.014.

Bibliography

D. Roylance, Engineering viscoelasticity, Department of Materials Science and Engineering–Massachusetts Institute of Technology, Cambridge MA (2001), 2139, 1-37.

A. Stern, Fracture mechanical characterization of the long-term behavior of polymers under static loads, Dissertation, University of Leoben, Austria, 1995.

R.K. Krishnaswamy, A.M. Sukhadia, M.J. Lamborn, Is Pent a true indicator of PE pipe slow crack growth resistance?, Bulletin, Performance Pipe, Plano, TX, Report No. PP818-TN, 2007.

N. Brown, Intrinsic lifetime of polyethylene pipelines, Polym. Eng. Sci. 47 (2007) 477–480. doi:10.1002/pen.

N.W.J. Brooks, A.P. Unwin, R.A. Duckett, I.M. Ward, Double yield points in polyethylene: structural changes under tensile deformation, J. Macromol. Sci. Part B. 34 (1995) 29–54. doi:10.1080/00222349508219486.

E. Lever, Design and pressure rating of PE fittings: stress concentrations, slow crack growth and use of ISO 9080 regression coefficients in material choice, Plast. Rubber Compos. 34 (2005) 15–19. doi:10.1179/174328905x29730.

X.C. Zhang, M.F. Butler, R.E. Cameron, The ductile-brittle transition of irradiated isotactic polypropylene studied using simultaneous small angle X-ray scattering and tensile deformation, Polymer (Guildf). 41 (2000) 3797–3807. doi:10.1016/S0032-3861(99)00594-7.

A. Makke, O. Lame, M. Perez, J.L. Barrat, Influence of tie and loop molecules on the mechanical properties of lamellar block copolymers, Macromolecules. 45 (2012) 8445–8452. doi:10.1021/ma301286y.

A.F. Yee, The yield and deformation behaviour of some polycarbonate blends, J. Mater. Sci. 12 (1977) 757–765. doi:10.1007/BF00548168.

L.P. Chen, A.F. Yee, E.J. Moskala, The molecular basis for the relationship between the secondary relaxation and mechanical properties of a series of polyester copolymer glasses, Macromolecules. 32 (1999) 5944–5955. doi:10.1021/ma981363a.

D.A. Dillard, R.G. Kander, T.C. Ward, Structure-property relationships: model studies on melt extruded uniaxially oriented high density PE films having well defined morphologies, Virginia Tech, 1997.

T.C. O'Connor, M.O. Robbins, Molecular models for creep in oriented polyethylene fibers, J. Chem. Phys. 153 (2020). doi:10.1063/5.0021286.

R.H. Boyd, Relaxation processes in crystalline polymers: experimental behaviour - a review, Polymer (Guildf). 26 (1985) 323–347. doi:10.1016/0032-3861(85)90192-2.

C. Bauwens-Crowet, J.C. Bauwens, G. Homès, Tensile yield-stress behavior of glassy polymers, J. Polym. Sci. Part A-2 Polym. Phys. 7 (1969) 735–742. doi:10.1002/pol.1969.160070411.

L. Farge, S. André, J. Boisse, Use of Digital Image Correlation to study the effect of temperature on the development of plastic instabilities in a semi-crystalline polymer, Polymer (Guildf). 153 (2018) 295–304. doi:10.1016/j.polymer.2018.07.076.

W.A. Spitzig, O. Richmond, Effect of hydrostatic pressure on the deformation behavior of polyethylene and polycarbonate in tension and in compression, Polym. Eng. Sci. 19 (1979) 1129–1139. doi:10.1002/pen.760191602.